INFLUENZA A VIRUS GENE EXPRESSION HETEROGENEITY REGULATES VIRAL SUPERINFECTION POTENTIAL AND HOST INNATE ANTIVIRAL RESPONSE

BY

JIAYI SUN

DISSERTATION

Submitted in partial fulfillment of the requirements
for the degree of Doctor of Philosophy in Microbiology
in the Graduate College of the
University of Illinois at Urbana-Champaign, 2020

Urbana, Illinois

Doctoral Committee:

Assistant Professor Christopher Brooke, Chair
Professor Rachel Whitaker
Associate Professor Thomas Kehl-Fie
Professor Steven Blanke

ABSTRACT

Influenza A virus (IAV) is an infectious respiratory pathogen that causes seasonal epidemics and sporadic pandemics in human, resulting in tens of thousands of deaths and tens of billions of dollars in economic costs every year in the U.S. alone. Its genome consists of eight gene segments each encoding one or more viral proteins. The expression of all eight genes is required to initiate productive infection. Interestingly, under the single particle infection condition, most IAV particles are semi-infectious particles (SIPs) that express an incomplete subset of the eight viral genes. The production and gene expression pattern of SIPs can vary hugely between IAV strains. However, the biological significance of this intrinsic gene expression heterogeneity at single particle level remains poorly understood. Here, I aim to investigate that whether and how this heterogeneity influences viral superinfection and host innate antiviral response.

To initiate productive infection, multiple SIPs must co-infect one cell to achieve complementation. Within a certain MOI range, increasing the abundance of SIPs in a viral population increases the percentage of productively infected cells that result from co-infection. One of the primary ways by which co-infection can occur is superinfection, the sequential infection of one cell by multiple viral particles. However, how SIPs affect IAV superinfection remain largely unknown. By combining single particle infection and multi-color flow cytometry, I directly assessed the effects of individual IAV genes on superinfection efficiency and revealed that superinfection susceptibility is negatively correlated with the quantity of viral gene segments expressed within an infected cell, regardless of their identity. As a result, cells infected with SIPs are more susceptible to

superinfection compared to cells infected with particles that express a complete set of viral genes, and viral populations that contain more SIPs undergo more-frequent superinfection. Further, I found that viral replicase activity in infected cells is responsible for inhibiting the subsequent infection. These findings identify viral gene expression heterogeneity as a major determinant of IAV superinfection potential.

Viral infection outcomes are governed by the complex interactions between infecting virus population and host response. Although viral gene expression within IAV population is extremely heterogeneous, little is known about how this heterogeneity influences host response to infection. By pairing Fluorescence-Activated Cell Sorting (FACS) with single cell RNA-seq (scRNAseq), I examined the combined host and viral transcriptomes of thousands of individual cells, each infected with a single IAV particle. I observed complex patterns of viral gene expression and the existence of multiple distinct host transcriptional responses to infection at single cell level. In addition, SIPs that fail to express the NS gene can play a dominant role in triggering innate anti-viral response to infection. Finally, human H1N1 and H3N2 virus infections differ significantly in patterns of host anti-viral gene transcriptional at single cell level. These results revealed that how patterns of viral gene expression heterogeneity can serve as a major determinant of host antiviral gene activation.

Altogether, these studies demonstrate that IAV gene expression heterogeneity has clear functional consequences on both viral superinfection potential and host innate response to

infection. More broadly, my works help establish the importance of understanding the effects of population heterogeneity on viral collective interactions and pathogenesis.

TABLE OF CONTENTS

CHAPTER 1: INTRODUCTION

1.1 Overview of IAV

Significance

Influenza A virus (IAV), together with type B, C, and recently identified type D, belong to the *Orthomyxoviridae* family(Hause et al. 2014). It is an infectious respiratory pathogen that causes influenza, also known as “flu”, in birds and a variety of mammals, including humans. In most human cases, infections are confined to the upper respiratory tract and the symptoms are relatively mild and similar to common cold, including fever, runny nose, sore throat, headache, cough, muscle pain and fatigue. However, in some severe cases, infections can spread to the lower respiratory tract and the patients can be killed by lethal pneumonia due to viral or secondary bacterial infection(Kuiken et al. 2012). According to the World Health Organization, circulating human IAV strains cause annual seasonal epidemics which result in about 1 billion infections, 3 to 5 million hospitalizations, and 300000 to 500000 deaths worldwide(Krammer et al. 2018). In addition, IAV strains of zoonotic origin can cause sporadic and unpredictable pandemics which have happened 4 times over the last 100 years. In 1918, a highly pathogenic IAV strain with genes of avian origin caused the “Spanish flu” pandemic, resulting in over 40 million deaths worldwide. The most recent “swine flu” pandemic occurred in 2009 and resulted in more than 150000 deaths worldwide. Results of phylogenetic analysis indicate that it was caused by a novel IAV strain with a mixture of avian, swine, and human flu genes(Smith et al. 2009).

Structure

The 13 kilobase IAV genome is divided into 8 negative sense, single-stranded RNA segments, referred as viral RNAs (vRNA), which encode for 10 essential viral proteins and several accessory proteins that are strain-dependent (McGeoch, Fellner, and Newton 1976). Within virus particles, the 8 vRNA segments are present in the form of viral ribonucleoprotein (vRNP) complex, where each vRNA is wrapped around multiple copies of viral nucleoprotein (NP), and the semi-complimentary 5' and 3' ends base pair with each other to form a hairpin structure bound by the viral polymerase heterotrimer, consisting of polymerase basic 1 (PB1), polymerase basic 2 (PB2), and polymerase acidic (PA) subunits(Hsu et al. 1987; Moeller et al. 2012; Fodor, Seong, and Brownlee 1993; Pflug et al. 2014; Arranz et al. 2012). The 8 vRNPs are bundled together to form a "1+7" configuration, with 1 central RNP surrounded by 7 other RNPs, and encapsidated within a viral protein coat formed by matrix 1 (M1)(Noda et al. 2006). The viral capsid also provides support underneath the viral envelope, a host-derived lipid bilayer decorated by viral membrane proteins haemagglutinin (HA), neuraminidase (NA), and matrix 2 (M2)(Gamblin and Skehel 2010; Harris et al. 2006). The size and morphology of influenza A particles are highly variable, ranging from spheres of 80 nm in diameter to filaments of 20 μm in length(Badham and Rossman 2016). Studies have suggested that both viral protein M1 and lipid composition of host membrane at the budding site play important roles in determining the morphology of virus particles(Calder et al. 2010; Hutchinson et al. 2014; Gerl et al. 2012).

Classification

IAV strains are classified into different subtypes based on the antigenicity of viral glycoproteins HA and NA, the two main targets of the host B cell response(Katz et al. 2014). Each IAV subtype is characterized by the specific combination of antigenically distinct HA and NA. Up to now, 16 antigenically distinct HA (H1-16) and 9 antigenically distinct NA (N1-9) have been identified in viruses isolated from wild aquatic birds, which serve as the natural reservoir for IAV(Yoon, Webby, and Webster 2014). Besides birds and humans, IAV is also capable of circulating in other animal species, such as pigs, bats, and horses. These animal reservoirs allow IAV to maintain significant diversity in the gene pool of antigenically distinct HA and NA, and the unique ability to adapt to various animal hosts makes IAV almost impossible to eradicate(Hurt et al. 2016; Webster et al. 1992). Recently, 2 additional HA (H17 and H18) and NA (N10 and N11) subtypes have been found in influenza A-like viruses isolated from bats(Tong et al. 2012; 2013). Despite the numerous possible combinations of HA and NA, only H1N1, H2N2, and H3N2 have persisted in humans(Morens, Taubenberger, and Fauci 2009). Among these 3 subtypes, only H1N1 and H3N2 are currently circulating and therefore are often included in the annual flu vaccines(Houser and Subbarao 2015).

Antigenic drift

Despite the widespread pre-exposure and vaccination, IAV continues to be a major threat to global public health, largely due to its ability to constantly evolve and escape pre-existing humoral immunity(Molinari et al. 2007). One way of evading the antibody-mediated inhibition is through accumulating point mutations in HA and NA that alter the

antigenicity. This mechanism, known as antigenic drift, depends upon the error-prone nature of the viral RNA-dependent RNA polymerase (RdRp) that lacks proof-reading capability(Drake 1999). The estimated mutation rate of the IAV RdRp is 1.8 to 2.5 × 10^{-4} substitutions per nucleotide, resulting in an average of 2 to 3 substitutions in every newly synthesized viral genome(Pauly, Procario, and Lauring 2017a). Currently, HA is the main component of inactivated flu vaccines, therefore the antigenic drift of HA is most extensively studied and constantly monitored to guide vaccine production(Barr et al. 2014; G. K. Hirst 1943). By pairing computational analysis with site-direct mutagenesis, multiple studies have suggested that the epitopes on HA globular head recognized by neutralizing antibody exhibit high level of mutational tolerance(Plotkin and Dushoff 2003; Thyagarajan and Bloom 2014), and one to a few amino acid substitutions in the head can lead to significant antigenic drift(Koel et al. 2013). According to surveillance, antigenic drift is more evident in circulating seasonal human influenza viruses than in animal influenza viruses, possibly due to the longer lifespan of humans(de Jong et al. 2007; Lewis et al. 2011). Despite being poorly studied, antigenic drift in NA and escape mutations in T cell epitopes have been observed and begun to receive increased attention(Sandbulte et al. 2011; Voeten et al. 2000).

Antigenic shift

Another way of developing resistance to pre-existing antibody response is by swapping the HA or NA gene between different IAV subtypes, known as antigenic shift(Morens, Taubenberger, and Fauci 2009). This process occurs through reassortment, which is the exchange of intact gene segments between viruses due to imperfect genome

packaging(Lowen 2017). Given reassortment only happens between viruses co-infecting the same cell, cellular co-infection of different IAV subtypes is required for antigenic shift to occur. Although cross-species transmission is constantly detected in regions where human directly contact poultry or swine, the antigenic shift between human and animal strains happens less frequently, largely due to the functional incompatibility of viral components from different genetic backgrounds(Chengjun Li et al. 2008; Greenbaum et al. 2012). However, when antigenic shift happens, the new viruses produced will have the potential of causing pandemics in human since most people have no pre-existing immunity against them. To date, every influenza virus that has caused a major pandemic (except the 1976 H1N1 pandemic) was generated through reassortment of human and zoonotic strains(Sobel Leonard et al. 2017). Yet, factors that dictate the efficiency of reassortment between different IAV subtypes remain poorly characterized, leaving prediction of the next pandemic extremely difficult.

1.2 IAV life cycle

Binding

Upon reaching a cell, the receptor-binding site of HA on the viral membrane recognizes the terminal sialic acid residues of glycoconjugates on host cell surface(Hamilton, Whittaker, and Daniel 2012; Weis et al. 1988). This HA-mediated receptor binding process then triggers the internalization of virus particles into host cell via clathrin-dependent endocytosis or macropinocytosis(Rust et al. 2004; C. Chen and Zhuang 2008). It is believed that HAs from avian strains preferentially bind to α-2,3-linked sialic acids(Nobusawa et al. 1991), whereas HAs from human strains preferentially bind to α-

2,6-linked sialic acids(Gambaryan et al. 1997). As a result, the distribution of α-2,3 and α-2,6-linked sialic acid receptors in host tissue is considered to be a major determinant of host range and tissue tropism of IAV. However, highly pathogenic avian viruses can occasionally infect humans despite lacking the airborne transmission between hosts(Herfst et al. 2012; Imai et al. 2012; Linster et al. 2014). Multiple studies have also revealed that single amino acid substitutions in HAs from avian viruses introduced into mammals are enough to alter their receptor binding specificities(M. Matrosovich et al. 2000). Clearly, the match between HA receptor binding preference and sialic acid linkage is not absolute and can easily be altered.

Fusion

After entering host cell, the virus traffics to endosome where acidification facilitates viral genome release. The low pH in endosome first triggers conformational change in HA which exposes the fusion peptide on the N-terminus of HA2 subunit(Bullough et al. 1994). After exposure, the fusion peptide inserts itself into endosomal membrane and the HA2 trimers then fold back to create a hairpin that brings viral and endosomal membrane in close proximity. Lastly, the hairpin structure collapses into a six-helix bundle to bring the two membranes closer, resulting in lipid stalk formation and eventually fusion(Harrison 2015; J. M. White and Whittaker 2016). The decrease in endosomal pH also leads to proton influx into the viral capsid via M2 ion channel, which weakens the interactions between M1 and vRNPs, and facilitates the release of vRNPs into cytosol at the membrane fusion site(Pinto and Lamb 2006; Martin and Helenius 1991; Bui, Whittaker, and Helenius 1996).

Genome trafficking

Recent studies combining imaging and RNA labeling techniques discovered that from attachment to cell surface, IAV can deliver genome into nucleus in as little as 1 hour(Chou et al. 2013). Timewise, cell entry and fusion can occur within 10 min, whereas nuclear import takes up most of the remaining time(Dou et al. 2017). Single-molecule FISH-based vRNP tracing revealed that viral genome is released relatively close to the nucleus, and the 8 vRNPs are likely to traffic together as a complex before reaching nuclear envelope, supporting the observation of high nuclear import efficiency of 8 vRNPs(Lakdawala et al. 2016). The current model of nuclear import is that the nuclear localization signals (NLS) on numerous NP molecules first recruit importin-α, which is recognized by importin-β transport receptor. The importin-β then directs the vRNP-importin-α-importin-β complex to nuclear pore and interacts with pore complex to facilitate the entry into the nucleoplasm(P. Wang, Palese, and O'Neill 1997; Wu, Weaver, and Panté 2007). In consistent with this model, one study showed that NP of avian viruses and mammalian viruses prefer different isoforms of importin-α, indicating the importin-α specificity is a determinant of host range and interspecies transmission(Gabriel et al. 2011).

vRNA replication

To initiate vRNA replication, the vRNP-associated viral polymerase first transcribes complimentary RNA (cRNA) using vRNA as template. First, 2 free rNTPs base pair with the first 2 nucleotides at the 3' end of vRNA, locking the template to the polymerase

active site within the PB1 subunit(Newcomb et al. 2009; York et al. 2013). The 2 rNTPs are then ligated into a dinucleotide "primer" to elongate cRNA(Robb et al. 2016). Next, the newly synthesized cRNA associates with multiple copies of NP and one copy of heterotrimeric viral polymerase to form cRNP. To transcribe vRNA, the cRNP-associated viral polymerase using cRNA as template. Like cRNA transcription, the dinucleotide at 3' end of cRNA is formed to synthesize vRNA. However, recent structures raise an alternative mechanism, that is, the 2 rNTPs base pair with the 4^{th} and 5^{th} base at the 3' end of cRNA to form dinucleotide, and the dinucleotide dissociates and reanneals with the 1^{st} and 2^{nd} base(Deng, Vreede, and Brownlee 2006; Jorba et al. 2009; S. Zhang et al. 2010). In either way, the dinucleotide is positioned at 3' end of cRNA to initiate vRNA elongation, and the synthesized vRNA associates with multiple NPs and one viral polymerase trimer to form vRNP.

mRNA transcription

During infection, viral mRNA transcription starts prior to the unprimed vRNA replication and is much more efficient due to priming(Reich et al. 2014). The vRNP-associated viral polymerase first acquires capped oligos from host mRNAs to prime transcription, known as "cap snatching"(Plotch et al. 1981). This process is mediated by cap-binding domain of PB2 that binds to the 5' caps of nascent host mRNAs(Guilligay et al. 2008), and endonuclease domain of PA that cleaves 10 to 13 nucleotides down to the 5' end(Dias et al. 2009). The PB2 then directs the capped primer to the catalytic site of PB1 where it gets elongated using vRNA as template. As the polymerase reaches the poly-U sequence at the 5' end of vRNA template, transcription is terminated with polyadenylation through

a “stuttering” mechanism where the elongating 3’ end keeps being repositioned to the uracil-rich region(Poon et al. 1999). At last, the newly transcribed viral mRNAs get exported into cytoplasm for translation by cellular ribosomes(Jorba et al. 2009). Each viral mRNA molecule encodes for one essential viral protein except that M and NS are spliced by cellular spliceosomes and encode for M1, M2, non-structural 1 (NS1), and nuclear export protein (NEP), respectively(Lamb et al. 1980; Lamb, Lai, and Choppin 1981; Inglis and Brown 1981). Despite a variance in splicing efficiency among IAV strains, it is generally thought that the splice product NEP is equally expressed as NS1, whereas the expression of splice product M2 gradually increases as infection goes(Inglis and Brown 1984; Valcárcel, Portela, and Ortín 1991; Backström Winquist et al. 2012).

Membrane protein synthesis

Like secreted cellular proteins, IAV membrane proteins are synthesized by ER-associated ribosomes and are eventually decorated onto the plasma membrane from which viral envelope originates. The signal recognition particles (SRP) first interact with the cleavable ER-targeting signal on HA and the transmembrane domain (TMD) on NA and M2. This process targets ribosome-nascent chain complexes (RNC) to the SRP receptors in ER membrane(Dou et al. 2014; Daniels et al. 2003). The ribosomes on RNC then associate with a protein-conducting channel, or “translocon”, initiating the translocation of polypeptide chains into ER lumen(Gilmore, Walter, and Blobel 1982; Görlich et al. 1992; Bowie 2005). Mutations that alter the hydrophobicity of ER-targeting sequence have been shown to modulate the expression level of viral membrane proteins(Nordholm et al. 2013). Both HA and NA receive multiple N-linked glycans post-translationally,

while the copy number and positioning of glycosylation are strain or subtype-dependent(Mandon, Trueman, and Gilmore 2013). These glycans recruit lectin chaperones and associated oxidoreductase to aid the formation of multiple intramolecular disulfide bonds essential to the co-translational folding of HA and NA monomers(N. Wang et al. 2008; Hebert et al. 1997). Functionally active HA molecules are formed by trimerization of 3 individual monomers, while NA tetramer is formed by pairing 2 co-translationally dimerized NA monomers(Saito, Taylor, and Webster 1995). During infection, significant amount of trimeric HA and tetrameric NA are produced via protein concentration-dependent oligomerization, while the tetrameric M2 is formed in much less abundance(Holsinger and Lamb 1991). The ratio of HA to NA on viral envelope is usually around 4:1, whereas HA to M2 ratio can range from 10:1 to 100:1(Holsinger and Lamb 1991; Zebedee and Lamb 1988). It remains largely unclear how IAV regulates the timing and expression level of different viral proteins, given the lack of temporal variation in viral mRNA transcription(Kawakami et al. 2011).

HA proteolytic activation

The newly synthesized HA monomer is fusion incompetent precursor HA0 which has to be cleaved into HA1 and HA2 subunits to gain fusion capacity prior to being endocytosed into infected cells(R. T. Huang, Rott, and Klenk 1981; Maeda, Kawasaki, and Ohnishi 1981). In HA0 from highly pathogenic avian strains, the multibasic cleavage sites are cleaved by furin, a ubiquitously expressed, calcium-dependent serine endoprotease that resides within trans-Golgi network(Böttcher-Friebertshäuser et al. 2014; Stieneke-Gröber et al. 1992). Whereas in HA0 from human strains, the monobasic cleavage site is cleaved

by proteases in human respiratory epithelial cells, including human airway trypsin-like protease (HAT) and transmembrane protease serine S-1 member 2 (TMPRSS2)(Böttcher et al. 2006). HAT is mainly found at plasma membrane of epithelial cells in upper respiratory tract, where it cleaves both membrane-associated HA and HA in virus particles attaching to the cells(Zhirnov, Ikizler, and Wright 2002). TMPRSS2 is present in trans-Golgi network of epithelial cells in both upper and lower respiratory tract, where it only cleaves HA trafficking towards the membrane(Bertram et al. 2012).

RNP assembly

Besides the 3 membrane proteins, the other 7 essential viral proteins, PB1, PB2, PA, NP, M1, NS1, and NEP are translated by cytosolic ribosomes and imported back into the nucleus(York and Fodor 2013). Using the same mechanism that vRNP nuclear import utilizes, PB2 and NP are imported individually, whereas PB1 and PA are imported as heterodimer(Cros, García-Sastre, and Palese 2005). Within the nucleus, NP monomers oligomerize and bind to the 12 nucleotide stretches of newly synthesized vRNA or cRNA(Lee et al. 2017). This NP-RNA association is likely regulated by NP phosphorylation(Mondal et al. 2015). The PB2 associates with dimerized PB1 and PA to form viral polymerase heterotrimer which binds to the hairpin structure of NP-associated vRNA or cRNA to finalize the vRNP or cRNP assembly. The M1 is likely an adaptor protein that links vRNPs to NEP which targets vRNPs to cellular exportin-1-dependent nuclear export pathway, as well as a blocker that covers NLS in NP to prevent re-import of vRNPs exported to cytoplasm(Shimizu et al. 2011; Akarsu et al. 2003; S. Huang et al. 2013). The last essential viral protein out of the 7 is the viral RNA-binding protein NS1,

which is produced and imported into nucleus during early stage of infection to inhibit host interferon signaling and link viral mRNAs with cellular nuclear export factors to facilitate mRNA export into cytoplasm(Ayllon and García-Sastre 2015; Satterly et al. 2007).

Genome packaging

Previous studies proposed that PB2 of cytoplasmic vRNPs associate with Rab11 on recycling endosomes and traffic towards plasma membrane along with microtubules(Amorim et al. 2011, 11; Momose et al. 2011), whereas recently an alternative model proposed that vRNPs bind to Rab11 close to ER network that undergoes tubulation caused by infection to travel towards cell surface(de Castro Martin et al. 2017). Cross section images of budding virus particles revealed that most viral genomes share a common pattern of 7 vRNPs surrounding 1 central vRNP, known as the "7+1" array, which likely depends upon physical interactions of individual vRNP segments(Noda et al. 2006; Sugita et al. 2013; Fournier et al. 2012; Gavazzi et al. 2013; Noda et al. 2012). These interactions likely occur after nuclear export of vRNPs and prior to budding, but the exact location where they happen remains unknown. Numerous studies have shown that the 5' and 3' UTRs together with terminal coding regions of the vRNA, known as "packaging signal", are required for the highly selective and efficient packaging of 8 vRNPs(Hutchinson et al. 2010; Fujii et al. 2003). Recently, a study indicated that viral promoter and non-coding regions are crucial for the packaging of each individual vRNP segment, while the terminus of segment-specific coding regions are responsible for selective packaging of the full set of 8 distinct vRNP segments(Goto et al.

2013). Outside of the canonical packaging signal, sequence elements within internal coding region are also suggested to contribute to maximizing the packaging efficiency(Williams et al. 2018).

Budding

The envelopes of virus particles are enriched with cholesterol and sphingolipids, suggesting the viral budding occurs in lipid rafts of apical plasma membrane(Lingwood and Simons 2010). The HA concentrates in lipid rafts due to the fatty acid modifications on C-terminal cysteine(Takeda et al. 2003; Zurcher, Luo, and Palese 1994; Kordyukova et al. 2008), and the NA enrichment at budding site is attributed to the C-terminus of the TMD(Barman et al. 2004). The M1 in cytoplasm has been proposed to be recruited to the budding region by associating with cytoplasmic tails of HA and NA(Ali et al. 2000). Upon reaching the plasma membrane, M1 oligomerizes underneath to form viral capsid layer and the vRNPs are thought to directly bind to M1 to ensure encapsidation(J. Zhang, Pekosz, and Lamb 2000; Noton et al. 2007). Expression of HA and NA in lipid rafts alone can induce positive membrane curvature and budding(B. J. Chen et al. 2007; Lai et al. 2010; Yondola et al. 2011; Chlanda et al. 2015), whereas the oligomerized M1 is likely to also significantly curve the membrane which provides an explanation for its role in determining the shapes of budding virus particles(Elleman and Barclay 2004). The other membrane protein M2 is found to locate at the boundary of the budding region and incorporate the hydrophobic face of its cytoplasmic amphipathic α-helix into membrane leaflet to generate negative membrane curvature, which potentially brings the opposing membranes of the budding neck closer to each other and eventually results in

scission(Rossman et al. 2010; Rossman and Lamb 2013). Although many details of the budding process remain unknown, it seems that IAV uses multiple viral proteins to induce membrane curvature and facilitate viral budding through a combination of cone-shaped lipids recruitment, membrane-bending protein association, and molecular crowding on membrane leaflet.

Cell release

The release of virus particles that bud out of host cell surface is mediated by sialidase activity of NA which hydrolyzes glycosidic bond attaching the terminal sialic acids to sugar molecules underneath(Burnet 1948; Burnet, Mccrea, and Anderson 1947). By cleaving the sialic acids, NA prevents HA from binding to cell surface and facilitates viral release(Webster and Laver 1967). Since both HA and NA are glycosylated, NA has also been shown to cleave sialic acids on N-linked glycans from HA and NA in the viral envelopes which promotes separation of virus particles and inhibits viral aggregation(Palese et al. 1974).

Post-release movement

After being released from cell surface, virus particles not only move through the mucus layer rich in heavily glycosylated mucins and infect nearby naïve cells to promote within-host transmission, but also make their way towards the luminal side of mucus and get exhaled into the air via aerosols or droplets to facilitate inter-host transmission(Kutter et al. 2018). Upon entering a new host, virus particles penetrate mucus layer at the inoculation site to reach the epithelial cells underneath and initiate infection. Studies have

shown that NA-mediated sialic acid cleavage releases viruses from mucins covered with sialylated O-linked glycans, thereby enhancing the viral movement through mucus(Cohen et al. 2013). As a result, decrease in NA activity in the presence of mucus inhibits both viral infection and transmission(Zanin et al. 2015; M. N. Matrosovich et al. 2004). Unlike HA, NA from human IAV strains prefer to cleave α-2,3 linked sialic acids compared with α-2,6-linked sialic acids(Air 2012; Mochalova et al. 2007). The sialic acid preference of a particular viral HA-NA combination, as well as the host sialic acid profile at the infection site, largely dictate the receptor-binding affinity of HA and the receptor-cleaving activity of NA, therefore governing tissue tropism, host range, viral fitness and transmissibility of IAV(de Vries et al. 2020).

1.3 IAV gene expression heterogeneity

Definition

Although the expression of 10 functional essential viral proteins encoded by 8 viral gene segments is required for productive infection, most IAV particles fail to express at least one functional essential viral protein under single-particle infection condition(Brooke et al. 2013). It has been shown that 70% to 99% of virus particles across different IAV strains are unable to initiate productive infection and cannot be detected using plaque assay, a commonly used technique to measure viral titer(Donald and Isaacs 1954). Instead, they can be detected through hemagglutination assay or real-time PCR that quantifies total physical virus particles and genome equivalents, respectively. These "non-infectious" particles, the silent majority of viral populations, consist of defective-interfering particles (DIPs) and semi-infectious particles (SIPs)(Nayak, Chambers, and

Akkina 1985; Heldt et al. 2015; Brooke 2014). DIPs are characterized as viruses with one or more gene segments harboring large internal deletion which encode for short, non-functional viral gene products. DIPs can only propagate under high MOI condition where they can be complemented by other co-infecting viruses(Von Magnus 1951). In contrast with DIPs, SIPs lack a unique molecular signature. They refer to viruses that encode for incomplete, variable subset of the 10 functional essential viral proteins. SIPs are constantly produced during viral infection which makes them the dominant virion type in most viral populations(Brooke 2017). Like DIPs, SIPs cannot initiate productive infection by themselves. They must complement each other during high MOI co-infection to avoid becoming dead-end products. In this thesis, IAV gene expression heterogeneity is defined as variation in gene coding capacity of individual virions.

Origins

IAV gene expression heterogeneity arises from a variety of mechanisms that are not mutually exclusive. Results from EM imaging analysis revealed that up to 20% of virus particles contain less than 8 gene segments(Nakatsu et al. 2016). In addition, it has been shown that IAV can package host ribosomal RNA into virus particles to complete the "7+1" array(Noda et al. 2018). Therefore, despite being highly selective and efficient, IAV genome packaging is imperfect which can lead to failure in delivery of 8 distinct viral gene segments into infected cells. Numerous studies have indicated that the viral genome trafficking and nuclear import are also imperfect(Babcock, Chen, and Zhuang 2004; Schelker et al. 2016). The viral genome in cytoplasm is constantly at risk of being degraded before reaching nuclear envelope, while the interferon inducible antiviral factor

myxovirus resistance 1 (Mx1) may actively interfere with the nuclear import(Chou et al. 2013; Götz et al. 2016). As a result, it is highly likely that not all gene segments packaged into virus particles are successfully imported into nucleus. Further, random mutations in critical regulatory elements and coding regions of viral genes may hinder transcription and result in truncation or mis-folding of viral proteins(Pauly, Procario, and Lauring 2017b). Importantly, it is possible that a perfectly packaged virus without any lethal mutations may still end up being a SIP due to random failure of replication steps(Diefenbacher, Sun, and Brooke 2018). Together, through imperfect packaging, lethal mutations, and failure of trafficking, nuclear import, transcription and translation, IAV populations maintain a significant amount of heterogeneity in viral gene coding capacity at single particle level.

Phenotypic effects

Viral gene expression heterogeneity is observed not only in cell culture, but also in animals infected with lab-adapted or clinical IAV strains(Nakatsu et al. 2016; Brooke et al. 2014). Interestingly, the quantity and composition of SIPs produced by different IAV strains can vary hugely(Brooke et al. 2013). The gene expression profile of a given viral population is likely governed by a combination of viral genotype, host cell environment, and stochastic events during infection. Low dose UV irradiation of virus decreases the average gene expression frequency and artificially increases SIPs content. It has been shown that increasing the fraction of SIPs increases reassortment frequency by promoting co-infection, suggesting SIPs may facilitate viral evolution(Fonville et al. 2015). Recently, a study showed that a single amino acid substitution in NP selectively decrease

NA segment abundance and packaging rate, increasing the fraction of SIPs that do not express NA. The stoichiometric decrease of NA segment in a viral population decreases the relative expression level of NA in multiply infected cells, suggesting SIPs may regulate viral gene expression through gene dosing effects(Brooke et al. 2014). Despite a lot still being unknown, it is clear that IAV gene expression heterogeneity can have significant functional consequences and SIPs are not merely byproducts resulting from unavoidable errors of infection.

1.4 IAV collective interactions

Co-infection and superinfection

Co-infection occurs when one cell is infected by multiple virus particles. Studies have shown that under multi-round replication, co-infected cells are detected with high frequency in IAV-infected mice and guinea pigs(Brooke et al. 2014; Fukuyama et al. 2015). Since co-infection mediates reassortment and facilitates productive infection of SIPs through complementation, the co-infection frequency could be a major determinant of viral replicative and evolutionary potential(George K. Hirst 1973). Further, co-infection frequency governs the average copy number of viral genomes delivered into each infected cell which has been suggested to play important roles in viral replication dynamics and interferon induction(Phipps et al. 2020). In nature, not all infections happen simultaneously, and it is likely that a sizable proportion of co-infected cells result from multiple sequential infections. The subsequent infection of cells that are already infected is known as superinfection. The key signature of superinfection is that when it happens to the infected cells, the primary virus has already initiated replication. Like

many other enveloped viruses, IAV has been shown to potently and rapidly inhibit superinfection, a phenomenon known as superinfection exclusion (SIE)(I.-C. Huang et al. 2008). However, the existence of potent universal SIE is at odds with the observations of frequent co-infection and wide-spread reassortment from numerous studies(Brooke et al. 2014; Rambaut et al. 2008; Nelson et al. 2008). Thus, defining the mechanism of SIE is important for better understanding the collective interactions of IAV.

Reassortment

Reassortment is the biological process that multiple distinct viruses co-infect the same cell and exchange one or more viral gene segments to generate progeny with novel genotypes. As homologous recombination seems to be extremely rare, reassortment serves as the primary mechanism of genetic recombination for IAV(Boni et al. 2008). Reassortment occurs frequently between compatible strains in cell culture, laboratory animals, and wild birds, with little bias towards certain combinations of gene segment variants(Tao, Steel, and Lowen 2014; Tao H et al. 2015; Dugan et al. 2008). Sporadically, reassortment can occur between human and zoonotic strains which has been responsible for causing all major flu pandemics over the past century. Reassortment between some IAV strains can be inhibited or limited to only produce specific genotypes, possibly due to incompatibility of packaging signals or viral proteins(Phipps et al. 2017; White MC et al. 2017; Essere et al. 2013). To date, how frequent reassortment occurs during human infections remains largely unclear(Leonard et al. 2017). Recently, multiple studies showed that reassortment within single viral populations occurs with high frequency and without restrictions, allowing the reshuffling of gene segments with

beneficial or deleterious mutations(Marshall et al. 2013; Murcia et al. 2010). Therefore, reassortment without segment mismatch may serve as an adaptation driving force that optimizes fitness of the viral populations by combining beneficial alleles and purging deleterious alleles. Together, reassortment within a viral population and between viral populations both generate enormous genotypic diversity that fuels rapid viral evolution, promoting optimization of viral fitness, adaptation to new hosts, and evasion of host immune responses(Steel and Lowen 2014).

1.5 Interactions of IAV and host innate immune response

Overview of host innate immune response

The innate immune responses serve as the first line of defense against IAV infection. Mucus forms a physical barrier rich in mucins and collectins that can trap the virus particles and stopping them from reaching the epithelial cells underneath. Once the infection initiates, the pathogen recognition receptors (PRRs) in infected cells recognize pathogen-associate molecular patterns (PAMPs) produced by the virus, triggering signaling cascades that result in production of cytokines and type I/III interferons (IFNs)(Iwasaki and Pillai 2014). Among all the PRRs, toll-like receptors (TLRs), retinoic acid inducible gene-I (RIG-I)-like receptors (RLRs), and nucleotide oligomerization domain (NOD)-like receptors (NLRs) are involved in recognizing IAV infection and inducing IFNs(Blasius and Beutler 2010; Takeuchi and Akira 2009; Pang and Iwasaki 2011). IFN secretion eventually leads to expression of interferon-stimulated genes (ISGs) in infected and neighboring cells, which in turn inhibits viral replication and spread. Importantly, the activation of innate immune responses also contributes to initiation of

adaptive immune responses responsible for the viral clearance, whereas excessive inflammatory responses induced by highly pathogenic IAV strains can be detrimental and sometimes fatal to the host.

Recognition by TLRs

TLR3 and TLR7 are both expressed on the inside of cellular endosomes and recognize endosomal viral RNA. Upon IAV infection, TLR3 recognizes unidentified double stranded (ds) RNA species in human respiratory epithelial cells while TLR7 recognizes single stranded (ss) RNA genomes within virions in the endosomes(Alexopoulou et al. 2001; Diebold et al. 2004). Upon activation of TLR3 signals, TLR3 interacts with the adaptor TIR domain-containing adaptor inducing IFN-β (TRIF) in human respiratory epithelial cells, macrophages and dendritic cells, and TRIF activates the TRAF family member-associated NF-κB activator (TANK)-binding kinase-1 (TBK1) and inhibitor of κB kinase ε (IKKε), leading to phosphorylation of interferon regulatory factor 3 (IRF3) and induction of type I IFNs(Chengye Li et al. 2020). The TLR3 activation induces antiviral state to restrict viral replication but also recruits inflammatory cells that can cause damage to the hosts. It has been shown that $TLR3^{-/-}$ mice have increased viral loads in the lungs but survive longer than wild-type mice upon challenge of lethal dose IAV(Le Goffic et al. 2006). Upon activation of TLR7 signals, TLR7 interacts with adaptor myeloid differentiation factor-88 (MyD88) to activate IRF7 via IKKα, leading to expression of IL-6 and type III IFNs in bronchial epithelial cells and type I IFNs in plasmacytoid dendritic cells (pDCs)(Honda et al. 2005). TLR7 activation induces

production of IFNs and pro-inflammatory cytokines and plays important roles in promoting antibody responses upon sublethal IAV infection(Jeisy-Scott et al. 2012, 7).

Recognition by RLRs

The RLR family consists of RIG-I, melanoma differentiation-associated gene 5 (MDA5) and laboratory of genetics and physiology 2 (LGP2), which recognize replicating viral RNA in the cytosol. Among them, RIG-I is the most well-studied IAV sensor that recognizes cytosolic dsRNA and 5'-triphosphate containing ssRNA generated from viral replication in infected epithelial cells, conventional DCs and alveolar macrophages(Pichlmair et al. 2006; Kato et al. 2005). After viral RNA recognition by the carboxy-terminal domain, the helicase domain of RIG-I binds to ATP and exposes the caspase-recruitment domains (CARD). The exposed CARD domains are then ubiquitinated by E3 ligases TRIM25 which results in interactions of RIG-I and mitochondrial antiviral signaling adaptor (MAVS)(Kowalinski et al. 2011; Luo et al. 2011). MAVS can recruit TNF-receptor-associated factor 6 (TRAF6), receptor-interacting protein (RIP)1, NF-κB essential modulator (NEMO), TAK1, IKKα and IKKβ to activate NF-κB which leads to the production of pro-inflammatory cytokines. In addition, MAVS can also recruit TRAF3, TANK, TBK1, and IKKε to activate IRF3 which leads to the production of type I IFNs(Chengye Li et al. 2020).

Antiviral activity of ISGs

After being secreted, the type I (IFNα and IFNβ) and III (IFNλ) IFNs bind to their receptors on the same cell or surrounding cells. The receptor binding activates Janus

protein tyrosine kinase 1 (JAK1) and tyrosine kinase 2 (TYK2) which leads to phosphorylation of the signal transducer and activator of transcription 1 (STAT1) and STAT2 transcription factors(Levy, Marié, and Durbin 2011). The phosphorylated STAT1 and STAT2 then associate with IRF9 to form the heterotrimeric ISG factor 3 (ISGF3) complex which enters the nucleus and binds to IFN-stimulated response elements (ISREs) within the promoter regions of ISGs to promote their transcription(Hoffmann, Schneider, and Rice 2015). Many ISGs induced by IAV infection have been shown to limit viral replication through a variety of mechanisms. The human Mx1 binds to viral NP in the cytosol to inhibit viral transcription, while interferon-induced transmembrane protein 1 (IFITM1), IFITM2, and IFITM3 have been shown to inhibit fusion of viral and endosomal membrane(Turan et al. 2004; Bailey et al. 2014). Protein kinase R (PKR) promotes type I IFN production by stabilizing their mRNA(Schulz et al. 2010). It also inhibits viral protein synthesis by phosphorylating α subunit of eukaryotic initiation factor 2 (eIF2α) and activates NF-κB by phosphorylating its inhibitor IκB(Kumar et al. 1994; Patel and Sen 1998).

Inhibition of innate immune response by NS1

The viral protein NS1 encoded by NS segment suppresses host innate immune response to ensure efficient viral replication(Klemm et al. 2018). It has been shown that IAV with decreased NS1 expression or expressing malfunctional NS1 are highly attenuated when replicating in cells capable of producing type I IFN(Talon, Salvatore, et al. 2000; Nogales et al. 2014). Numerous studies have demonstrated that NS1 interferes with the function of many cellular proteins involved in different pathways of innate immune response to

infection. NS1 suppresses IFN production by directly interacting with TRIM25 to inhibit the activation of RIG-I and inhibiting the activity of transcription factors IRF3 and NF-κB(Gack et al. 2009; Talon, Horvath, et al. 2000; X. Wang et al. 2000). Additionally, NS1 binds to dsRNA to inhibit the activation 2'-5' oligoadenylate synthetase (OAS)-ribonuclease L (RNaseL) which degrades viral ssRNA(Min and Krug 2006). Moreover, NS1 inhibits activity of PKR by direct interactions and sequestration of dsRNA(S. Li et al. 2006). Finally, NS1 in some IAV strains have been reported to interfere with maturation, polyadenylation, and nuclear export of host mRNA, resulting in shutoff of host protein synthesis(Satterly et al. 2007; Noah, Twu, and Krug 2003; Z. Chen, Li, and Krug 1999).

1.6 Aims of this thesis

IAV gene expression is extremely heterogeneous, and the biological significance of this heterogeneity is desperately in need of further investigation. Due to this heterogeneity, the dominant constituent of IAV populations are SIPs which require co-infection and complementation to initiate productive infection. Reassortment is one of the major mechanisms that facilitate IAV evolution and can only occur in cells co-infected by multiple distinct viruses. Therefore, co-infection rate is a major determinant of IAV replicative and evolutionary potential. One of the primary mechanisms by which co-infection can happen is superinfection, the sequential infections of one cell by multiple viruses. Huang et al. demonstrated that NA activity is necessary and sufficient to potently inhibit IAV superinfection by removing SA-containing receptors on surface of infected cells(I.-C. Huang et al. 2008). In support of this finding, Dou et al. recently reported a

narrow time window of 3 hours during which superinfection can occur(Dou et al. 2017). However, Marshall et al. showed that superinfection occurs up to 8 hours after the primary infection and results in robust co-infection and reassortment(Marshall et al. 2013). Further, multiple studies showed that co-infection and complementation are quite common in respiratory tracts of IAV-infected mice and guinea pigs(Brooke et al. 2014; Fukuyama et al. 2015). Together, factors that dictate IAV superinfection potential remain to be characterized.

In this thesis, I investigated how gene expression heterogeneity influences IAV superinfection potential (chapter 2). By combining single particle infection and multi-color flow cytometry, I directly quantified superinfection efficiency in infected cells that express different combinations of viral genes. The results showed that superinfection susceptibility is negatively correlated with the quantity of viral gene segments expressed within an infected cell, regardless of their identity. In addition, cells infected with SIPs are more susceptible to superinfection compared to cells infected with particles that express a complete set of viral genes, and viral populations that contain more SIPs undergo more-frequent superinfection. Further, I found that viral replicase activity in infected cells is responsible for inhibiting the subsequent infection. These findings raise a novel mechanism of superinfection exclusion and identify viral gene expression heterogeneity as a major determinant of IAV superinfection potential.

Besides viral gene expression heterogeneity, I also tried to define other factors that govern IAV superinfection potential (chapter 3). Specifically, I found that superinfection

potential decrease with increase of MOI of the primary infection. In addition, IAV superinfection exclusion is largely independent of host innate immune response and is likely to occur post viral binding. These findings validate previous results and shed new light on mechanisms of IAV superinfection exclusion.

Under low MOI condition where most infected cells are infected with single virus particles, viral gene expression patterns vary significantly between individual infected cells due to the existence of extreme gene expression heterogeneity within IAV populations. Thus, the overall infection outcome is likely governed by the complex interplay of viral heterogeneity and host response at single cell level. Due to the technical challenge, most studies on host response to IAV infection remain at bulk level which masks the cell-to-cell heterogeneity in both viral and host gene expression. Several studies have taken advantage of the recent progress in single cell RNA sequencing (scRNAseq) technique to characterize single cell heterogeneity during IAV infection(Heldt et al. 2015; Russell, Trapnell, and Bloom 2018; Russell et al. 2019). However, these efforts are more or less hampered by the limited number of cells analyzed or experimental set up that confounded the results. How patterns of single cell heterogeneity in IAV-infected cells shape infection dynamics and viral pathogenesis remain poorly understood.

In this thesis, I investigated how viral gene expression heterogeneity influences host innate antiviral response to IAV infection (chapter 4). By pairing Fluorescence-Activated Cell Sorting (FACS) with single scRNAseq, I examined the combined host and viral

transcriptomes of thousands of individual cells, each infected with a single IAV particle. Even under the condition where viral input and infection time are largely equivalent for all infected cells, I observed complex patterns of viral gene expression and the existence of multiple distinct host transcriptional responses to infection at single cell level. In addition, I found that SIPs that fail to express the NS gene can play a dominant role in triggering innate anti-viral response to infection. Finally, human H1N1 and H3N2 virus infections differ significantly in patterns of host anti-viral gene transcriptional at single cell level. These results reveal how patterns of viral gene expression heterogeneity can serve as a major determinant of host anti-viral gene activation.

CHAPTER 2: IAV GENE EXPRESSION HETEROGENEITY REGULATES VIRAL SUPERINFECTION POTENTIAL

2.1 Introduction

Influenza A virus (IAV) is estimated to cause hundreds of thousands of deaths across the world every year during seasonal epidemics, despite widespread preexposure and vaccination(Iuliano et al. 2018). In addition to the yearly burden of seasonal influenza viruses, novel zoonotic IAV strains periodically emerge into humans from swine or birds, triggering unpredictable pandemics that can dramatically increase infection and mortality rates(Taubenberger and Morens 2010). Defining the specific factors that influence the evolution of influenza viruses is critical for designing more-effective vaccines, therapeutics, and surveillance strategies.

The prevalence of coinfection can play an enormous role in determining the replicative and evolutionary potential of IAV populations. This is a function of both the segmented nature of the viral genome and the enormous amount of genomic heterogeneity present within IAV populations(Brooke 2014; 2017). Coinfection allows reassortment, i.e., the production of novel viral genotypes through the intermixing of the individual IAV genome segments(Lowen 2017; McDonald et al. 2016). Reassortment events have contributed to the emergence of every major influenza pandemic of the past century(Taubenberger and Kash 2010). Coinfection also facilitates the complementation and productive replication of the semi-infectious particles (SIPs) that make up the majority of IAV populations(Brooke et al. 2013; 2014; George K. Hirst 1973; Russell, Trapnell, and Bloom 2018; George K. Hirst and Pons 1973). Finally, increasing the frequency of coinfection can accelerate viral replication kinetics and virus output by

increasing the average multiplicity of infection (MOI)(Dou et al. 2017; D. O. White and Cheyne 1966; D. White et al. 1965). Thus, to better understand how IAV populations transmit and evolve, we must identify the specific host and viral factors that govern coinfection.

One of the primary means by which coinfection can occur is superinfection, the sequential infection of one cell by multiple viral particles. For some viruses, superinfection appears to occur freely(Ramig 1990; Keirstead and Coombs 1998). In contrast, a diverse range of viruses actively inhibit superinfection through a variety of mechanisms, a phenomenon known as superinfection exclusion (SIE)(Nethe, Berkhout, and van der Kuyl 2005; Schaller et al. 2007; Tscherne et al. 2007; Zou et al. 2009; X.-F. Zhang et al. 2017; Laliberte and Moss 2014; Folimonova 2012; Simon et al. 1990; Ludlow et al. 2005). The only in-depth study of IAV superinfection performed to date concluded that the viral neuraminidase (NA) protein acts to potently and rapidly inhibit IAV superinfection by depleting infected cells of the sialic acid receptors required for viral entry(I.-C. Huang et al. 2008). More recently, Dou et al. reported a narrow time window during which IAV superinfection was possible(Dou et al. 2017). These findings are consistent with recent studies that have argued that reassortment is rare during human infection(Leonard et al. 2017; Xue et al. 2017). However, the existence of a potent mechanism of IAV SIE is at odds with both the frequent coinfection observed in a variety of experimental settings and the widespread occurrence of reassortment at the global scale(Rambaut et al. 2008; “Multiple Reassortment Events in the Evolutionary History of H1N1 Influenza A Virus Since 1918” n.d.; Holmes et al. 2005; Nelson et al. 2008;

Westgeest et al. 2014; Maljkovic Berry et al. 2016). Marshall et al. showed that superinfection occurring at up to 8 h after a primary infection leads to robust coinfection and reassortment in cell culture(Marshall et al. 2013). Extensive coinfection and complementation have also been observed in the respiratory tracts of IAV-infected mice and guinea pigs(Brooke et al. 2014; Fukuyama et al. 2015). Collectively, these results suggest that IAV superinfection can be restricted, but to what extent and through which specific mechanisms remain crucial open issues.

Here, we reveal that IAV superinfection potential is regulated by the extent of genomic heterogeneity within the viral population. We observed that superinfection susceptibility is influenced in a dose-dependent fashion by the number of viral genes expressed by the initially infecting virion. Further, we show that superinfection occurs more frequently in IAV populations with more SIPs than in those with fewer. Finally, we demonstrate that SIE is mediated by the presence of active viral replication complexes and is completely independent of the gene coding sequence. Taken together, our results reveal how genomic heterogeneity influences IAV superinfection potential and demonstrate how SIPs can modulate collective interactions within viral populations.

2.2 Results

Influenza virus SIE occurs in multiple cell types and is independent of type I interferon (IFN) secretion

A previous study of IAV SIE concluded that NA expression completely blocks susceptibility to superinfection by 6 h post-infection (hpi)(I.-C. Huang et al. 2008). To

explore the potential mechanisms of IAV SIE in greater detail, we developed a flow cytometry-based assay that allows us to precisely measure the effects of previous infection on superinfection efficiency. To clearly identify cells infected by the first virus or by the superinfecting virus or by both, we used two recombinant viruses that express antigenically distinct hemagglutinin (HA), NA, and NS1 proteins that we could distinguish using specific monoclonal antibodies (MAbs) that we had on hand (Fig. 2.6). For the primary infection, we used a recombinant version of H1N1 strain A/Puerto Rico/8/34 (rPR8). For the secondary infection, we used a recombinant virus (rH3N2) that contained the HA and NA gene segments from H3N2 strain A/Udorn/72, the NS gene segment from A/California/04/09, and the remaining 5 segments from PR8.

We first asked whether prior infection with rPR8 affected cellular susceptibility to superinfection with rH3N2. We infected Madin-Darby canine kidney (MDCK) cells with rPR8 at an MOI of <0.3 50% tissue culture infective doses ($TCID_{50}$)/cell, and at 3 hpi (all times post-infection are expressed relative to the time at which the first virus was added) we added the PR8-HA-specific neutralizing MAb H17-L2 to block secondary spread of rPR8 within the culture. At 6 hpi, we infected with rH3N2 at a MOI of <0.3 $TCID_{50}$/cell (6 hr). To prevent spread of both rPR8 and rH3N2, we added 20 mM NH_4Cl at 9 hpi(Martin and Helenius 1991; Ohkuma and Poole 1978). In parallel, we performed simultaneous coinfections (0 hr) with rPR8 and rH3N2 to measure coinfection frequencies under conditions SIE should not be possible. At 19 hpi, we harvested cells and examined primary and secondary virus infections by flow cytometry, using H1 expression and H3 expression as markers of rPR8 infection and rH3N2 infection,

respectively. We observed that the H3-positive ($H3^+$) frequency within $H1^+$ cells was significantly reduced when rPR8 infection preceded rH3N2 by 6 h compared with when rPR8 and rH3N2 were added simultaneously (Fig. 2.1A). This indicated that rPR8 infection significantly reduces the susceptibility of cells to superinfection by 6 hpi.

We next asked whether the SIE effect was cell type specific and whether it depended on activation of the type I interferon (IFN) system. We performed the experiment described above in MDCK cells, A549 cells, human embryonic kidney HEK293T (293T), and Vero cells (which are incapable of type I IFN secretion)(Desmyter, Melnick, and Rawls 1968; Emeny and Morgan 1979). We observed that the levels of SIE were comparable among all cell lines tested, suggesting that SIE occurs in multiple distinct cell types and does not depend upon IFN secretion (Fig. 2.1B,2.7).

SIE does not depend upon viral neuraminidase activity

In an attempt to confirm the previously reported role for NA activity in SIE, we directly measured the effect of NA expression on SIE in our system(I.-C. Huang et al. 2008). We took advantage of our previous observation that IAV populations consist primarily of SIPs that fail to express one or more viral genes(Brooke et al. 2013). When carrying out the primary infection at a low MOI, we generate populations of infected cells that are either positive or negative for expression of a given viral gene. We can then assess the effects of specific viral proteins on superinfection susceptibility by comparing superinfection frequencies between infected cells that do or do not express the protein in question (Fig. 2.2A).

We performed the same superinfection experiment as described above in MDCK cells; however, we used slightly different viruses to ensure that the NA specificity of the primary virus was well matched to the HA specificity of the secondary virus. The primary virus used here encoded the HA gene from A/Udorn/72 and the NA gene from PR8 (rH3N1), while the secondary virus encoded the HA gene from PR8 and the NA gene from A/Udorn/72 (rH1N2). The remaining 6 segments for both viruses came from PR8.

At 19 hpi, we harvested and stained with MAbs against H1, N1, and H3. To compare rH3N1 infected cells that did or did not express NA, we individually gated cells into $H3^+$ $N1^+$ and $H3^+$ $N1^-$ subpopulations (Fig. 2.2A). Comparison of $H1^+$ frequencies between $H3^+$ $N1^+$ and $H3^+$ $N1^-$ cells revealed that NA expression in infected cells was clearly associated with decreased susceptibility to superinfection (Fig. 2.2B). This finding was consistent with the previously reported role for NA in IAV superinfection exclusion(I.-C. Huang et al. 2008). Importantly, while SIE was more pronounced in the $H3^+$ $N1^+$ cells, we also observed a significant decrease in superinfection susceptibility within the $H3^+$ $N1^-$ cell population by 6 hpi, suggesting that viral factors other than NA also act to restrict superinfection.

To directly test whether NA enzymatic activity was required for the increased potency of SIE that we observed in NA^+ cells, we asked whether treatment with the NA inhibitor (NAI) zanamivir could diminish this effect. We observed that the addition of zanamivir at

1 uM (a concentration that completely blocked rH3N1 NA enzymatic activity) did not decrease the strength of SIE in NA^+ cells (Fig. 2.2B,2.8). We also examined the effects of two substitutions (NP:F346S and NA:K239R) that decrease cellular NA expression relative to wild-type PR8 on superinfection efficiency(Brooke et al. 2014; Hensley et al. 2011) (Fig. 2.9A). In accordance with our zanamivir results, these mutants did not exhibit higher superinfection frequencies than wild-type PR8 (Fig. 2.9B). Taken together, these results reveal that superinfection is more effectively inhibited by virions that express NA than by those that do not, but that NA enzymatic activity is dispensable for this effect.

Superinfection susceptibility is determined by the number of viral genes expressed in cell

On the basis of our observation that superinfection was also inhibited within $N1^-$ cells (Fig. 2.2B), we hypothesized that expression of other viral gene products might also inhibit superinfection. We examined the effects of HA and NS1 expression on superinfection susceptibility, using rPR8-specific MAbs. Surprisingly, we found that both HA expression and NS1 expression within rPR8-infected cells were associated with significant decreases in superinfection by rH3N2 and that the results were comparable to the effect associated with NA expression (Fig. 2.3A,B). To further dissect how viral gene expression patterns influence SIE, we individually gated all seven possible combinations of HA, NA, and NS1 expression by rPR8 (HA^+ NA^+ $NS1^+$, HA^+ NA^+, HA^+ $NS1^+$, NA^+ $NS1^+$, HA^+, NA^+, $NS1^+$) and directly compared their rH3N2 infection frequencies (the gating scheme is shown in Fig. 2.10A). We observed that the fraction of cells superinfected with rH3N2 was inversely correlated with the number of rPR8 genes

expressed (among the three we examined), regardless of their specific identities (Fig. 2.3C,D). Thus, susceptibility to IAV superinfection is determined by the number of viral genes expressed in the host cell by the initially infecting virion.

Superinfection is more prevalent in IAV populations with more SIPs

If the number of viral genes expressed in a cell determines superinfection susceptibility, then decreasing the average number of functional viral genes successfully delivered by individual virions should increase the overall incidence of superinfection. We tested this by artificially decreasing the functional gene segment content of rPR8 through exposure to UV irradiation(Fonville et al. 2015). Exposure to low-dose UV irradiation generates SIPs that carry gene-lethal UV-induced lesions at frequencies proportional to genome segment length. On the basis of our previous findings, we hypothesized that superinfection frequencies would increase with longer exposure of rPR8 to UV.

We used UV (302-nm wavelength) to irradiate rPR8 for either 30 s or 60 s and confirmed that the $TCID_{50}$ concentration was reduced and the SIP concentration was increased as a function of treatment duration (Fig. 2.4A-C). We then performed superinfection assays as described above, comparing rH3N2 superinfection frequencies following infection by untreated or UV-irradiated rPR8 in MDCK cells. To fairly compare superinfection frequencies between viral populations with differing particle-to-infectivity ratios, we normalized our rPR8 infections based on equivalent numbers of particles capable of expressing NA (NA-expressing units [NAEU])(Brooke et al. 2014).

We first examined the effect of UV treatment on superinfection when rPR8 and rH3N2 were added to cells simultaneously (at 0hr). This was a critical control because UV treatment can increase the measured incidence of coinfection, independently of SIE effects, purely by creating a larger pool of SIPs that show up in our assays only when complemented by secondary infection(Fonville et al. 2015). Consistent with this, we observed a small increase in coinfection frequency with UV treatment when the two viruses were added simultaneously (Fig. 2.4D,E). When rH3N2 was added 6 h after rPR8, however, we observed a much more pronounced increase in superinfection frequency with UV treatment, consistent with our hypothesis that superinfection can be regulated by the proportion of SIPs present within the viral population (Fig. 2.4D-F).

SIE is mediated by active IAV replication complexes and is independent of the gene coding sequence

Our data reveal that IAV superinfection potential is determined by the number of viral genes expressed within a cell, independent of their specific identity. This suggests that the viral gene products themselves are dispensable for SIE. We thus hypothesized that active replication and/or transcription of viral RNAs by the viral replicase complex might be responsible for decreasing cellular susceptibility to subsequent infection. To test this, we cotransfected 293T cells with pDZ vectors encoding the individual viral replicase proteins (PB2, PB1, PA, and NP) together with a pHH21 vector encoding either the HA vRNA gene segment (HA_{vRNA}) or a vRNA-derived reporter gene segment in which the enhanced green fluorescent protein (eGFP) open reading frame (ORF) is flanked by the 5′ and 3′ untranslated-region (UTR) sequences from the NA segment ($eGFP_{vRNA}$). These

UTR sequences are required for replication and transcription of the reporter RNA by the viral replicase. At 24 h post-transfection, we infected cells with rH3N2 at a MOI of 0.2 $TCID_{50}$/cell and measured infectivity at 8 hpi using an M2-specific MAb.

Infection frequencies were decreased ~50% in cells expressing the replicase components plus the $eGFP_{vRNA}$ construct compared with control cells transfected with the replicase-expressing constructs plus an empty pHH21 vector (Fig. 2.5A). In analyses of differences in the levels of rH3N2 infectivity between cotransfected cells ($eGFP^+$, HA^+) and uncotransfected cells ($eGFP^-$, HA^-) within the same culture wells, the inhibitory effects mediated by $eGFP_{vRNA}$ or HA_{vRNA} expression were found to be comparable (Fig. 2.5B,2.11). Importantly, this effect was not seen when we left out the plasmid encoding PA (RNP_{PA-}) or used an eGFP reporter RNA that lacked the viral UTR sequences ($eGFP_{ORF}$) (Fig. 2.5A). Taken together, these data indicate that inhibition of infection requires both an intact replicase complex and an RNA template containing the viral UTR sequences but not the viral coding sequence.

Our data demonstrate that IAV SIE is mediated by the specific activity of viral replication complexes. One potential explanation is that large amounts of recently synthesized negative sense vRNA within the cell might outcompete incoming genome segments for replication and expression. To test this, we transfected 293T cells with a pHH21 vector that overexpresses the $eGFP_{vRNA}$ segment and measured susceptibility to rH3N2 infection 24 h later using an NP-specific MAb. Compared to the empty vector control, we observed no effect of $eGFP_{vRNA}$ vRNA overexpression on cellular susceptibility to infection

(Fig. 2.5C). Similarly, we observed no effect when we overexpressed the cRNA and vRNA forms of the HA gene segment, either individually or together (Fig. 2.5C). It must be noted that bulk levels of viral RNA were roughly 5-fold lower in these cells than in cells that express the viral replicase, so we cannot rule out a role for the intracellular abundance of viral RNA as a determinant of susceptibility to subsequent infection (Fig. 2.12).

Another potential explanation is that viral mRNA or protein overexpression might inhibit subsequent infection. To test this, we transfected 293T cells with pCI vectors that overexpress mRNA and protein of eGFP and HA and measured susceptibility to rH3N2 infection 24 h post-transfection using the M2-specific MAb. Compared to the empty vector control, mRNA/protein overexpression of eGFP or HA had no effect on infection susceptibility (Fig. 2.5D,2.13). Collectively, these data demonstrate that IAV superinfection exclusion is triggered by the activity of viral replication complexes.

2.3 Discussion

Superinfection plays an enormous role in influencing the outcome of IAV infection, both by promoting reassortment and by facilitating the multiplicity reactivation of SIPs and defective interfering particles(Brooke 2017). Despite this importance, the specific factors that govern the occurrence of superinfection have remained obscure. Here, we reveal that IAV superinfection susceptibility is regulated by the number of viral genes successfully expressed by a virion. We further demonstrate that the presence of SIPs within viral populations significantly increases the frequency of superinfection. This represents a

completely novel mechanism of viral superinfection exclusion and identifies a clear functional consequence of the enormous genomic heterogeneity within IAV populations.

The only other published study that examined IAV SIE in detail concluded that NA expression mediates SIE by depleting the pool of available sialic acid receptors on the cell surface(I.-C. Huang et al. 2008). In this study, we directly quantified the contribution of NA expression to SIE during IAV infection and found that the SIE effect of NA expression is actually comparable to that of other viral genes. We also show that treatment with NAIs has no appreciable effect on superinfection susceptibility. The conclusions of the study by Huang et al. were based primarily on two observations: (i) overexpression of NA within cells rendered them refractory to infection by an HA-pseudotyped virus, and (ii) IAV superinfection occurred only when cells were treated with NAIs. While we cannot conclusively explain the discrepancies between the two studies, we can offer a couple of plausible explanations. First, the cellular overexpression studies in Huang et al. likely involved levels of cellular NA expression that are far beyond those seen during IAV infection. Second, the observation that NAI treatment dramatically increases superinfection frequencies may be explained by the effects of cell death. In their experiments, Huang et al. infected cells at a relatively high MOI, did not block secondary spread of the virus within cultures, and assessed superinfection frequency at 20 hpi or later. Under those conditions, many of the initially infected cells may have been dead or dying and thus lost from the analysis. That may be especially true of superinfected cells, which tend to be infected at a higher than the average effective MOI. Even under low-MOI conditions, we had to limit the time frame of our experiments

and block secondary spread of virus to prevent cell death from skewing our results. NAI treatment may act to help preserve coinfected cells so that they are detected at the endpoint of the experiment, thus increasing the measured superinfection rate.

Our results reveal that SIE is triggered in a dose-dependent fashion by the number of functional viral gene segments delivered by the initially infecting virion. The surprising irrelevance of the specific IAV gene segments involved is explained by our finding that the viral coding sequence of a gene segment can be replaced with that of eGFP without any loss of inhibitory effect. This suggests a direct role for viral replicase activity itself in triggering SIE rather than any effect of the viral gene segments themselves. We hypothesize that the overall levels of replicase activity in the cell, particularly during the early stages of infection, are determined by the number of functional RNPs delivered to the cell. Thus, cells infected by SIPs that deliver fewer functional RNPs exhibit lower overall levels of replicase activity, resulting in less-potent SIE.

The specific mechanism by which the activity of viral replicase complexes may inhibit subsequent infection remains unclear; however, one potential explanation is that the activity of viral replication complexes triggers a cell-intrinsic antiviral response. As each incoming gene segment brings its own replicase complex, this could potentially explain the gene dose-dependent suppression of superinfection that we observed. While our experiments in Vero cells demonstrated that the secretion of type I IFN is not required for SIE, they do not preclude the involvement of type I IFN-independent mechanisms. These could include either the type III IFN-mediated induction of antiviral effectors or the

engagement of completely IFN-independent antiviral mechanisms(Dixit et al. 2010; Wack, Terczyńska-Dyla, and Hartmann 2015; Odendall and Kagan 2015). Future studies will be aimed at delineating the role of the host in the regulation of IAV superinfection.

Our results demonstrate that SIPs can directly influence the prevalence of superinfection and thus, potentially, the frequency of reassortment. Fonville et al. used a UV irradiation-based method similar to that shown here to demonstrate that increasing the frequency of SIPs within a viral population increases the overall reassortment rate(Fonville et al. 2015). The explanation given for this effect was that increasing the abundance of SIPs increases the proportion of the viral population that depends upon coinfection to replicate. As a result, within a certain MOI range, a greater share of productively infected cells is coinfected and subject to reassortment. In our study, we confirmed this effect by observing a slight increase in coinfection frequency with increasing UV dose when rPR8 and rH3N2 were added simultaneously (Fig. 2.4E). When we controlled for this, however, we still observed a significant increase in superinfection frequency as we increased the proportion of SIPs through UV treatment (Fig. 2.4D-F). Thus, the relationship between SIPs and SIE that we describe here is completely independent of the increased multiplicity reactivation observed by Fonville et al. and likely represents the effects of decreasing the strength of SIE. Between these two studies, it is clear that SIPs can modulate the frequency of IAV coinfection and reassortment through two distinct mechanisms.

IAV strains can differ significantly with respect to the relative production and gene expression patterns of SIPs(Brooke et al. 2013; 2014). This raises the possibility that strains with distinct SIP production phenotypes may differ in their reassortment potential, given the influence of SIPs on coinfection and reassortment frequencies. If this is the case, it would suggest a significant role for production of SIPs in governing the evolutionary potential of IAV populations.

The relationship between viral gene expression patterns and superinfection exclusion that we report here demonstrates that viral genomic heterogeneity has distinct functional consequences during infection. A crucial implication is that all infected cells cannot be thought of as equal but may in fact exhibit distinct phenotypes based on the number and identity of viral genome segments that they harbor(Diefenbacher, Sun, and Brooke 2018). The relationship between viral genomic heterogeneity and the phenotypic diversity of infected cells likely extends to cellular features beyond superinfection susceptibility.

It remains to be seen whether the relationship between viral gene dose and superinfection susceptibility that we describe here exists for other segmented viruses besides IAV. Beyond the segmented viruses, it has become increasingly clear that collective interactions mediated by cellular coinfection significantly influence the replicative and evolutionary dynamics of non-segmented viruses as well(Sanjuán 2017). More work is needed to better understand the factors that govern coinfection for different virus families, both *in vitro* and *in vivo*.

In summary, our work reveals a unique mechanism of IAV superinfection regulation that is governed by viral genomic heterogeneity. Critically, we show that the abundance of SIPs within a viral population directly influences the prevalence of superinfection; suggesting that IAV strains may differ in their superinfection potential and thus in their potential for reassortment. This finding has significant consequences for understanding how SIP production can influence the evolutionary potential of IAV populations. More broadly, we demonstrate how genomic diversity within viral populations can have clear functional consequences during infection.

2.4 Materials and methods

Plasmids

The A/Puerto Rico/8/34 and A/Udorn/72 reverse genetics plasmids were generous gifts from Adolfo Garcia-Sastre and Kanta Subbarao, respectively. The pCI vector was graciously provided by Joanna Shisler. pHH21::eGFP$_{vRNA}$ (eGFP ORF flanked by the NA UTRs) was kindly gifted by Andrew Mehle. Generation of pHH21::HA$_{vRNA}$ has been previously described. The following primer pairs were used to generate the indicated constructs: for pHH21::eGFP$_{ORF}$ (BsmBI), 5′-CGTCTCCTATTTTACTTGTACAGCTCG and 3′ CGTCTCCGGGATGGTGAGCAAGGGC; for pHH21::HA$_{cRNA}$ (BsmBI), 5’CGTCTCATATTAGCAAAAGCAGG and 3′ CGTCTCAGGGAGTAGAAACAAGGG; for pCI::eGFP$_{ORF}$ (EcoRI/SalI), 5′-AGAATTCATGGTGAGCAAGG and 3’AGTCGACTTACTTGTACAGC; for

pCI::HA_{ORF} (EcoRI/SalI), 5′-AGAATTCATGGAAGATTTTGTGCG and 3′ AGTCGACCTAACTCAATGCATGTGT.

Cells

Madin-Darby canine kidney (MDCK) and human embryonic kidney HEK293T (293T) cells were maintained in Gibco's minimal essential medium (MEM) with GlutaMax (Life Technologies). Vero cells were maintained in Dulbecco's modified Eagle medium (Life Technologies). Human lung epithelial A549 cells were maintained in Gibco's F-12 medium (Life Technologies). MDCK, Vero, and A549 cells were obtained from Jonathan Yewdell; 293T cells were obtained from Joanna Shisler. All media were supplemented with 8.3% fetal bovine serum (Seradigm). Cells were grown at 37°C and 5% CO_2.

Viruses

Recombinant A/Puerto Rico/8/1934 (rPR8) and rH3N2 viruses were generated using 8-plasmid rescue systems. The rH3N2 virus is a reassortant with the HA and NA segments from A/Udorn/72 (H3N2), the NS segment from A/California/04/09 (H1N1), and the other 5 segments from PR8. The rPR8 clones differ from the published sequence (GenBank accession no. AF389115 to AF389122) at two positions: PB1 A549C (K175N) and HA A651C (I207L) (numbering from initiating Met). Molecular clone-derived mutants (rPR8 NP:F346S and rPR8 NA:K239R) were generated using standard site-directed PCR mutagenesis. rH3N1 and rH1N2 viruses used in superinfection studies were similarly generated through reverse genetics, using the HA and NA segments from A/Udorn/72 (H3N2) respectively and the remaining segments from PR8. All viruses were

rescued by transfecting subconfluent 293T cells with 500 ng of each of the appropriate reverse genetics plasmids using JetPRIME (Polyplus) according to the manufacturer's instructions. Plaque isolates derived from rescue supernatants were amplified into seed stocks in MDCK cells. Working stocks were generated by infecting MDCK cells at a MOI of 0.0001 $TCID_{50}$/cell with seed stock and collecting and clarifying supernatants at 48 hpi. All viral growth was carried out in MEM with 1 ug/ml trypsin treated with L-(tosylamido-2-phenyl) ethyl chloromethyl ketone (TPCK-treated trypsin; Worthington), 1 mM HEPES, and 100 ug/ml gentamicin. The titers of the virus stocks were determined via standard 50% tissue culture infectious dose ($TCID_{50}$) assay.

Superinfection assay

For the 6-h sequential-infection group, confluent mammalian cells (MDCK, Vero, A549, or 293T) in six-well plates were infected with rPR8 at a MOI of <0.3 $TCID_{50}$/cell for 1 h. At 1 h post-adsorption, monolayers were washed with phosphate-buffered saline (PBS) and incubated in serum-containing medium. At 3 hpi, neutralizing anti-PR8-HA mouse MAb H17-L2 (5 ug/ml) was added to cultures to prevent spread of rPR8. At 6 hpi, monolayers were superinfected with rH3N2 at an MOI of <0.3 $TCID_{50}$/cell in the presence of H17-L2 (which does not interfere with rH3N2 infection) (Fig. 2.7). At 1 h post-adsorption, monolayers were washed with PBS and incubated in serum-containing medium with H17-L2. At 9 hpi of rPR8 (3 hpi of rH3N2), the medium was changed to MEM with 50 mM HEPES and 20 mM NH_4Cl to block spread of both viruses. At 19 hpi of rPR8 (13 hpi of rH3N2), monolayers were trypsinized into single-cell suspensions.

For the 0-h simultaneous infection group, cells were infected with a mixture of rPR8 and rH3N2 at the same MOIs as in 6-h superinfection group. The NH_4Cl medium was added to block viral spread at 3 hpi, and cells were harvested at 19 hpi.

All cells were simultaneously fixed and permeabilized using foxP3 fix/perm buffer (eBioscience). Fixed cells were stained with Alexa Fluor 488-conjugated mouse anti-H1 MAb H36-26 (which does not compete with H17-L2), Pacific Orange-conjugated mouse anti-N1 MAb NA2-1C1, Pacific Blue-conjugated mouse anti-NS1 MAb NS1-1A7, and Alexa Fluor 647-conjugated mouse anti-H3 MAb H14-A2 (all MAbs were gifts from Jon Yewdell). After staining was performed, cells were washed, run on a BD LSR II flow cytometer, and analyzed using FlowJo version 10.1 (Tree Star, Inc.). Importantly, the expression patterns of H1, H3, N1, and NS1 allowed clear gating of positive and negative populations.

NA activity inhibition assay

The NA inhibitor zanamivir (Sigma) (10 ug/ml) was 2-fold serially diluted in assay buffer [33 mM 2-(N-morpholino) ethane-sulfonic acid (pH 6.5), 4 mM $CaCl_2$] and mixed with 2.2×10^6 $TCID_{50}$ of rH3N1 virus in a final volume of 50 ul. On a 96-well half-well flat-bottom plate (Corning 3686), 25 ul of the virus-NAI mixture was mixed with 20 ul of the fluorogenic substrate MUNANA [2′-(4-methylumbelliferyl)-α-D-N-acetylneuraminic acid] (Sigma) diluted in assay buffer [33 mM 2-(N-morpholino)ethane-sulfonic acid (pH 6.5), 4 mM $CaCl_2$]. In the mixture, the final concentration was 200 uM for the substrate and ranged from 0.0625 uM to 1 uM for zanamivir. No-drug controls and no-virus

controls were also included. Immediately after the addition of the substrate, fluorescence was measured every 5 min over a 30-min period on a SpectraMax M2 microplate reader (Molecular Devices). Michaelis-Menten kinetics were determined for each dilution of zanamivir to estimate the maximum rate of metabolism (V_{max}) values.

Quantification of NA expression

$H1^+$ $N1^+$ MDCK cells infected with rPR8WT, rPR8 NP:F346S, or rPR8 NA:K239R in the superinfection assay (6-h group) were gated, and histograms for NA expression were plotted. The geometric mean fluorescence intensities (GMFI) for NA were determined using FlowJo version 10.1 (Tree Star, Inc.).

UV treatment and analysis

rPR8 stocks were placed in six-well plates (500 ug/well) on ice. Plates were placed 5 cm underneath a 302-nm-wavelength UVP-57 handheld UV lamp (UVP) and irradiated for 30 s or 60 s. $TCID_{50}$ titers and single virion expression patterns of untreated and UV-treated virus were determined on MDCK cells, and the superinfection assays described above were performed using these viruses and rH3N2.

Transfection assay

293T cells (80% confluent) in six-well plates were transfected with the following plasmids using jetPRIME (Polyplus): RNP (500 ng each of pDZ::PB2, pDZ::PB1, pDZ::PA, and pDZ::NP) plus 1 ug of pHH21 vector; RNP plus 1 ug of pHH21::$eGFP_{vRNA}$ ($eGFP_{ORF}$ flanked with NA UTRs); RNP plus 1 ug of

pHH21::eGFP$_{ORF}$; RNP plus 1 ug of pHH21::HA$_{vRNA}$; RNP$_{PA-}$ (500 ng each of pDZ::PB2, pDZ::PB1, pDZ, and pDZ::NP) plus 1 ug of pHH21::eGFP$_{vRNA}$; RNP$_{PA-}$ plus 1 ug of pHH21::HA$_{vRNA}$; 6 ug of pHH21 vector; 3 ug of pHH21 vector plus 3 ug of pHH21::eGFP$_{vRNA}$; 3 ug of pHH21 vector plus 3 ug of pHH21::HA$_{vRNA}$; 3 ug of pHH21 vector plus 3 ug of pHH21::HA$_{cRNA}$; 3 ug of pHH21::HA$_{vRNA}$ plus 3 ug of pHH21::HA$_{cRNA}$; 3 ug of the pCI vector; 3 ug of pCI::eGFP$_{ORF}$; 3 ug of pCI::HA$_{ORF}$. All plasmid-encoded viral sequences were derived from PR8. At 24 h post-transfection, monolayers were infected with rH3N2 at a MOI of 0.2 TCID$_{50}$/cell. At 8 hpi, cells transfected by RNP$^+$ pHH21, and pCI plasmids were harvested and stained with Alexa Fluor 488-conjugated mouse anti-H1 MAb H36-26 and Alexa Fluor 647-conjugated mouse anti-M2 MAb O19. Cells transfected with pHH21 plasmids were permeabilized, fixed, and stained with Alexa Fluor 647-conjugated mouse anti-NP MAb HB-65. After staining, cells were washed and run on a BD LSR II flow cytometer, and virus infection frequencies, as measured by fractions of M2$^+$ or NP$^+$ cells, were quantified using FlowJo version 10.1 (Tree Star, Inc.).

Intracellular viral RNA quantification

Subconfluent 293T cells in six-well plates were infected with rPR8 at an MOI of 0.5 HA-expressing units (HAEU)/cell or were transfected with the following plasmids using jetPRIME (Polyplus): 3 ug of pHH21 vector plus 3 ug of pHH21::HA$_{vRNA}$; RNP (500 ng each of pDZ::PB2, pDZ::PB1, pDZ::PA, and pDZ::NP) plus 1 ug of pHH21::HA$_{vRNA}$. At 6 hpi and 24 h post-transfection, cells were harvested, and RNA was extracted using a RNeasy minikit (Qiagen). cDNA of cellular mRNA and cDNA of HA vRNA were

reverse transcribed with oligo(dT)$_{20}$ or MBTuni (5′-ACGCGTGATCAGCAAAAGCAGG) reverse transcriptase (RT) primers using Superscript III (Invitrogen). Quantitative real-time PCR on cDNA was carried out using Power SYBR green PCR Master Mix (Thermo Fisher) on a QuantStudio 3 thermal cycler (Thermo Fisher). The strand-specific primers for quantitative real-time PCR of HA vRNA and GAPDH (glyceraldehyde-3-phosphate dehydrogenase) mRNA were as follows: for GAPDH317F, CTGGGGCTCACTTGAAAGG; for GAPDH388R, CAAACATGGGGGCATCAG); for HA, F (forward) (AAGGCAAACCTACTGGTCCTGTT) and R (reverse) (AATTGTTCGCATGGTAGCCTATAC). Delta threshold cycle (ΔC_T) values for viral RNA were calculated by subtracting GAPDH C_T values from HA C_T values.

Statistical analysis

Unpaired, two-sided Student's *t* tests were applied to the data shown in Fig. 1B, 2B, 3A, 3B, and 4F. An unpaired, two-sided Welch's *t* test was applied to the data shown in Fig. 3D. All statistical analyses were performed with GraphPad Prism 7.0a.

2.5 Figures

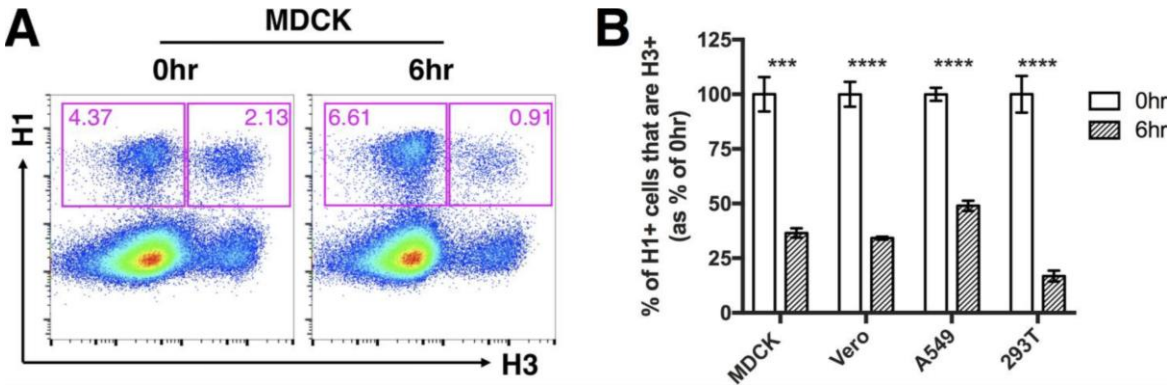

Figure 2.1 A 6-h delay between primary infection and superinfection allows robust superinfection exclusion. The indicated mammalian cell lines were infected with rPR8 virus and were simultaneously (0hr) or sequentially (6hr) infected with rH3N2 virus; all infections were performed at MOI = <0.3 $TCID_{50}$/cell. (A) Representative fluorescence-activated cell sorter (FACS) plots showing expression of H1 versus H3 within MDCK cells. (B) $H3^+$ frequencies within $H1^+$ cells following simultaneous or sequential infection, in the indicated cell lines. The values for both the 0-h and 6-h groups are shown as percentages of the mean values of the 0-h control group to clearly illustrate the percentages of reduction in cellular susceptibility in the 6-h group. Data are presented as means (n = 3 cell culture wells) ± standard deviations. ***, $P < 0.001$; ****, $P < 0.0001$ (t test).

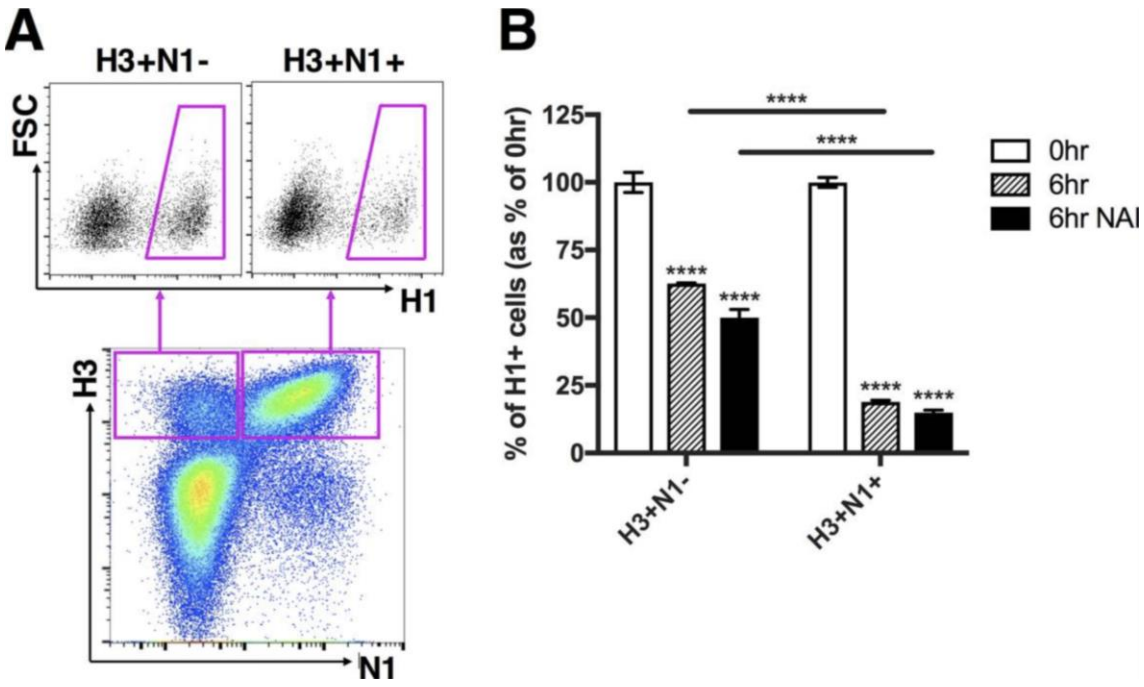

Figure 2.2 Superinfection exclusion is more potent in infected cells that express NA but is independent of NA enzymatic activity. MDCK cells were infected with rH3N1 virus and were simultaneously (0hr) or sequentially (6hr) infected with rH1N2 virus; all infections were performed at MOI = <0.3 $TCID_{50}$/cell. During the 5-h gap and 1-h adsorption of the secondary infection (rH1N2), cells were incubated in either medium alone or media with 1 μM zanamivir (NAI). (A) Representative FACS plots comparing $H1^+$ frequencies between $H3^+$ $N1^-$ and $H3^+$ $N1^+$ cells. (B) $H1^+$ frequencies within $H3^+$ $N1^-$ and $H3^+$ $N1^+$ cells following simultaneous (0hr) or sequential (6hr) infection. Values of both the 0-h and 6-h groups (with or without the presence of NAI) are normalized to the means of 0-h controls, and data are presented as mean values (n = 3 cell culture wells) ± standard deviations. ****, $P < 0.0001$ (t test).

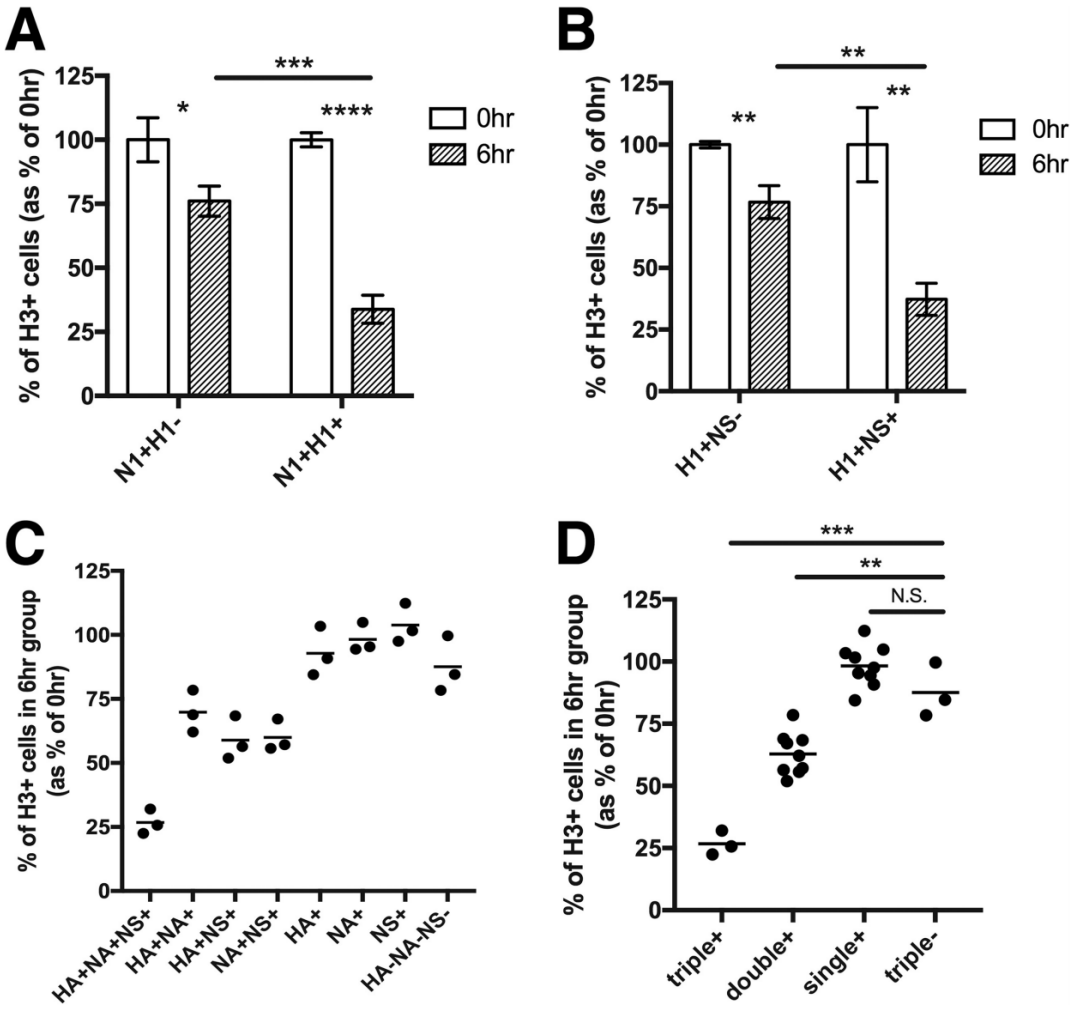

Figure 2.3 Superinfection is more frequent in cells that express fewer viral genes. MDCK cells were infected with rPR8 and were simultaneously (0hr) or sequentially (6hr) infected with rH3N2; all infections were performed at MOI = <0.3 $TCID_{50}$/cell. (A and B) Representative FACS plots comparing $H3^+$ frequencies between (A) $N1^+$ $H1^-$ and $N1^+$ $H1^+$ cells and (B) $H1^+$ NS^- and $H1^+$ NS^+ cells. (C) Superinfection assay performed as described for panels A and B; however, cells are gated into all 8 possible combinations of HA, NA, and NS1 expression by rPR8, and $H3^+$ percentages are compared between these subpopulations. Data represent the values of 6hr groups normalized to the means of 0hr controls. Each data point represents the $H3^+$ frequency for the indicated cell population within a single cell culture well, shown as a percentage of the mean $H3^+$ frequency of the same cell subpopulation in the 0hr controls. (D) Data from panel C grouped by total numbers of the three examined viral gene products (HA, NA, and NS1) expressed by rPR8 rather than by their specific identities. **, $P < 0.05$; **, $P < 0.01$; ***, $P < 0.001$; ****, $P < 0.0001$; N.S., not significant (*t* test).

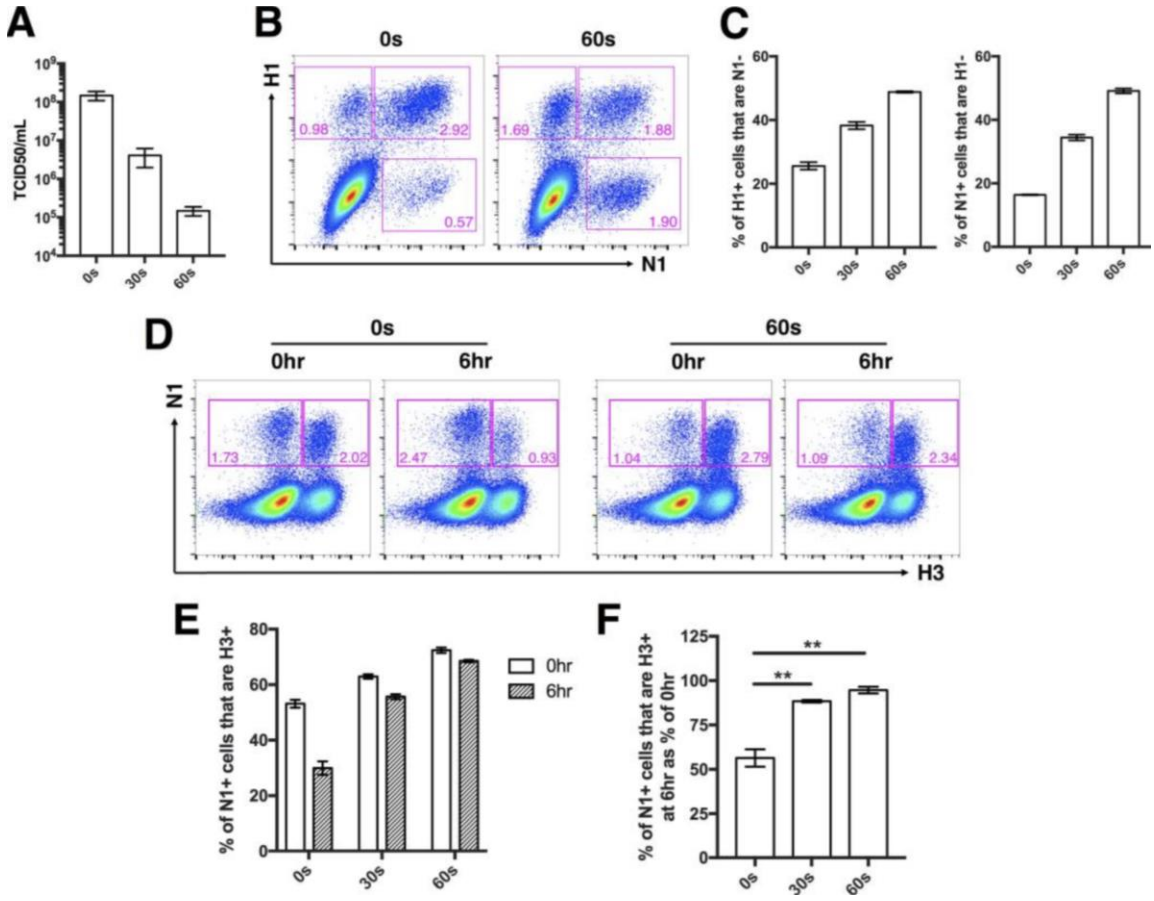

Figure 2.4 Superinfection is more common in viral populations that contain more SIPs. rPR8 was irradiated by the use of a 302-nm-wavelength UV lamp for 30 s or 60 s. (A) $TCID_{50}$ titers of untreated rPR8 (0 s) or rPR8 subjected to UV treatment for 30 s and 60 s. Pooled data from two independent experiments are shown. (B) Representative FACS plots showing HA versus NA expression patterns of untreated rPR8 (0 s) and rPR8 subjected to UV treatment for 60 s. (C) Quantification of $H1^-$ and $N1^-$ SIPs in untreated rPR8 (0 s) or rPR8 subjected to UV treatment for 30 s and 60 s. (D) MDCK cells were infected with untreated rPR8 (0 s) or with rPR8 subjected to UV treatment for 30 s and 60 s at an MOI of 0.04 NAEU/cell and were simultaneously (0hr) or sequentially (6hr) infected with rH3N2 at MOI < 0.3 $TCID_{50}$/cell. Representative FACS plots showing expression of N1 versus H3 in cells infected with untreated rPR8 (0 s) or with rPR8 subjected to UV treatment for 60 s. (E) rH3N2 infection percentages within $N1^+$ cells infected with untreated rPR8 (0 s) or with rPR8 subjected to UV treatment for 30 s and 60 s. (F) Values corresponding to the 6hr groups in panel E normalized to means of 0hr controls. For panels E and F, data are presented as mean values (n = 3 cell culture wells) ± standard deviations. **, $P < 0.01$ (t test).

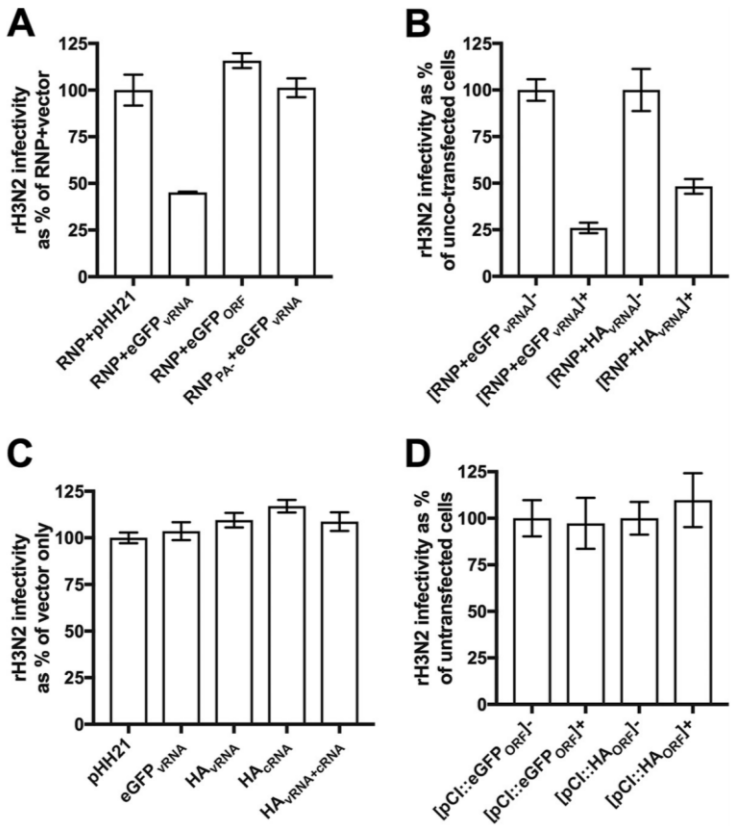

Figure 2.5 Viral replicase activity inhibits subsequent infection. (A) Subconfluent 293T cell monolayers were transfected with: vectors encoding the complete set of viral replicase proteins (PB2, PB1, PA, and NP) together with empty pHH21 vector with the PolI promoter (RNP+pHH21), pHH21 encoding a reporter viral RNA with eGFP ORF plus 5′ and 3′ viral UTR sequences (RNP + $eGFP_{vRNA}$), pHH21 encoding eGFP ORF without the viral UTRs (RNP + $eGFP_{ORF}$), and vectors encoding an incomplete set of viral replicase proteins (PB2, PB1, and NP only; no PA) along with pHH21 encoding the reporter viral RNA (RNP_{PA-} + $eGFP_{vRNA}$). At 24 h post-transfection, cells were infected with rH3N2 at MOI = 0.2 $TCID_{50}$/cell. At 8 hpi, cells were harvested and assessed for rH3N2 infection via flow cytometry. For each group, rH3N2 infectivities are presented as the percentages of the mean rH3N2 infectivity in the RNP + pHH21 vector control group. (B) Experiment performed as described for panel A with cotransfection of plasmids encoding the complete set of viral replicase proteins plus either pHH21::$eGFP_{vRNA}$ or pHH21::HA_{vRNA}. Data representing rH3N2 infectivity in cotransfected cells ($eGFP^+$ or HA^+) are normalized to uncotransfected cells ($eGFP^-$ or HA^-) in the same samples. (C) Experiment performed as described for panel A with transfection of empty vector (pHH21) or vectors encoding indicated RNA products. rH3N2 infectivities are presented as the percentages of the mean rH3N2 infectivity in the vector control group. (D) Experiment performed as described for panel A with transfection of empty vector (pCI) or vectors encoding eGFP or HA protein. Data representing rH3N2 infectivity in transfected cells ($eGFP^+$ or HA^+) are normalized to untransfected cells ($eGFP^-$ or HA^-) in the same samples. Data are presented as mean values (n = 2 cell culture wells) ± standard deviations.

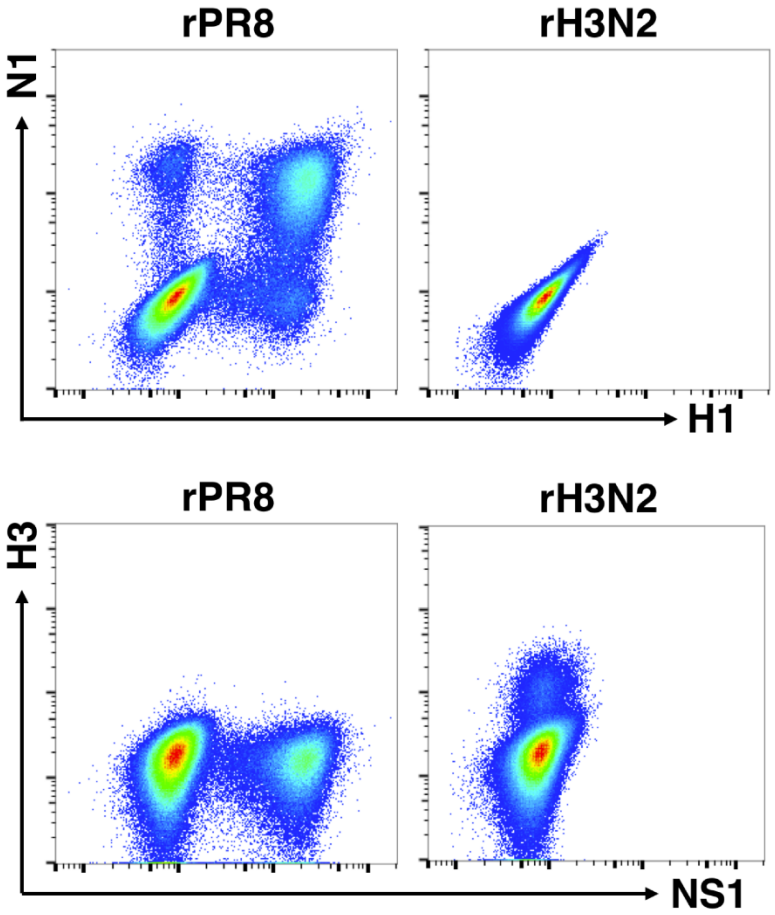

Figure 2.6 Levels of expression of HA, NA, and NS1 by rPR8 and rH3N2 can be differentiated using specific MAbs. MDCK cells were infected with rPR8 or rH3N2 at a MOI of <0.3 $TCID_{50}$/cell. At 19 hpi, cells were harvested, fixed, permeabilized, stained against H1 (H36-26), N1 (NA2-1C1), NS1 (1A7), and H3 (H14-A2), and run on an LSR II flow cytometer. The results of analyses of expression of H1 versus N1 and of NS1 versus H3 are shown in representative FACS plots.

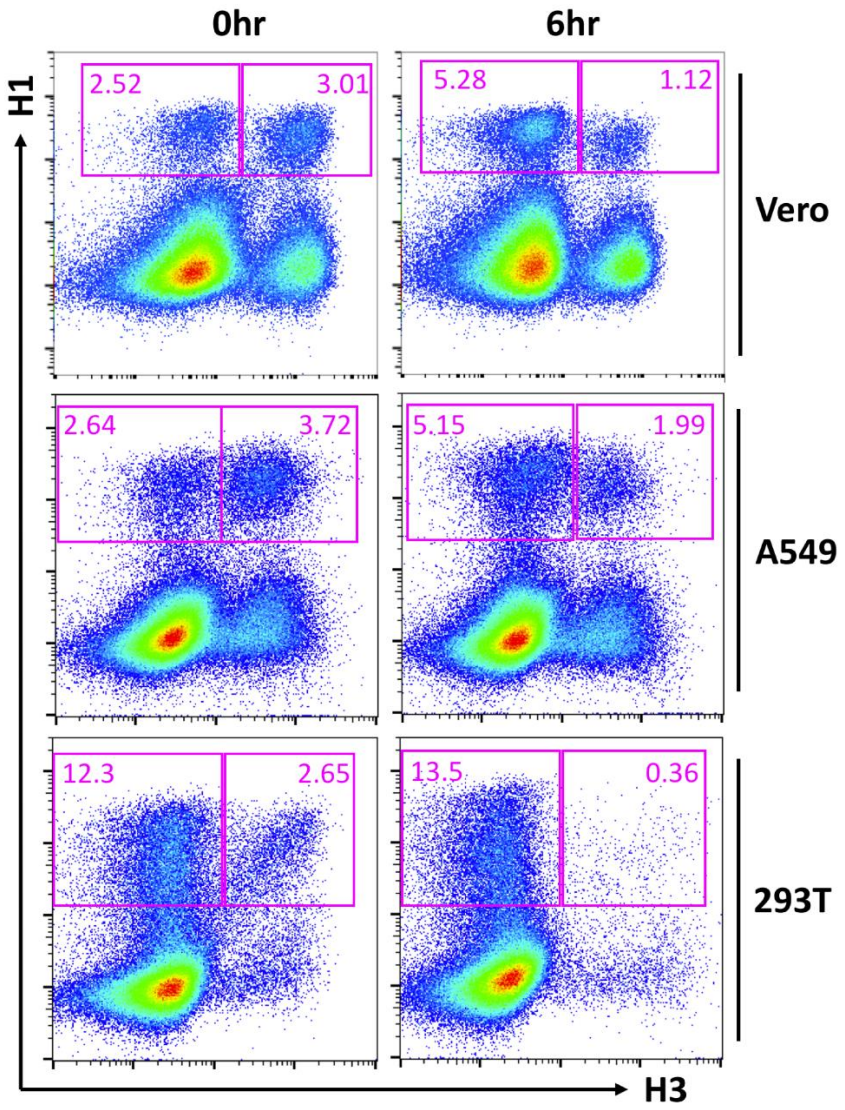

Figure 2.7 Superinfection is inhibited in multiple cell lines. Levels of H1 expression versus H3 expression in Vero cells, A549 cells, and 293T cells observed in the experiments described in the Fig. 1 legend are shown as representative FACS plots.

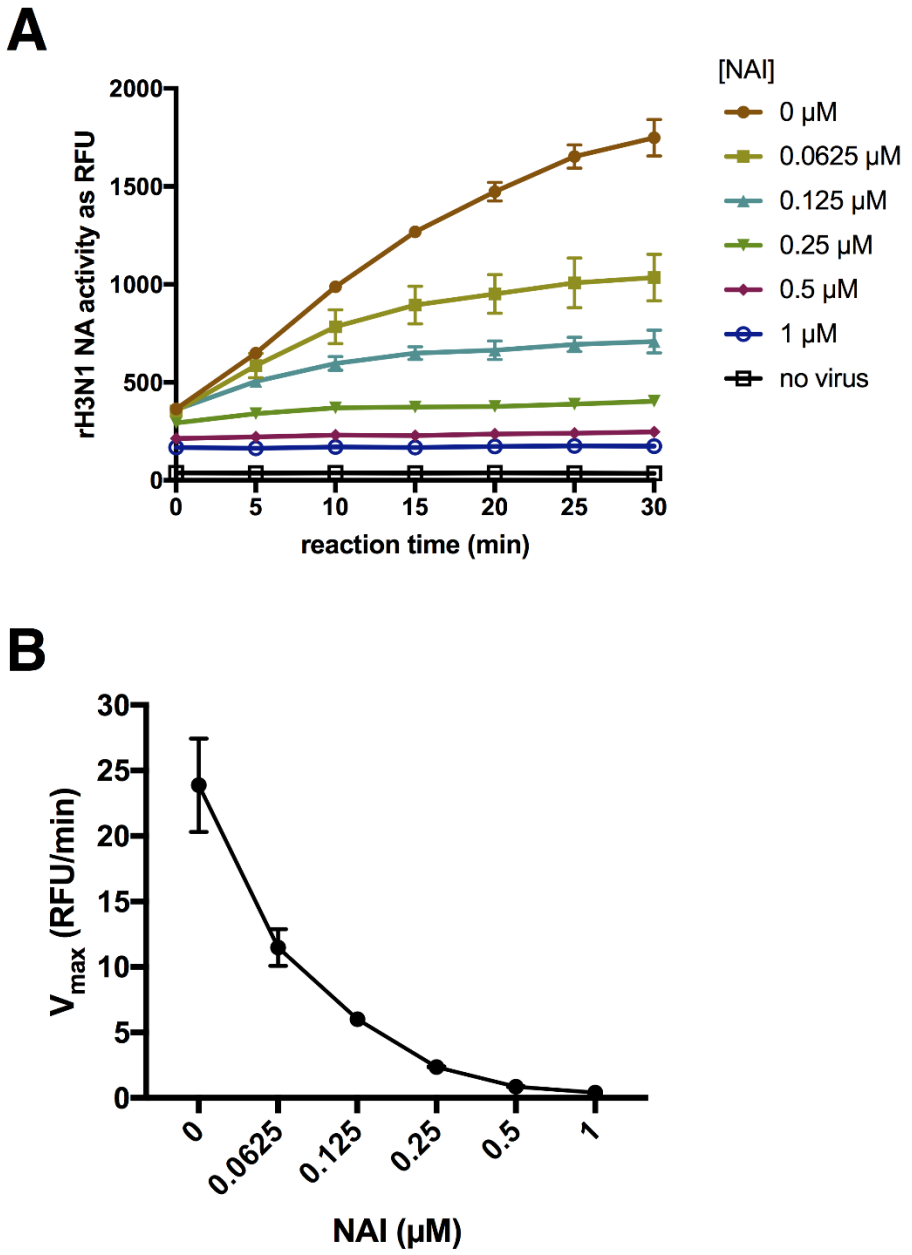

Figure 2.8 Viral NA activity is blocked by 1 μM zanamivir. (A) NA activity of rH3N1 virus used in the experiment described in the Fig 2 legend. Data represent results of determinations of relative fluorescence units (RFU) against time under conditions of increasing concentrations of zanamivir. (B) V_{max} of reactions performed as described for panel A. Data are presented as mean values ($n = 2$ enzymatic reactions) ± standard deviations.

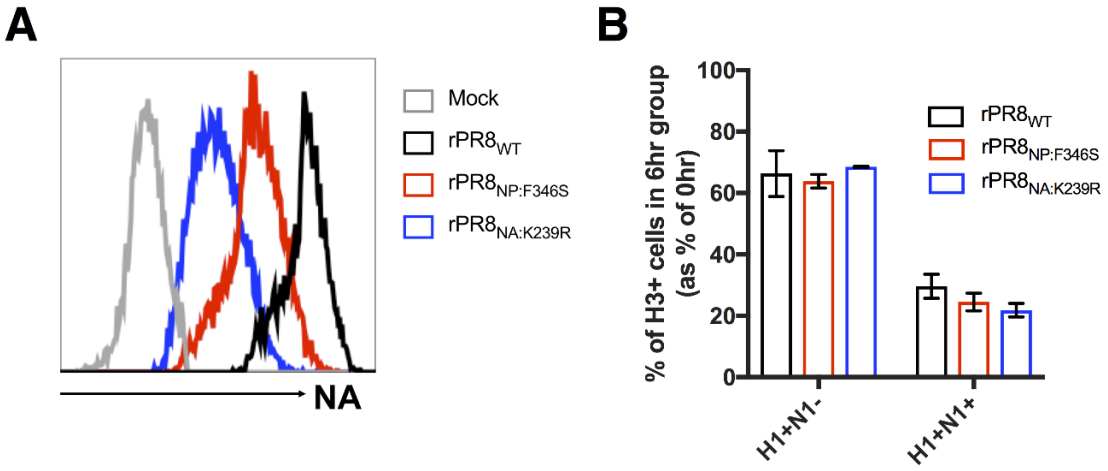

Figure 2.9 Superinfection exclusion is independent of NA expression level. MDCK cells were infected with $rPR8_{WT}$, $rPR8_{NP:F346S}$, or $rPR8_{NA:K239R}$ and were simultaneously (0hr) or sequentially (6hr) infected with rH3N2; all infections were performed at MOI = <0.3 $TCID_{50}$/cell. (A) Comparison of NA expression levels within $H1^+$ $N1^+$ cells between $rPR8_{WT}$, $rPR8_{NP:F346S}$, and $PR8_{NA:K239R}$ at 19 hpi. (B) Comparison of $H3^+$ frequencies within $H1^+$ $N1^-$ and $H1^+$ $N1^+$ cells between the three indicated viruses. Values from h 6 groups are normalized to means of h 0 controls. Data are presented as mean values ($n = 3$ cell culture wells) ± standard deviations.

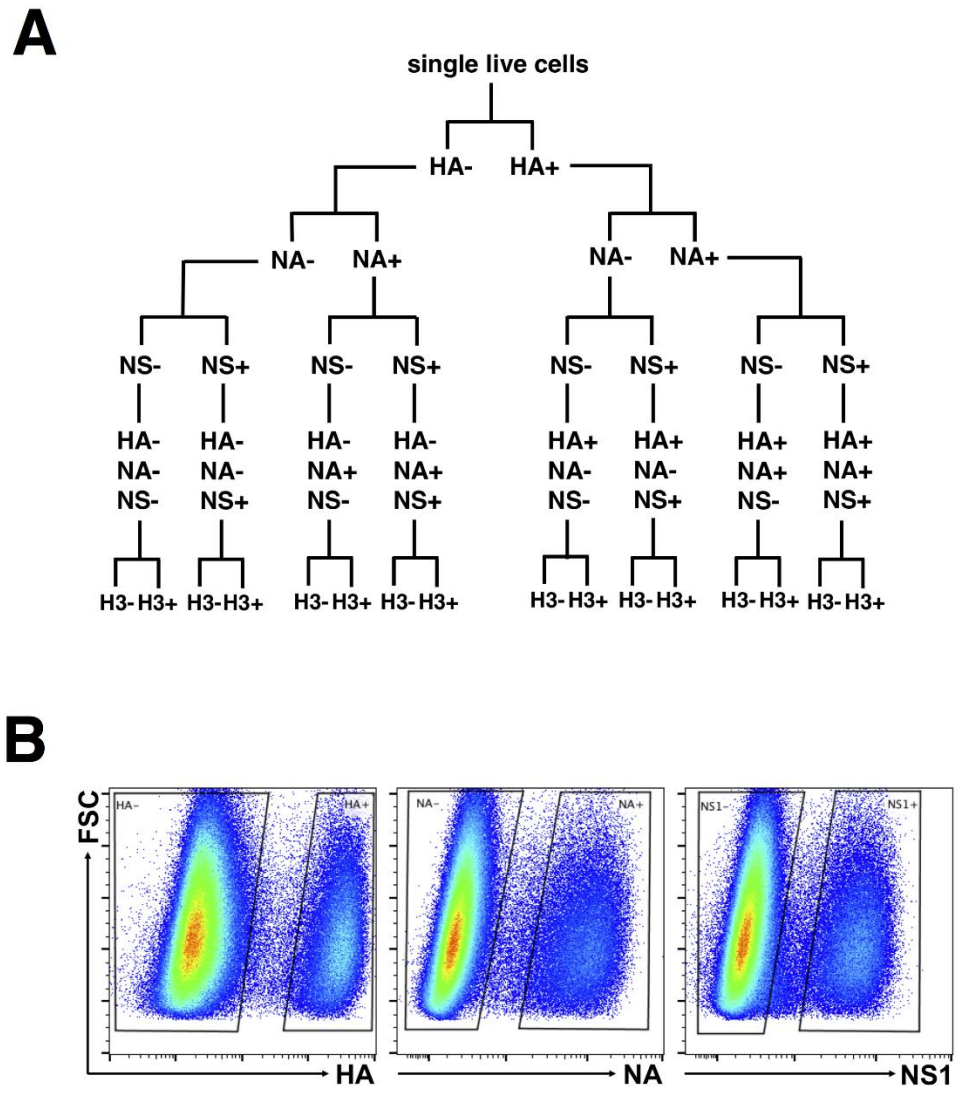

Figure 2.10 Gating scheme used for measuring the effect of the number of viral genes expressed on superinfection frequencies. (A) Cells from the experiment described in the Fig. 3 legend were assessed for expression of HA, NA, and NS1 sequentially. The fractions of $H3^+$ cells (indicative of superinfection rates) were quantified and compared between the cell populations with the indicated viral gene expression patterns. (B) Representative FACS plots showing the gates used to assess HA, NA, and NS1 expression in this experiment.

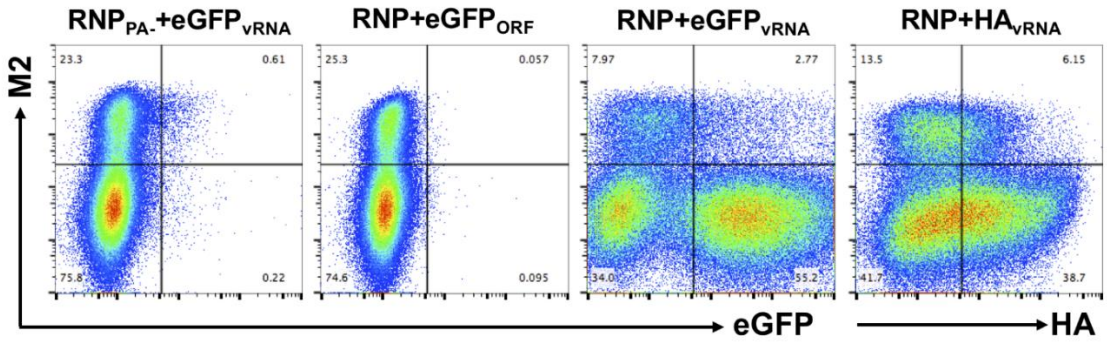

Figure 2.11 Cells cotransfected with plasmids encoding viral replicase and viral RNA are less susceptible to subsequent infection. Cells from the experiments described in the Fig. 5A,B legends were assessed for expression of M2 (indicative of rH3N2 infection) versus eGFP and HA (indicative of cotransfection) as shown in representative FACS plots.

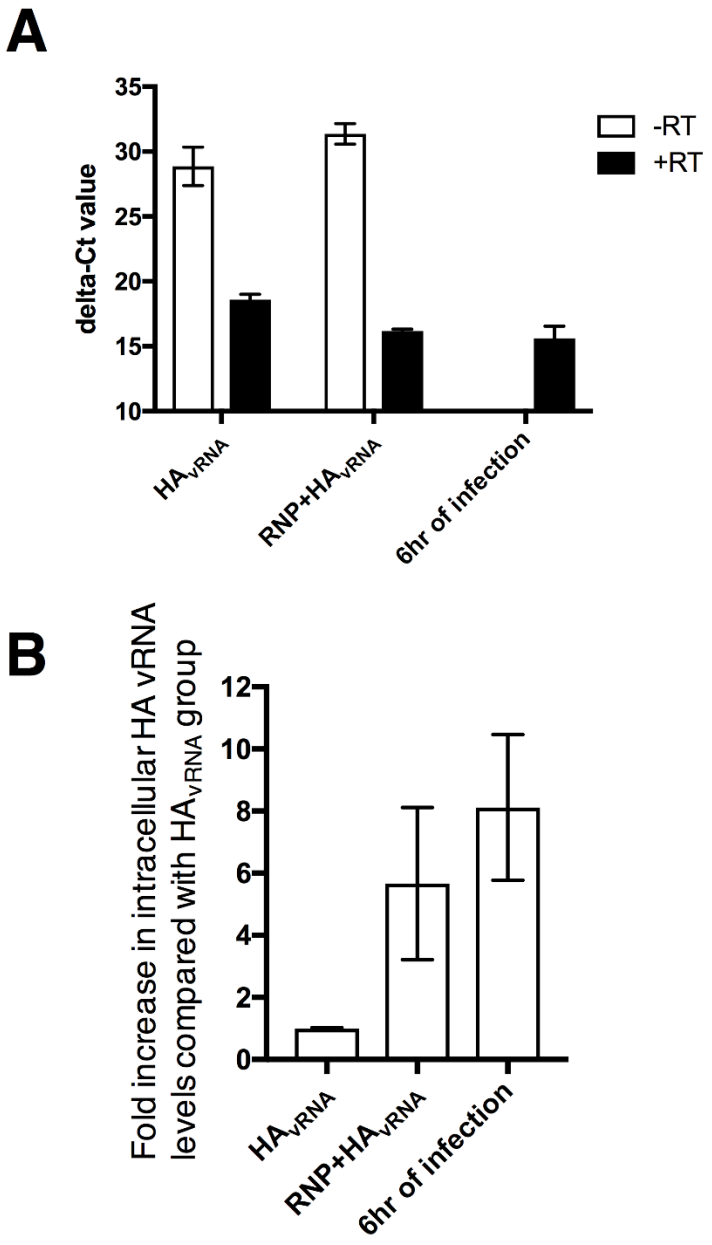

Figure 2.12 Comparison of intracellular viral RNA levels measured under different experimental conditions. (A) Relative amounts of HA vRNA in 293T cells transfected with pHH21::HA_{vRNA} or cotransfected with plasmid-derived viral replicase complex plus pHH21::HA_{vRNA} for 24 h or infected with rPR8 for 6 h at MOI = 0.5 HAEU/cell were determined by strand-specific quantitative real-time PCR, including the no-reverse-transcription control. Data shown are delta threshold cycle (ΔC_T) values for HA vRNA versus GAPDH mRNA. (B) Relative amounts of HA viral RNA shown as fold differences compared with HA_{vRNA}. Data are presented as mean values ($n = 2$ cell culture wells) ± standard deviations.

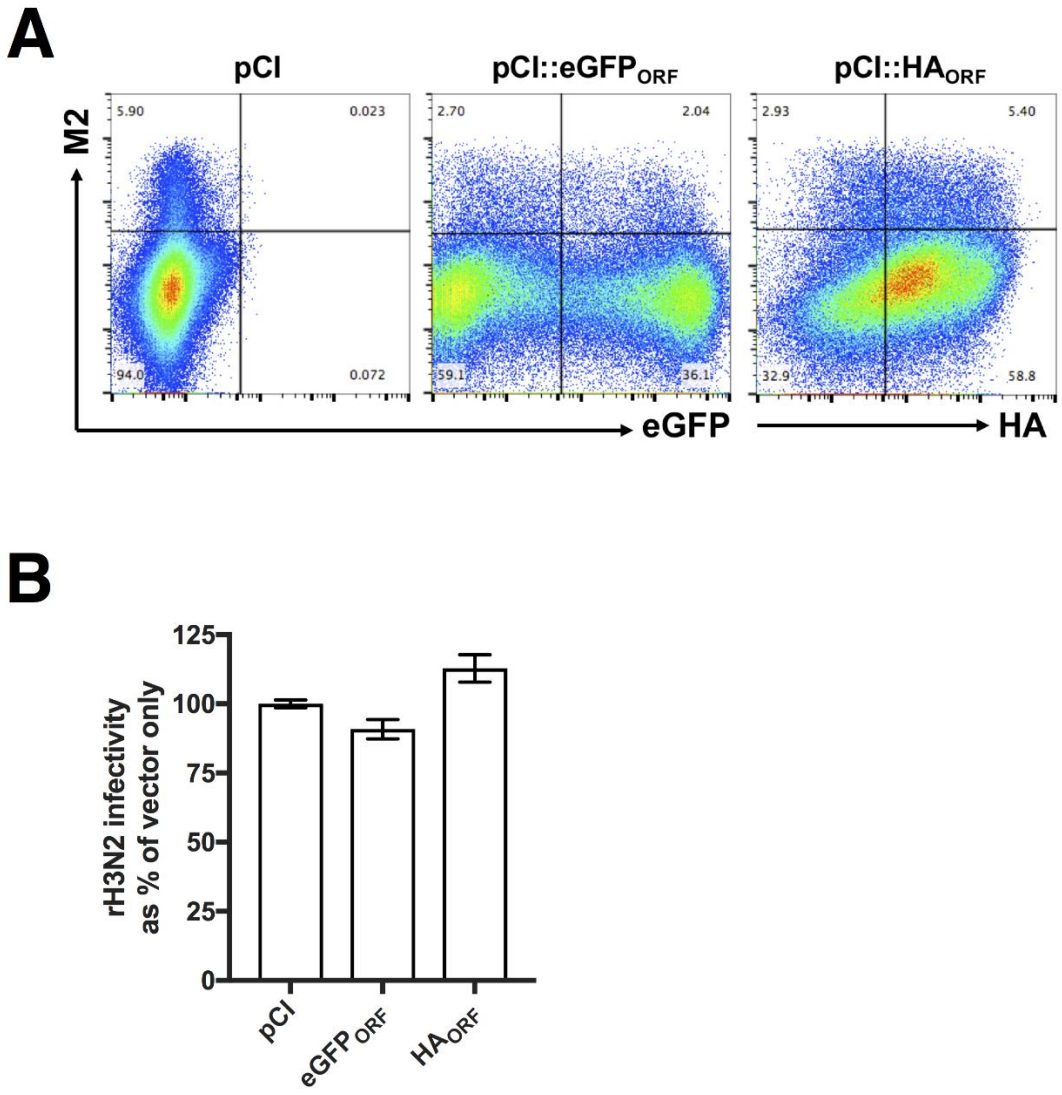

Figure 2.13 Overexpression of viral mRNA and protein in cells does not inhibit subsequent infection. (A) Cells from the experiment described in the Fig. 5D legend were assessed for expression of M2 (indicative of rH3N2 infection) versus eGFP and HA (indicative of transfection) in representative FACS plots. (B) rH3N2 infectivity data from panel A are shown as percentages of pCI vector. Data are presented as mean values ($n = 2$ cell culture wells) ± standard deviations.

CHAPTER 3: DEFINING NOVEL DETERMINANTS OF IAV SUPERINFECTION EXCLUSION

3.1 Introduction

Superinfection exclusion (SIE) occurs when the host cell infected by a virus become refractory to the subsequent infection of another virus. To date, SIE has been observed in multiple RNA viruses, including IAV (IAV)(I.-C. Huang et al. 2008; Nethe, Berkhout, and van der Kuyl 2005; Schaller et al. 2007; Zou et al. 2009; X.-F. Zhang et al. 2017; Laliberte and Moss 2014). It is clear that the extent of SIE regulates viral co-infection rate, the fraction of cells infected by multiple virus particles(Marshall et al. 2013). Since both multiplicity reactivation (complementation of semi-infectious particles) and reassortment (exchange of gene segments between different IAVs) require co-infection to occur, SIE is a major determinant of IAV replicative and evolutionary potentials(Brooke 2017). Despite the huge importance, the mechanisms that mediate SIE in IAV remain poorly understood. Here, we aim to define novel viral and host determinants of SIE to better understand the mechanisms.

3.2 Results

SIE is enhanced by cellular co-infection

We previously showed that under low MOI condition where co-infection is rare, increasing the number of functional gene segments delivered to a given cell resulted in more potent SIE, limiting the potential for cellular co-infection in a cell-type independent manner. Therefore, we hypothesized that increases in cellular MOI of the primary infection would shorten the time window during which superinfection is possible, enhancing SIE. To more quantitatively describe the relationship between MOI and SIE,

we collaborated with Dr. Katia Koelle who developed different mathematical models and tested which model best explains our experimental data.

To define how cellular MOI affects subsequent superinfection potential, we measured the extent of SIE across a range of bulk MOIs in MDCK cells. We generated 2 antigenically distinct reassortant viruses (rH3N1 and rH1N2) that could be differentiated using specific monoclonal antibodies. We infected MDCK cells with rH3N1 at a range of intended MOIs resulting in groups with average bulk MOIs of 0.25, 1.13, 3.00, 15.43, and 53.72 TCID50/cell (based on subtracting post-adsorption inoculum GE titers from pre-adsorption inoculum titers as detailed in methods). At 6 hpi, we superinfected with a constant bulk input MOI of 0.5 TCID50/cell of rH1N2. To measure the baseline co-infection rates in the absence of SIE effects, we included co-infection controls for each input MOI where we simultaneously co-infected with rH3N1 and rH1N2 viruses. At 19 hpi, we examined the infection status of cells by flow cytometry, using H3 and H1 expression as markers of rH3N1 infection and rH1N2 infection, respectively.

As expected, during simultaneous co-infection (where no SIE occurs), we observed that the fraction of co-infected cells (H3+H1+) increased with the input MOI of rH3N1 virus and plateaued when almost all rH1N2-infected cells (H1+) were co-infected with rH3N1 (Fig 3.1A). These simultaneous co-infection data were used to develop and parameterize an appropriate “null” model of co-infection in the absence of SIE. To capture the possibility of overdispersion of viral particles, the null model assumed that cells could belong to either a low susceptibility class of cells or a high susceptibility class of cells.

In contrast to what was observed under simultaneous co-infection conditions, under superinfection conditions we observed that the fractions of both double-infected (H3+H1+) cells and rH1N2-infected (H1+) cells decreased with increasing rH3N1 input MOI (Fig 3.1B). To determine whether these patterns could simply be explained by higher numbers of cells being infected with rH3N1 at higher rH3N1 input MOIs, we assessed how well two different models of super-infection fit the experimental data. The first model assumed that all rH3N1-infected cells had the same reduced probability of becoming infected with rH1N2 (input-independent). The second model assumed that the probability of being infected with rH1N2 decreased with cellular rH3N1 MOI (input-dependent). Similar to the co-infection null model, both models assumed that cells fall into either a high or low susceptibility class. We fit each of these two models to the SIE data. The input-independent model underestimated the extent of rH1N2 infection to a greater extent than the input-dependent model (Fig 3.1B). The input-independent model further systematically underestimated the extent of double (H3+H1+) infection at low rH3N1 input MOI, while systematically overestimating these measurements at high rH3N1 input MOI (Fig 3.1B). In contrast, the input-dependent model was better able to reproduce the double (H3+H1+) infection measurements across all experimental MOIs (Fig 3.1B). As anticipated from these patterns, we found that the input-dependent model was significantly better supported by the data than the input-independent model. In Fig 3.1C, we show the relationship between cellular input and susceptibility to superinfection predicted by this input-dependent model, indicating a rapid decline in susceptibility to superinfection with rH1N2 at 6 hpi at increasing levels of rH3N1 virus input.

These results demonstrate that the strength of SIE increases with the increase of primary infection MOI, which is in consistent with our previous finding that susceptibility to superinfection is inversely correlated with the cellular dosage of replication complexes delivered by incoming virions. Thus, the MOI-dependence of SIE may serve as a negative feedback loop that restricts the maximum number of virions that can successfully infect a given cell.

SIE is largely independent of host innate immune response

The host innate immune response serves as the first line of defense against viral infection. It is possible that the antiviral state induced by innate immune response to infection suppresses the subsequent infection. We hypothesized that SIE is mediated by host innate antiviral response triggered by the primary infection. We anticipated that there are multiple antiviral signaling pathways that contribute to SIE.

To determine which antiviral pathway is involved in SIE, we compared SIE between wild-type cells and cells lacking expression of specific individual host factors involved in different antiviral pathways. We repeated superinfection with rH3N1 and rH1N2 viruses as described before at low MOI (<0.3 TCID50/cell) in wild-type and CRISPR knockout (KO) human foreskin fibroblasts (hFF) lacking expression of IRF3 (transcription factor of type I IFN), PKR (ISG that inhibits viral protein synthesis), STING (sensor of cytosolic DNA associated with viral infection)(Franz et al. 2018), MyD88 (adaptor protein involved in TLR signaling), and MAVS (activator of NF-κB and IRF3). Surprisingly, the level of SIE measured by the decrease in superinfection rate in 6-hr

group relative to 0-hr group were comparable between wild-type and most KO hFF, indicating expression of the host factors are not required for SIE (Fig 3.2A,B). The only group in which we observed a moderate decrease of SIE was the STING KO. We thus validated this result by repeating the experiment in A549 cells which is a more biologically relevant cell line. However, there was no difference in SIE between wild-type and STING KO A549 cells (Fig 3.2C). Finally, we repeated the experiment in IFIT2 KO HEK293 cells to test the effects of IFIT2, an ISG that is highly relevant to IAV infection(Zhou et al. 2013). Again, we observed no difference in SIE (Fig 3.2D). In these experiments, the hFF and A549 cells were gifted by Dr. Victor DeFillippis and the HEK293 cells were gifted by Dr. Andrew Mehle.

These results indicate that SIE does not solely depend on expression of the host factors or the antiviral signaling pathways that we tested. Consistent with our previous finding that SIE is independent of type I IFN secretion, our data suggest that SIE is largely independent of host innate immune response.

SIE cannot be fully explained by decrease in viral binding efficiency

To better understand the mechanisms of SIE, we wanted to determine the viral replication step that is inhibited during superinfection. By determining when and where SIE actually occurs, we can focus on investigating the viral and host factors involved in that particular viral replication step. We set out to test whether SIE occurs at the beginning of viral life cycle, binding of virus particles to the host cell surface. Previously we have shown that

SIE is independent of viral NA activity, we thus hypothesized that SIE does not occur at the step of viral binding.

Since the level of SIE is positively correlated with MOI of the primary infection (Fig 3.1C), we amplified SIE to increase the chance of seeing any effects by repeating superinfection experiment described above with rH3N1 and rH1N2 viruses at high MOI (3 TCID50/cell). As expected, with a MOI of 3, over 95% of the superinfection in 6-hr group was blocked by the primary infection (Fig 3.3A). To determine whether this blockage occurred at the binding step, we measured rH1N2 titers in the inoculum before and after the 1-hr adsorption using RT-qPCR and calculated the titers of rH1N2 adsorbed to cell monolayers by subtracting titers of post-adsorption inoculum from pre-adsorption inoculum. As shown in Fig 3.3B, around 80% of rH1N2 adsorbed to cell monolayers in 0-hr group where there was no SIE and around 60% of rH1N2 adsorbed in 6-hr group, indicating a 25% decrease in binding efficiency which is significantly lower than the 95% blockage in superinfection.

Together, although our data showed that the binding efficiency is decreased in 6-hr delayed superinfection, it seems to be a minor contributor to SIE, suggesting the majority of SIE likely occurs post-binding.

3.3 Discussion

In this study, we first demonstrated that the primary infection MOI is positively correlated with the level of SIE which is in consistent with our previous findings. This

dose-dependent fashion indicates that the extent of cellular co-infection is a major determinant of viral replication and transmission. Under low MOI conditions where co-infection is rare, most infected cells are infected by single semi-infectious particle and the average number of functional viral gene segments within each infected cell are relatively low. As a result, SIE remains less potent, so most infected cells can be complemented via superinfection. Under high MOI condition where co-infection is common, most infected cells contain more than one copy of viral genomes so that the SIE is highly activated, leaving infected cells refractory to superinfection. Clearly superinfection-mediated multiplicity reactivation under low MOI increases viral replicative potential, but what is the biological significance of inhibiting superinfection under high MOI remains unclear.

While we showed that SIE is independent of multiple antiviral signaling pathways that have been shown to play crucial roles against IAV infection, it is still possible that SIE is mediated by combinations of more than one antiviral pathway we tested or by the pathways we didn't test, such as activation of inflammasome. In addition, the host innate immune response is highly variable among infections of different IAV strains in different cell types. Thus, we cannot completely rule out the role of host antiviral mechanisms on SIE even if our data strongly suggest they are irrelevant.

Interestingly, despite we previously showing that SIE is independent of NA activity, we still observed a 25% drop in viral binding efficiency in 6-hr delayed superinfection. Importantly, not all virus particles that bind to cell surface are going to be endocytosed. SIE can occur in any post-binding stage of viral replication cycle, including endocytosis,

membrane fusion, nuclear import and replication of viral genome. Images from high resolution microscopy on fluorescently labeled genomes of superinfecting virus showed that SIE occurs as early as 3 hours post-infection and a sizable number of viral genomes fail to make it to nucleus(Dou et al. 2017). Importantly, this study also revealed that viral genomes that entered the nucleus were not replicating, indicating SIE also occurs after nuclear import. Therefore, combining our results on viral binding, it is very likely that SIE results from the additive inhibitory effects on superinfecting viruses at multiple stages of viral replication cycle. To determine what percentages of superinfection are inhibited at each step of replication cycle, a time course study with single-molecule resolution microscopy is needed to more accurately localize and quantify the genomes from superinfecting viruses.

To conclude, this study revealed that viral co-infection level is positively correlated with the strength of SIE and host innate antiviral response is likely not a major contributor to SIE. In addition, decrease in viral binding efficiency is a minor contributor to SIE, indicating majority of SIE occurs post binding. Altogether, our results shed new light on the mechanisms of SIE and provide insights on basic biology IAV infection.

3.4 Materials and methods

Cells

Madin-Darby canine kidney (MDCK) and human embryonic kidney HEK293T (293T) cells were maintained in Gibco's minimal essential medium (MEM) with GlutaMax (Life Technologies). Vero cells and human foreskin fibroblast (hFF) cells were maintained in

Dulbecco's modified Eagle medium (Life Technologies). Human lung epithelial A549 cells were maintained in Gibco's F-12 medium (Life Technologies). MDCK and Vero cells were obtained from Jonathan Yewdell; wild-type and CRISPR KO hFF and A549 cells were obtained from Victor DeFillippis; wild-type and CRISPR KO HEK293 cells were obtained from Andrew Mehle. All media were supplemented with 8.3% fetal bovine serum (Seradigm). Cells were grown at 37°C and 5% CO_2.

Viruses

Recombinant rH3N1 and rH1N2 viruses were generated using 8-plasmid rescue systems. The rH3N1 virus is a reassortant with the HA segment from A/Udorn/72 (H3N2) and the other 7 segments from A/Puerto Rico/8/1934 (PR8). The rH1N2 virus is a reassortant with the NA segment from A/Udorn/72 (H3N2) and the other 7 segments from A/Puerto Rico/8/1934 (PR8). The PR8 clones differ from the published sequence (GenBank accession no. AF389115 to AF389122) at two positions: PB1 A549C (K175N) and HA A651C (I207L) (numbering from initiating Met). All viruses were rescued by transfecting subconfluent 293T cells with 500 ng of each of the appropriate reverse genetics plasmids using JetPRIME (Polyplus) according to the manufacturer's instructions. Plaque isolates derived from rescue supernatants were amplified into seed stocks in MDCK cells. Working stocks were generated by infecting MDCK cells at a MOI of 0.0001 $TCID_{50}$/cell with seed stock and collecting and clarifying supernatants at 48 hpi. All viral growth was carried out in MEM with 1 ug/ml trypsin treated with L-(tosylamido-2-phenyl) ethyl chloromethyl ketone (TPCK-treated trypsin; Worthington), 1 mM HEPES, and 100 ug/ml

gentamicin. The titers of the virus stocks were determined via standard 50% tissue culture infectious dose ($TCID_{50}$) assay.

Superinfection assay

For the 6hr superinfection group in Fig 3.1, confluent MDCK cells in six-well plates were infected with rH3N1 virus at intended MOIs of 0.05, 0.25, 1, 2.5, and 10 TCID50/cell respectively at 4°C. 1 hour post-adsorption, remaining inoculum was collected, monolayers were washed with PBS and incubated in MEM + 8.3% FBS. At 6 hpi, monolayers were superinfected with rH1N2 at MOI=0.5 TCID50/cell at 4°C. One-hour post-adsorption, monolayers were washed with PBS and incubated in MEM + 8.3% FBS. At 9 hpi of rH3N1 (3 hpi of rH1N2), the media was changed to MEM with 50 mM HEPES and 20 mM NH4Cl to block spread of both viruses. For the 0hr co-infection group, cells were infected with a mixture of rH3N1 and rH1N2 at the same MOIs as in 6hr superinfection group. At 3 hpi, 20 mM NH4Cl was added to block viral spread. For both 0hr and 6hr groups, at 19 hpi of rH3N1 (13 hpi of rH1N2), cell monolayers were trypsinized into single-cell suspensions and stained with Alexa Fluor 647-conjugated mouse anti-H3 MAb H14-A2 and Alexa Fluor 488-conjugated mouse anti-H1 mAb H28-E23 (gifts of Dr. Jon Yewdell). After staining, cells were washed with PBS, run on a BD LSR II, and analyzed using FlowJo version 10.1 (Tree Star, Inc.). For superinfection in Fig 3.2, the MOI of both rH3N1 and rH1N2 were less than 0.3 $TCID_{50}$/cell, whereas the MOI of both rH3N1 and rH1N2 were 3 $TCID_{50}$/cell for superinfection in Fig 3.3.

Measurement of adsorbed virus titers by RT-qPCR

To quantify the actual amount of rH3N1 and rH1N2 virus adsorbed to cell monolayers within the 1-h adsorption in Fig 3.1 and Fig 3.3, we quantified virus genome equivalents present in both pre- and post-adsorption inoculum by RT-qPCR and use pre-adsorption genome equivalents to minus post-adsorption genome equivalents. Specifically, viral RNA was isolated from viral supernatant with Zymo vRNA 96-well extraction kit (Zymo Research) according to manufacturer's instructions, eluted with 30 uL RNase free water, and stored at −70°C. For cDNA synthesis, 5 uL vRNA, 0.5 uL 10 mM dNTP mix (Sigma-Aldrich), and 1.0 uL Uni12 (AGCAAAAGCAGG) were incubated at 65°C for 5 minutes then transferred to ice for 2 minutes. 1 uL SUPERase In RNase inhibitor (20 U/uL; Thermo Fisher Scientific) was added to each mixture and incubated on ice again for 2 minutes. 6.5 uL dH_2O, 4 uL 5X First-Strand Buffer, 1 uL 100 mM DTT, and 1 uL SuperScript III RT (200 U/uL; Thermo Fisher Scientific) were added to each reaction and incubated at 55°C for 60 minutes and heat inactivated at 70°C for 15 minutes. Genome equivalents (GE) of rH3N1 were estimated by RT-qPCR of N1 gene segment (F-AAATCAGAAAATAACAACCATTGGA, R- ATTCCCTATTTGCAATATTAGGCT) and GE of rH1N2 were estimated by RT-qPCR of H1 gene segment (F-AAGGCAAACCTACTGGTCCTGTT, R-AATTGTTCGCATGGTAGCCTATAC). In duplicate for each sample, 10 uL Power SYBR Green PCR master mix (Thermo Fisher Scientific), 0.5 uL 10 uM forward and reverse primers, 8 uL dH_2O, and 1 uL cDNA were added to 0.2 mL MicroAmp Optical 96-well reaction plate (Thermo Fisher Scientific). RT-qPCR was performed on the QuantStudio 3 (Thermo Fisher Scientific) platform and the cycling conditions were as follows: 95°C for 10 minutes, 40 cycles of 95°C for 15

seconds and 60°C for 60 seconds. The standard curves established with pDZ-N1 and pDZ-H1 plasmids were used to estimate GE/uL and then each sample was corrected for dilution factor to give a final GE/mL.

Statistical modeling of superinfection exclusion

The statistical modeling was performed by Dr. Katia Koelle using our experimental data. We first developed and parameterized an appropriate 'null' model, where both viruses are introduced simultaneously, and superinfection exclusion would not be anticipated. In this model, we assumed that cells differed in their susceptibility to viral infection. This assumption reflects our finding that viral particles are unlikely to be Poisson-distributed across cells. In our null model, we did not adopt a negative binomial model to implement the possibility of viral particle overdispersion, as we had earlier, because if both reassortant viruses were assumed to be distributed according to a negative binomial distribution, viral particles (together) would not be distributed according to a negative binomial distribution. We instead considered a model that implemented different cell susceptibility classes, which we found to better accommodate viral overdispersion of distinct viral strains. To maintain simplicity, we considered only two types of cells: cells that had high susceptibility to infection and cells that had low susceptibility to infection. We defined fraction y of the cell population to be in low susceptibility state; the remaining fraction $(1 - y)$ we assumed was in a high susceptibility state. We let a fraction x of the viral population enter the low susceptibility state cells; the remaining fraction of the viral population $(1-x)$ we assumed entered the high susceptibility state cells. Under this model, the MOI of specifically the low susceptibility class of cells is

given by (input MOI)*(x/y), and the MOI of specifically the high susceptibility class of cells is given by (input MOI)*(1 - x)/(1 - y). When $x = y$, the Poisson distribution assumption is recovered, and both classes of cells have the same input MOI. We fit this simple model to the co-infection data, estimating three parameters: the actual rH1N2 MOI, and the fractions x and y. The parameter values, estimated using an RSS approach, are actual rH1N2 MOI = 1.86 (95% CI = [1.71,2.03]), x = 2.14e-4 (95% CI = [0.334e-4, 13.8e-4]), and y = 0.0526 (95% CI = [0.0381,0.0725]). This parameterized model fit the experimental data well (Fig 3.1A). Since the parameter x was estimated to be close to 0, this model effectively implemented the zero-inflated Poisson model, which had slightly lower statistical support than the negative binomial distribution.

To analyze the data from the superinfection experiment, we set as given the three parameter values and simple two-state susceptibility model structure derived from the fitting of the data from the simultaneous co-infection experiment described above. We then considered two distinct models to determine how cellular MOI may impact the rate of superinfection exclusion: an input-independent model and an input-dependent model. The input-independent model assumed that all infected cells had the same lower chance of being superinfected than previously uninfected cells. The parameter s quantified the extent of susceptibility of the previously infected cells (1 being full susceptibility). The input-dependent model instead assumed that cells that were infected with rH3N1 could experience different probabilities of superinfection exclusion. These different probabilities depended on a rH3N1 virus input, with, presumably, higher levels of rH3N1 virus input corresponding to higher probabilities of superinfection exclusion. For the

input-dependent model, we specifically assumed a functional form given by r^i, where i denotes rH3N1 virus input and $0 \leq r \leq 1$. We estimated s for the input-independent model to be 0.0361 (95% CI = [0.0227, 0.0576]) and r for the input-dependent model to be 0.293 (95% CI = [0.214, 0.402]).

To perform model selection, we used the Akaike Information Criterion (AIC). AIC based on RSS values is given by the equation: $2k + n \ln(\text{RSS}) + \text{constant}$, where k is the number of estimated parameters and n is the number of data points. Since AIC is a relative measure of information loss and the model with the lowest AIC has the most support, we calculated ΔAIC values to perform model selection by taking the difference between a given model and the model with the lowest AIC value. Based on AIC, the input-dependent model is strongly preferred over the input-independent model (ΔAIC = 22.0).

3.5 Figures

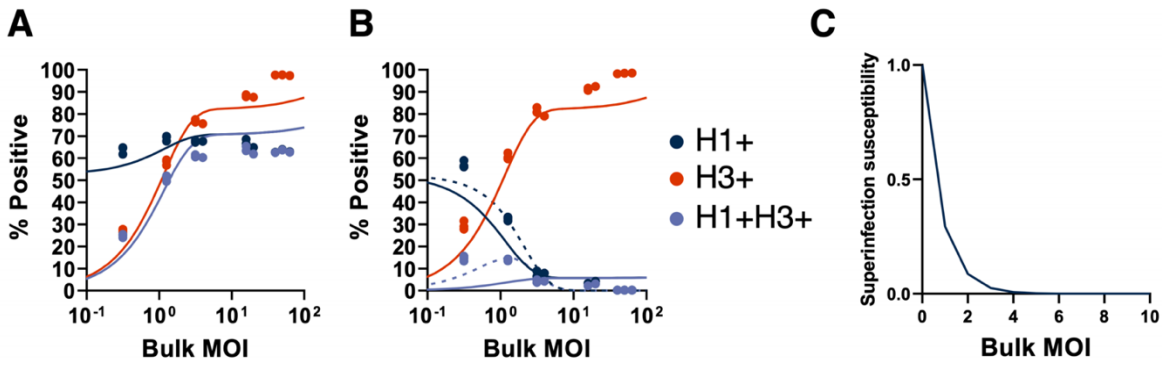

Figure 3.1 Cellular co-infection decreases the potential for superinfection. (A) MDCK cells were simultaneously co-infected with rH1N2 (at a constant MOI) and rH3N1 (at varying input MOIs shown; x-axis) under single cycle conditions; SIE would not be expected to occur during simultaneous co-infection. Plot shows the percentages of all cells infected with rH1N2 (H1+; includes co-infected cells; dark blue), all cells infected with rH3N1 (H3+; includes co-infected cells; red), and cells co-infected with both (H3+H1+; light blue), as determined by flow cytometry at 19 hpi. Solid lines indicate the two-susceptibility state null model fit to these data. (B) MDCK cells were infected with rH3N1 at varying input MOIs (x-axis) under single cycle conditions. 6 hours later, cells were superinfected with rH1N2 at an intended MOI of 0.5 TCID50/cell. Percentages of cells that were H1 + (including cells co-infected with rH3N1), H3+ (including cells co-infected with rH1N2), and H3+H1+ were determined by flow cytometry at 19 hpi. Lines indicate statistical fits of the input-independent (solid) and input-dependent (dashed) models. (C) Visualization of the input-dependent model of superinfection susceptibility where the susceptibility of infected cells to superinfection is shown relative to the susceptibility of uninfected cells.

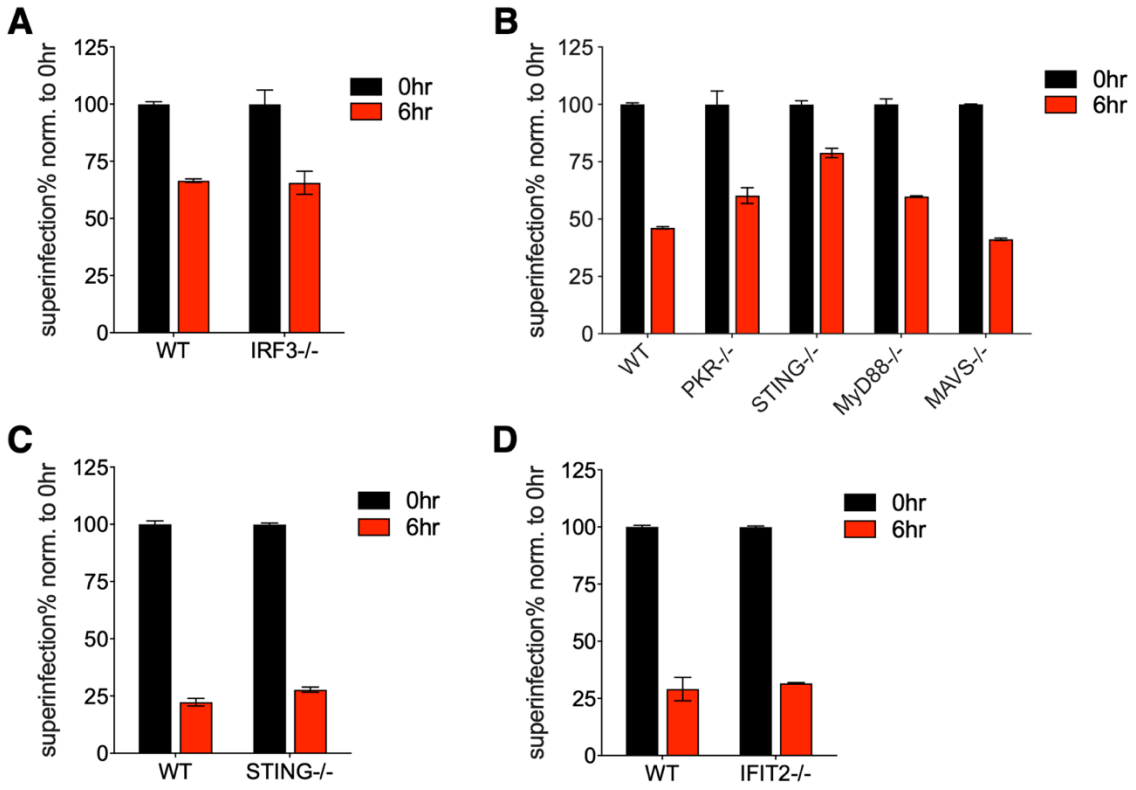

Figure 3.2 SIE is largely independent of the expression of specific individual host factors involved in innate immune response. The wild-type hFF (A,B), A549 cells (C), HEK293 cells (D), and their CRISPR KO cell lines lacking expression of indicated individual host factors were infected with rH3N1 virus and were simultaneously (0hr) or sequentially (6hr) infected with rH1N2 virus; all infections were performed at MOI<0.3 $TCID_{50}$/cell. $H1^+$ frequencies within $H3^+$ cells following simultaneous or sequential infection in the indicated cell lines were measured as indicatives of superinfection rate. The values for both the 0-h and 6-h groups are shown as percentages of the mean values of the 0-h control group to clearly illustrate the percentages of reduction in cellular susceptibility to superinfection in the 6-h group. Data are presented as means (n = 3 cell culture wells) ± standard deviations.

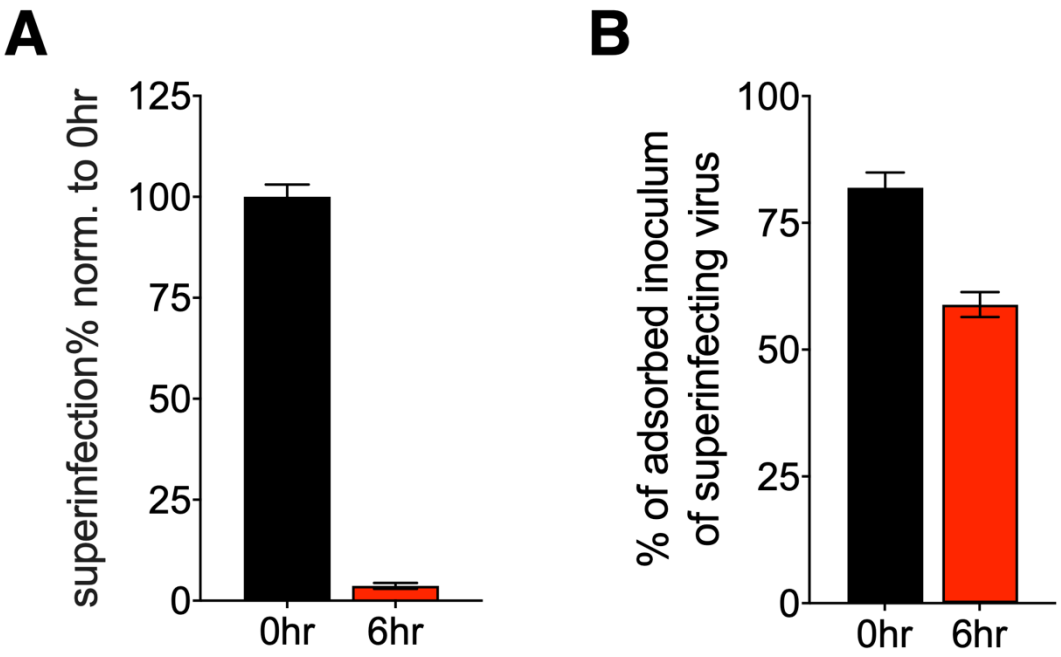

Figure 3.3 SIE cannot be fully explained by decrease in binding efficiency. (A) Vero cells were infected with rH3N1 virus and were simultaneously (0hr) or sequentially (6hr) infected with rH1N2 virus; all infections were performed at MOI=3 $TCID_{50}$/cell. $H1^+$ frequencies within $H3^+$ cells following simultaneous or sequential infection in the indicated cell lines were measured as indicatives of superinfection rate. The values for both the 0-h and 6-h groups are shown as percentages of the mean values of the 0-h control group to clearly illustrate the percentages of reduction in cellular susceptibility to superinfection in the 6-h group. (B) The percentages of rH1N2 virus inoculum adsorbed to cell monolayers during 1-h adsorption were measured by RT-qPCR for both 0-h and 6-h groups. Data are presented as means (n = 3 cell culture wells) ± standard deviations.

CHAPTER 4: SINGLE CELL HETEROGENEITY IN IAV GENE EXPRESSION SHAPES INNATE ANTIVIRAL RESPONSE

4.1 Introduction

RNA virus populations typically contain an enormous amount of sequence diversity due to an absence of virally encoded proofreading activity(Andino and Domingo 2015). In some cases, this genetic diversity can significantly influence infection outcomes(Bordería et al. 2015; Domingo-Calap et al. 2019; Xiao et al. 2017). In addition, influenza A virus (IAV) also exhibits substantial heterogeneity in the gene expression patterns of individual virions(Brooke 2017). Most IAV virions are only capable of expressing variable, incomplete subsets of viral genes(Brooke et al. 2013). The production and gene expression patterns of these semi-infectious particles (SIPs) can vary significantly between IAV strains(Brooke et al. 2014). Altogether, the high degree of diversity within IAV populations means that patterns of viral gene expression can vary significantly between individual infected cells.

Numerous studies have leveraged recent advances in single cell analysis methods to assess the extent of cellular heterogeneity present during infection by a variety of viruses, including IAV(Heldt et al. 2015; Russell, Trapnell, and Bloom 2018; Russell et al. 2019; Drayman et al. 2019; Guo et al. 2017; Ramos et al. 2019; Schulte and Andino 2014; Steuerman et al. 2018; Zanini et al. 2018; C. Wang et al. 2020). These studies connect to a larger body of work that has begun to explore single cell heterogeneity within different host cell populations and tissues(Lawson et al. 2018; Papalexi and Satija 2018; Stuart and Satija 2019).The extent to which IAV population diversity influences patterns of single

cell heterogeneity and the ways in which these patterns shape broader infection dynamics and outcomes remain poorly understood.

Here, we query the combined viral and host transcriptomes from thousands of individual cells, each infected by a single virion. This high-resolution dissection of viral and host gene expression patterns reveals that the transcriptional responses of individual infected cells can be highly divergent, resulting from the interplay between underlying cellular heterogeneity and viral population diversity. Thus, the host response to IAV infection consists of a heterogenous assemblage of highly variable single cell responses. This approach also reveals critical differences in the interactions of H1N1 and H3N2 viruses with the host antiviral machinery at the single cell level and implicates heterogeneity in NS segment expression as a major driver of the innate antiviral response to IAV infection. Altogether, these results establish the interplay between viral and host cell heterogeneity as a critical determinant of cellular infection outcomes.

4.2 Results

Generation of viral and host transcriptional data from thousands of singly infected cells

To assess the effects of viral population heterogeneity on the host response to infection, we examined the combined viral and host transcriptional profiles from thousands of single infected cells. To focus on the effects of viral heterogeneity, we wanted to remove the variability that could arise from variation in cellular MOI. To ensure that the vast majority of infected cells were each infected with a single virion, we infected A549 cells

with either the 2009 H1N1 pandemic strain A/California/07/2009 (Cal07), or the seasonal human H3N2 strain A/Perth/16/2009 (Perth09) at an MOI of 0.01, and blocked secondary spread in the culture through the addition of NH_4Cl(Martin and Helenius 1991). This resulted in only a tiny fraction of cells being infected, so to obtain sufficient numbers of infected cells for our analysis, we enriched infected cells by sorting based on surface expression of HA and/or M2 (Fig 4.1A). This approach had the added benefit of allowing us to sort HA-M2- bystander cells from the same culture to assess the paracrine effects of infection. In parallel, we sorted a group of mock-infected cells as a control.

We used the 10X Genomics Chromium platform to generate oligo-dT-primed single cell RNAseq libraries for mock, infected (HA+ and/or M2+), and bystander (HA-M2-) cells and sequenced them on an Illumina Novaseq. We demultiplexed the reads and mapped them to a customized hybrid reference containing both human and influenza sequences/annotation. Following quality control filtering, we had high quality combined viral and host transcriptomes from thousands of single virion-infected cells, as well as uninfected bystander and mock cells. Clustering of these three libraries by transcriptional similarity revealed that infected and uninfected cells largely clustered independently, as would be expected (Fig 4.1B,4.8). For Cal07 (but not Perth09), mock and bystander cells clustered independently, but it is possible this is due to a batch effects, as the mock and bystander cells came from different culture vessels.

Although we sorted infected cells based on the presence of viral markers, it is possible that some uninfected cells were included within the infected cell libraries due to a

combination of cell sorting errors, library index hopping, or cross-contamination with mRNA released from dying cells. To identify the truly infected cells within the infected libraries, we examined the distributions of percentage of viral counts within each cell (Fig 4.9). For cells in infected libraries of both Cal07 and Perth09, we observed clear bimodal distributions in the percentage of total viral counts. We assumed that cells within the lower peak (percentages of viral reads: < 1% for Cal07 and < 3% for Perth09) were actually uninfected. We calculated kernel density estimates on these distributions and used the first local minima to generate cutoff thresholds to differentiate truly-infected cells from uninfected cells (Fig 4.9A,C). Cells from infected libraries that fell below these thresholds clustered with the bystander cells, suggesting that these cells were truly uninfected (Fig 4.9B,D). We used this approach in subsequent analyses to define truly infected cells; however, it is possible that a small fraction of the cells we call as uninfected by these criteria are also truly infected yet exhibit very low levels of viral gene expression.

Enormous single cell heterogeneity in viral gene expression patterns

We first asked whether we observed the same degree of heterogeneity in viral gene expression between infected cells that has been reported previously(Brooke et al. 2013; Heldt et al. 2015; Russell, Trapnell, and Bloom 2018). We calculated the fraction of all transcripts within each cell that were viral in origin (Fig 4.2A). Similar to prior studies, total viral transcript levels ranged enormously between individual cells: from <1% up to ~90%. Notably, this heterogeneity arose under conditions where both viral input (1 virion/cell) and infection timing were largely equivalent across all cells.

Interestingly, the distributions for Cal07 and Perth09 were quite different, as Perth09-infected cells tended to have a much higher fraction of viral transcript. This could be a reflection of differences in gene expression kinetics, or of differences in the relative capacities of the two viruses to exploit the host cell machinery necessary for viral gene expression. This pattern of extreme cell-to-cell heterogeneity was also observed for individual viral transcripts, again consistent with previous reports (Fig 4.2B,C)(Russell, Trapnell, and Bloom 2018). We examined the degree to which individual pairs of viral genes were correlated with each other within infected cells that expressed all viral genes **(**Fig 4.10,4.11**).** For Cal07, we found that most pairs of viral transcripts were fairly well correlated, with one obvious exception: the NS segment (Fig 4.2D). Expression levels of the individual viral genes were generally less well correlated during Perth09 infection, compared with Cal07, and expression of both the M and NS segments by Perth09 was especially poorly correlated with the other viral genes (Fig 4.2E**)**.

We also found that the expression distributions for individual viral genes were highly over-dispersed compared with a Poisson distribution (Fig 4.2F). The tails of the expression distributions for several viral genes were an order of magnitude longer than those of the top 10 most abundant host transcripts (Fig 4.2G), emphasizing that viral gene expression is substantially noisier than host gene expression.

Significant heterogeneity in the host transcriptional response to infection

We next asked whether the observed variation in viral gene expression levels was associated with variation in host cell transcription. To test this, we first clustered all infected cells based on their host transcription patterns. We identified multiple distinct transcriptional response groups to infection by either Cal07 or Perth09, demonstrating that there is not one standard transcriptional response to IAV infection and that a single cell type can simultaneously generate multiple distinct responses to the same virus population (Fig 4.3A,D). It should be noted that these cluster definitions are not absolute and that substantial heterogeneity in the normalized expression levels of individual host genes existed within individual clusters.

We next asked whether the cell clustering patterns were correlated with levels of viral gene expression and/or cell cycle status. For Cal07, we did observe a relationship between overall viral gene expression levels and cluster structure, as the majority of cells with high levels of viral gene expression were concentrated in cluster 5 (Fig 4.3B). The clustering patterns of Cal07-infected cells also appeared to be partially influenced by cell cycle status, with cells in G2M phase disproportionately falling into cluster 0 (Fig 4.3C). While it is not surprising that cell cycle status would contribute to transcriptional heterogeneity during infection, these data highlight how little is known about how cell cycle status may influence the cellular response to infection. In contrast, we did not observe any clear relationships between viral gene expression levels, cell cycle status, and clustering pattern for Perth09-infected cells (Fig 4.3E,F).

We also observed the existence of multiple distinct clusters within mock cells (Fig 4.3G), raising the question of whether the observed heterogeneity in infected cells was simply a reflection of the intrinsic heterogeneity of the cell population prior to infection. In other words, does infection actually increase the overall heterogeneity in host gene expression patterns beyond that seen in mock cells? To quantify and compare heterogeneity in overall host transcription between the two cell populations, we calculated the multivariate homogeneity of dispersions for mock and infected cells using their host gene expression profiles (Fig 4.3H)(Anderson 2006). We found that infection significantly increased the overall single cell heterogeneity in host cell transcription patterns ($p<10^{-15}$ by pairwise t test). Altogether, our data are consistent with a model in which the interaction between viral population heterogeneity and pre-existing host cell heterogeneity gives rise to multiple distinct transcriptional responses at the single cell level.

Substantial heterogeneity in expression patterns of critical determinants of IAV infection outcome, including IFNs and ISGs

To explore the specific transcriptional differences that distinguished different clusters of infected cells, we performed single cell differential gene expression analysis which allowed us to compare the expression of host transcripts between different clusters(W. Chen et al. 2018; Finak et al. 2015). This approach revealed that the induction of numerous host genes known or likely to be involved in shaping IAV infection outcome varied significantly between clusters (Fig 4.4A,C). Most strikingly, for Perth09 (but not Cal07), expression of type III IFNs and several ISGs were heavily concentrated within a single cluster, cluster 5 (Fig 4.4C). Beyond obvious factors like the IFNs and ISGS, both

viruses, exhibited highly heterogeneous expression patterns of numerous other host genes likely to influence infection outcomes. For example, per-cell expression levels of NEAT1, a long non-coding RNA (lncRNA) involved in inflammasome formation, regulation of cytokine and chemokine expression, and nuclear paraspeckle formation(Landeras-Bueno and Ortín 2016; Sasaki et al. 2009; F. Zhang et al. 2016, 1; P. Zhang et al. 2019), varied significantly between infected cell clusters for both viruses (Fig 4.4B,D).

Hundreds of other host genes exhibited similarly heterogeneous patterns of expression between individual infected cells, though it must be pointed out that these measurements can be skewed somewhat by variation in viral RNA levels. Altogether, these data clearly demonstrate how numerous drivers of infection outcomes (not just IFNs) may be primarily expressed by limited subsets of infected cells.

Many infected cells have undetectable levels of one or more viral transcripts

The vast majority of IAV virions fail to express one or more viral genes, resulting in the expression of variable, incomplete subsets of viral gene products under low MOI conditions(Diefenbacher, Sun, and Brooke 2018). We asked whether this variation in functional viral gene content within individual cells contributes to the observed heterogeneity in host gene transcription. To assess the presence or absence of each individual viral gene within infected cells while avoiding false positives due to RNA cross-contamination, we used the same approach that we used to determine infection status of cells in infected libraries. Just as with overall viral gene expression, nearly all

individual viral genes exhibited clear bimodal patterns in the distributions of viral gene percentage within each cell on a log scale, suggestive of clear separations between positive and negative populations and allowing us to set cutoff thresholds based on the first local minima (Fig 4.12A,B). The only exceptions were PB2 and PA of Cal07. For these two genes that did not exhibit clear bimodal distribution, we set the cutoff thresholds at -1.5 (log10 scale) based on the distributions of polymerase gene expression in Perth09 and uninfected cells within the infected library of Cal07. It must be noted that while these cutoff thresholds represent our best effort to define the expression statuses of individual viral genes, they may not be perfectly accurate.

Using these cutoffs, we found that the fractions of infected cells that failed to express detectable transcripts ranged from ~35% to ~5% for the individual viral gene segments (Fig 4.5A,C). It is highly likely that our method of enriching for infected cells by sorting based on high level HA and/or M2 expression significantly biased these results. Regardless, we still observed substantial numbers of infected cells that fail to express detectable levels of individual viral transcripts, with roughly half of all infected cells failing to express detectable levels of at least one viral gene (Fig 4.5B,D). We were surprised to see so many cells that lacked detectable levels of the polymerase transcripts because we expected that sorting infected cells based on surface protein expression would bias cell collection against cells that could not synthesize new polymerase complexes. One important caveat with our approach is that we assessed transcript levels at 16 hpi and thus could have missed transient early expression of viral genes.

The absence of individual viral genes has a significant effect on the host transcriptional response to infection

We next asked how the expression status of individual viral genes influences the overall host response to infection to both Cal07 and Perth09. We grouped all infected cells into positive and negative populations based on the expression of each individual viral gene segment and compared host transcript expression between the two infected cell populations. For each viral gene, we generated a list of host transcripts that were reported as significantly different between positive and negative cells by both NBID and MAST tests. This approach allowed us to tease out the effects of individual viral gene segments from the more general effects of infection.

We identified hundreds of host genes with expression levels that varied significantly based on the expression status of individual viral genes (Fig 4.13A,B). Closer examination revealed that many of these hits were found for multiple viral genes, suggesting that they may correlate with overall viral gene expression levels or co-expression of multiple viral gene segments. When we focused on the host genes that only exhibited differential expression in association with the expression status of a single viral gene segment, we found that most were associated with the PA and NS segments (Fig 4.6A,D).

NS segment expression status is a major determinant of IFN and ISG induction by Perth09, but not Cal07

We focused on the NS segment, as the NS-encoded NS1 protein plays a well-established, multi-functional role in manipulating the host cell environment and the anti-viral response and could thus serve as a positive control for our approach(Ayllon and García-Sastre 2015; Hale et al. 2008; Krug 2015; Marc 2014). We found that approximately 4% of Cal07-infected cells and 9% of Perth09-infected cells had background or undetectable levels of NS segment transcript, and most of them came from cluster 5 with high viral transcript level which was in consistent with low correlation value between NS and other segments (Fig 4.6B,E). For Cal07, we observed over 300 host genes whose expression was uniquely influenced by NS. Notably, the expression of specific IFNs or ISGs was not significantly affected by NS expression status during Cal07 infection. In contrast, we did observe a significant reduction in SLFN5 expression frequency in infected cells that failed to express NS compared with those that did express NS (Fig 4.6C). SLFN5 is an interferon-stimulated gene (ISG) shown to negatively regulate STAT1-dependent anti-viral gene transcription(Arslan et al. 2017, 5). These results both validate the utility of our approach and identify the suppressor of antiviral gene transcription SLFN5 as a novel host target of the NS gene segment during Cal07 infection.

In contrast with Cal07 infection, NS segment expression status for Perth09 was significantly correlated with expression levels of numerous IFNs, ISGs, and other innate immune factors (Fig 4.6F). For example, the type III IFNs IFNL1 and IFNL2 were expressed by ~20% of Perth09-infected cells lacking detectable NS expression, but both

were only observed in ~2% of infected cells that did express NS. We also observed similar NS-dependent expression patterns for several ISGs (e.g. IFIT1, IFIT2, IFIT3, ISG15, ZC3HAV1, and OAS1), as well as the neutrophil-recruiting chemokine CXCL1. Thus, for Perth09 but not Cal07, single cell heterogeneity in NS segment expression status is a major determinant of the activation of the innate antiviral response.

H1N1 and H3N2 strains can differ significantly in single cell patterns of IFN and ISG transcription

Finally, we more broadly compared the activation of host innate anti-viral gene expression at the single cell level between Cal07 and Perth09. In Cal07-infected cells, expression of both type I and III IFNs were extremely rare, and only IFNL1 passed our quality control filter (detected in more than 4 cells) (Fig 4.7A)(Russell et al. 2019; Killip et al. 2017). For type I IFN (but probably not type III IFN), this could partially be a function of the relatively late timepoint that we examined, as IFNβ expression typically peaks earlier during infection(Österlund et al. 2012). Similarly, expression of multiple ISGs was also very rare in Cal07-infected cells, indicating a near-complete failure to initiate an innate anti-viral response. In bystander cells, both IFN and ISG expressions were also minimal, suggesting that the inhibition of IFN induction by Cal07 was sufficient to largely prevent paracrine ISG activation (Fig 4.7B).

In Perth09-infected cells, IFNL1 (type III IFN) transcription was roughly 20-fold more frequent compared with Cal07, indicating a significant difference in the ability of the host to initiate an IFN response to infection by these two strains (Fig 4.7C). Consistent with

this, some (but not all) ISGs were clearly expressed more frequently in bystander and Perth09-infected cells compared with Cal07, suggesting that Perth09 is less able to prevent paracrine activation (Fig 4.7D). Altogether, these data reveal clear differences in single cell patterns of IFN and ISG transcription between the human H1N1 and H3N2 strains tested.

4.3 Discussion

The host response to infection arises from the combined responses of many individual cells, both infected and uninfected. To understand the factors that govern host responses at the tissue and organismal levels, it is critical to define patterns of variation in single cell infection responses. Here, we demonstrate that IAV infection gives rise to a heterogeneous collection of divergent transcriptional responses at the single cell level. Notably, this heterogeneity occurred within a single cell type, under conditions where per-cell viral input and infection timing were normalized. Single cell responses *in vivo* may be significantly more variable. By comparing patterns of viral gene expression at the single cell level between two distinct strains of human IAV, we demonstrate how viral population heterogeneity can be a major driver of innate immune activation, in a virus strain-specific manner. These data establish a clear role for viral heterogeneity in modulating the host response to infection and highlight the power of single cell approaches to reveal new determinants of viral infection outcomes.

Variation in gene expression patterns between individual infected cells appears to arise from a combination of (1) genetic and genomic variation between individual virions, (2)

underlying heterogeneity within host cells, and (3) stochastic variation in infection processes. In line with previous reports of significant genetic and phenotypic heterogeneity within A459 and other transformed cell line populations, we observed substantial transcriptional heterogeneity between uninfected A549 cells that could not be simply explained by cell cycle status(Ben-David et al. 2018; Croce et al. 1999; Watanabe et al. 2002). As a result, virions that enter different cells establish infection within differing cellular environments that may be more or less supportive and primed for differing transcriptional responses to infection. This effect is likely enhanced by the stochastic variation inherent in different viral life cycle stages(Dou et al. 2017).

Layered on top of this intrinsic cellular heterogeneity and stochasticity is the genetic and genomic heterogeneity characteristic of IAV populations(Brooke 2017). We and others have previously demonstrated that well-characterized viral modulators of host cell function such as NS1 and PA-X are not ubiquitously expressed during infection(Brooke et al. 2013; Russell, Trapnell, and Bloom 2018). Here, we show that this variability in viral gene expression between individual infected cells has clear consequences for the host cell transcriptional response. It is clear that future efforts to understand the role of critical viral proteins such as NS1 in shaping infection outcome will have to account for heterogeneity in single cell expression patterns.

The comparison of Cal07 and Perth09 revealed clear commonalities and differences in single cell expression patterns between the two viruses that may have relevance for understanding differences in the apparent pathogenicity of different human H1N1 and

H3N2 viruses. The most obvious difference was seen in the activation of IFN and ISG transcription. In addition, while NS segment expression status significantly influenced the host response to both viruses, only Perth09 showed a clear relationship between NS levels and the activation of the host antiviral machinery. This finding is in line with previous studies that showed that (a) different human IAV strains differ in bulk induction of IFNβ, and (b) the 2009 pandemic H1N1 NS1 protein was less effective at suppressing transcription of human IFNs and ISGs compared with NS1 genes from other human IAV isolates(Hale et al. 2010; Hayman et al. 2006). While *de novo* NS segment transcription appeared to be largely dispensable for blocking IFN and ISG upregulation by Cal07 (at least under the conditions examined in this study), overall expression frequencies for select IFNs and ISGs were actually lower during Cal07 infection compared with Perth09, indicating that Cal07 is more effective at suppressing or evading IFN activation in A549 cells. Yet, it remains an open question how overall viral gene expression level might influence the host innate antiviral response, given the clear differences we observed between the two viruses. Overall, our data make clear that there is still a lot that we do not understand about the interplay between viral gene expression patterns, viral genotype, and the host antiviral response.

In this study, we took steps to eliminate two other sources of viral heterogeneity that are likely common during natural IAV infection. The first is presence of defective interfering particles (DIPs), which we minimized by generating our virus stocks under low MOI conditions, and subsequently verified (Fig 4.14). DIPs appear to be common within IAV populations, even in humans, and can have complicated effects on both viral and host

gene expression(Nayak, Chambers, and Akkina 1985; Russell et al. 2019; Alnaji et al. 2019; Saira et al. 2013; Vasilijevic et al. 2017; Vignuzzi and López 2019). We would predict that the presence of DIPs would further increase overall heterogeneity between individual cell responses to the virus. It is worth noting that we could not reliably detect the presence of DIP-associated transcripts within our data due to the unavoidably incomplete coverage of the viral gene segments generated by our short-read 3'-enriched sequencing approach. The second likely source of additional heterogeneity that we excluded from this study is variability in the cellular MOI. We and others have demonstrated that cellular co-infection can be common *in vivo*(Brooke et al. 2014; Marshall et al. 2013; Fukuyama et al. 2015; Jacobs et al. 2019). This suggests that the number of viral genomes entering individual cells is likely quite variable. We recently showed that this variability in cellular MOI can have distinct phenotypic consequences, both for viral replication dynamics and for IFN induction. Altogether, it appears likely that the heterogeneity that we describe here underrepresents what would be observed *in vivo*.

Our results extend our previous results and those of other groups in establishing the enormous amount of heterogeneity in viral gene expression that occurs at the single cell level, even under experimental conditions designed to minimize sources of variability(Dou et al. 2017; Brooke et al. 2013; Heldt et al. 2015; Russell, Trapnell, and Bloom 2018; Sjaastad et al. 2018). Critical phenotypes such as viral load dynamics, transmissibility, and pathogenicity must emerge from the collective output of heterogeneous populations of infected cells. This raises questions of how selection may

act upon patterns of viral heterogeneity to alter these emergent phenotypes and the extent to which these heterogeneity patterns are under viral genetic control. These questions are especially pertinent for segmented viruses like IAV but are relevant across diverse virus families.

Altogether, our results help establish the importance of considering the roles of viral and host cell heterogeneity in influencing the pathogenesis of viral infections. Similar to the way that viral populations are now viewed, our data clearly establishes that the host response to infection should be seen as a heterogeneous assemblage of single cell responses that collectively give rise to the bulk phenotypes that are generally measured. This creates the potential for complex interactions between responding cell subsets and raises the question of how such a heterogeneous system is effectively regulated. It also raises the possibility that viral and host response dynamics may be disproportionately driven by small subsets of cells that are obscured during bulk analysis. Dissection of these diverse constituents is likely to reveal new mechanisms that govern the pathogenesis of influenza virus infection.

4.4 Materials and methods

Plasmids

The A/California/04/09 and A/Perth/16/2009 reverse genetics plasmids were generous gifts from Drs. Jonathan Yewdell and Seema Lakdawala, respectively. Plasmids encoding A/California/07/09 were generated by introducing A660G and A335G substitutions into

HA and NP respectively, to match the amino acid sequences of A/California/07/09 HA and NP (NCBI accession numbers CY121680 and CY121683).

Cells

Madin-Darby canine kidney (MDCK) and human embryonic kidney HEK293T (293T) cells were maintained in Gibco's minimal essential medium with GlutaMax (Life Technologies). Human lung epithelial A549 cells were maintained in Gibco's F-12 medium (Life Technologies). MDCK and A549 cells were obtained from Dr. Jonathan Yewdell; 293T cells were obtained from Dr. Joanna Shisler. All media were supplemented with 8.3% fetal bovine serum (Seradigm). Cells were grown at 37°C and 5% CO2.

Viruses

Recombinant A/California/07/09 (Cal07) and A/Perth/16/2009 (Perth09) viruses were rescued via the 8-plasmid reverse genetics approach. For the rescue of both viruses, sub-confluent 293T cells were co-transfected with 500 ng of the following plasmids: pDZ::PB2, pDZ::PB1, pDZ::PA, pDZ::HA, pDZ::NP, pDZ::NA, pDZ::M, and pDZ::NS, using JetPrime (Polyplus) according to the manufacturer's instructions. Plaque isolates derived from rescue supernatants were amplified into seed stocks in MDCK cells. Working stocks were generated by infecting MDCK cells at a MOI of 0.0001 $TCID_{50}$/cell with seed stock and collecting and clarifying supernatants at 48 hpi. All viral growth was carried out in MEM with 1 ug/ml trypsin treated with L-(tosylamido-2-phenyl) ethyl chloromethyl ketone (TPCK-treated trypsin; Worthington), 1 mM HEPES, and 100 ug/ml

gentamicin. The titers of the virus stocks were determined via standard 50% tissue culture infectious dose ($TCID_{50}$) assay.

Viral infection and cell sorting for single cell RNAseq

Confluent A549 cell monolayers in 3 T-25 flasks were infected with Cal07 (or Perth09) at MOI of 0.01 $TCID_{50}$/cell for 1 h. At 1 hpi, monolayers were washed with phosphate-buffered saline (PBS) and incubated in serum-containing F-12 medium. At 3 hpi, the medium was changed to MEM with 50 mM HEPES and 20 mM NH_4Cl to block viral spread. At 16 hpi, monolayers were trypsinized and combined into single-cell suspension and washed with PBS. Cal07-infected cells were stained with Alexa Fluor 488-conjugated mouse anti-HA monoclonal antibody (mAb) EM4-CO4 (gift from Dr. Patrick Wilson) and Alexa Fluor 647-conjugated mouse anti-M2 mAb O19 (gift from Dr. Jonathan Yewdell). Perth09-infected cells were first stained with human anti-HA stem antibody FI6 (Gift from Dr. Adrian McDermott) and then stained with Alexa Fluor 488-conjugated donkey anti-human IgG (Jackson ImmunoResearch). After staining, cells were washed with PBS twice, and single live cells were sorted as “infected” or “bystander” populations based on the expression of HA and M2 on a BD FACS ARIA II sorter. Importantly, uninfected A549 cells from a separate flask were also trypsinized, stained, and sorted as “mock” population which served as a negative control.

Single cell RNAseq cDNA library generation

Sorted cell samples were counted and checked for viability on a BD20 cell counter (BIO-RAD) before they were diluted to equivalent concentrations with an intended capture of

4000 cells/sample. Each individual sample was used to generate individually barcoded cDNA libraries using the 10x Chromium Single Cell 3' platform (Pleasanton, CA) following the manufacturer's protocol. The Chromium instrument separates single cells into Gel Bead Emulsions (GEMs) that facilitate the addition of cell-specific barcodes to all cDNAs generated during oligo-dT-primed reverse transcription. The experiment with Cal07 used V2 reagent and the experiment with Perth09 used V3 reagent (all steps followed the manufacturer's protocol).

Illumina Library preparation and sequencing

Following ds-cDNA synthesis, individually barcoded libraries compatible with the Illumina chemistry were constructed. The libraries were sequenced on an Illumina NovaSeq 6000 using S4 flowcell for the experiment with Cal07 and S3 flowcell for the experiment with Perth09. Raw data can be found on the NCBI Gene Expression Omnibus under the GEO accession number GSE143167.

Single cell RNAseq analysis

The three Cal07-associated 10x Chromium Single Cell v2 libraries (Infected, Bystander, and Mock) were demultiplexed and reference mapped using Cell Ranger Count (version 2.2) for alignment to a combined human+virus reference (human: hg38, version 1.2.0; Cal07: Genbank Accessions: CY121680-CY121687), and then combined using Cell Ranger Aggr. The three Perth09-associated 10x Chromium Single Cell v3 libraries (Infected, Bystander, and Mock) were processed and combined using Cell Ranger (version 3.1) for alignment to a combined human+virus reference (human: hg38, version

1.2.0; Perth09: Genbank Accessions: KJ609203.1- KJ609210.1). The resulting raw count matrix for each virus set was imported into an R pipeline using SimpleSingleCell(Lun, McCarthy, and Marioni 2016), where it was filtered for empty droplets(Lun et al. 2019). Cell cycle status was determined next by running the Cyclone tool in the scran R package(Lun, McCarthy, and Marioni 2016). Additional filtering was then performed on low feature cells (i.e. droplets removed if < 400 features/cell), low expressing features (i.e. features removed if < 4 cells/feature), and potential doublets (droplets removed if cell UMI counts > 2-fold of the median raw count number of host genes in cells of 3 libraries combined).

Overall cellular infection status (infected/uninfected) and individual virus gene presence/absence was determined by examining the distributions of percentage of viral counts within each cell on the log10 scale to magnify the differences at the low end. Thresholds for calling cells “not infected” overall and for individual viral gene presence/absence were set by calculating kernel density estimates on the distributions and finding the first local minima. For genes without clear bi-modal distributions (PB2 and PA of Cal07) the threshold was set to -1.5 (log10 scale), which was a consistent minimum in other low-expression viral genes and extremely close to the maximum value of PB2 and PA in uninfected cells within the Cal07 infected library. The filtered and annotated matrix was then imported into a Seurat pipeline for additional analysis and visualization(Stuart et al. 2019), including normalization using the SCTransform method (all 3 libraries together for the combined tSNE but then each library separately for individual tSNE)(Hafemeister and Satija 2019), differential gene expression analysis

using the MAST(Finak et al. 2015) and NBID tools(W. Chen et al. 2018), graph-based clustering of the cells(Macosko et al. 2015), and PCA/tSNE dimensional reduction visualization.

Differential Gene Expression Analysis (DGE) for the Seurat clusters were performed by first sub-setting for 'Infected' status cells and then testing for each cluster versus all other clusters. The DGE gene list for each cluster consisted of genes with FDR < 0.01 in MAST test results generated from 10x Genomics Cell Ranger raw count matrix output. The DGE for missing individual virus genes were performed by first sub-setting the count matrices to contain only 'Infected' status cells and then using the individual virus gene status factors to test for cells with 'Present' versus 'Absent'. The DGE gene list for each viral segment was produced by intersecting genes with FDR < 0.01 in both MAST and NBID test results to minimize false positives.

All code used for single cell analysis, along with associated documentation, is available from: https://github.com/BROOKELAB/SingleCell

Multivariate homogeneity of groups dispersions analysis

In the analyses, each host gene represents a variable/coordinate and thus each cell can be seen as a point in the multivariate space. Multivariate homogeneity of groups dispersion analysis(Anderson 2006) was performed on log transformed host gene expressions of the two group of cells, i.e. mock cells and infected cells, using the betadisper function in the R package (http://www.R-project.org/) vegan. Distances between the points (i.e. cells)

and their respective group centroid in the principal coordinates were then used to test homogeneity of variances and calculate the p-value. Note that similar analyses were performed on linear host gene expression values and results remain the same, i.e. overall host gene expressions are significantly more heterogenous than those in mock cells.

DVG detection in viral stocks

Viral RNA was extracted from 140 ul of each viral stock tested using the QIAamp viral RNA kit (Qiagen) and eluted in 60 ul distilled water. For cDNA reactions, 3 ul of RNA was mixed with 1 ul (2 uM) MBTUni-12 primer (5-ACGCGTGATCAGCAAAAGCAGG-3), 1 ul (10 mM) dNTPs, and 8 ul distilled water. The mixture was incubated for 5 min at 65°C and then placed on ice for 2 min. Subsequently, the mixture was removed from ice and the following were added: 1 ul SuperScript III (SSIII) RT (Invitrogen), 4 ul first-strand buffer, 1 ul DTT, and 1 ul RNase-in (Invitrogen). The reaction mixture was incubated at 45°C for 50 min, followed by a 15 min incubation at 70°C for inactivation. cDNA product (5 ul) was mixed with the following for PCR amplification: 2.5 ul (10 uM) MBTUni-12 primer, 2.5 ul (10 uM) MBTUni-13 primer (5-ACGCGTGATCAGTAGAAACAAGG-3), 0.5 ul Phusion polymerase (NEB), 10 ul high-fidelity buffer, 1 ul (10 mM) dNTPs, and 28.5 ul distilled water. The PCR protocol used was 98°C (30 s) followed by 25 cycles of 98°C (10 s), 57°C (30 s), 72°C (90 s), and a terminal extension of 72°C (5 min). PCR products were run on 1% agarose gel and visualized on a BIO-RAD Gel Doc Universal Hood II Molecular Imager.

4.5 Figures

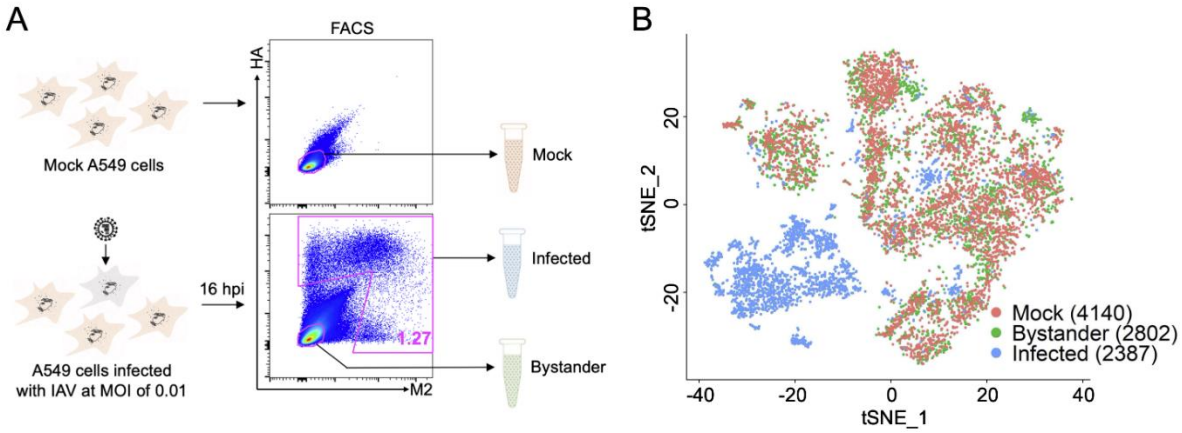

Figure 4.1 Generation of viral and host transcriptional data for thousands of singly infected cells. (A) Schematic depicting our strategy for generating single cell RNAseq libraries from thousands of cells infected at low MOI. In brief, we infect A549 cells with Cal07 or Perth09 at MOI = 0.01 to ensure that infected cells are infected with a single virion. We then block secondary spread with NH_4Cl treatment to make sure infection timing is uniform across all infected cells. Finally, we sort "infected" and "bystander" cells based on surface expression of HA and/or M2 and immediately generate single cell RNAseq libraries from these sorted cell populations using the 10X Chromium device. In parallel, mock cells are sorted and used as uninfected controls. (B) tSNE dimensionality reduction plot showing the extent of overlap between 3 indicated cell populations from Perth09 experiment clustered based on transcriptional similarity.

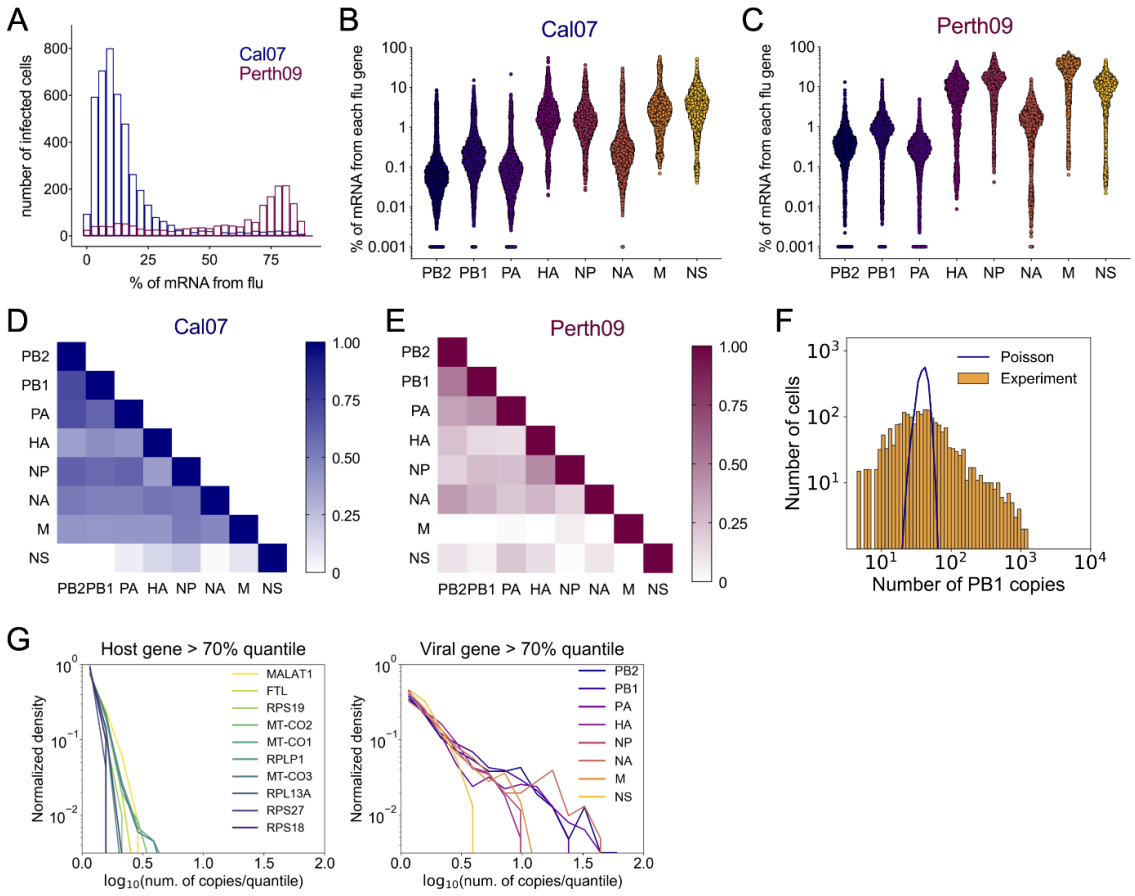

Figure 4.2 Enormous heterogeneity in viral gene expression patterns. (A) Distributions of Cal07 and Perth09-infected A549 cells, binned by the fraction of total cellular poly(A) RNA that is viral in origin. (B) Plots show the fraction of total poly(A) RNA per cell that maps to the indicated viral gene segment of Cal07. Each dot represents a single cell, cells with no detectable reads mapping to the indicated segment were arbitrarily assigned a value of 0.001 to show up on the log10 scale. (C) Same figure as (B) for Perth09. (D) R^2 correlation values plotted as heat map for all pairwise comparisons of Cal07 viral transcripts within infected cells positive for all viral genes. (E) Same figure as (D) for Perth09. (F) Distribution of normalized Cal07-PB1-derived reads per cell (orange) compared with a Poisson distribution of equal mean (blue line) on a log-log scale. (G) Distributions of top 10 most abundant host transcripts (left panel) and Cal07 viral gene expression (right panel) normalized by the 70th quantile on a log-log scale.

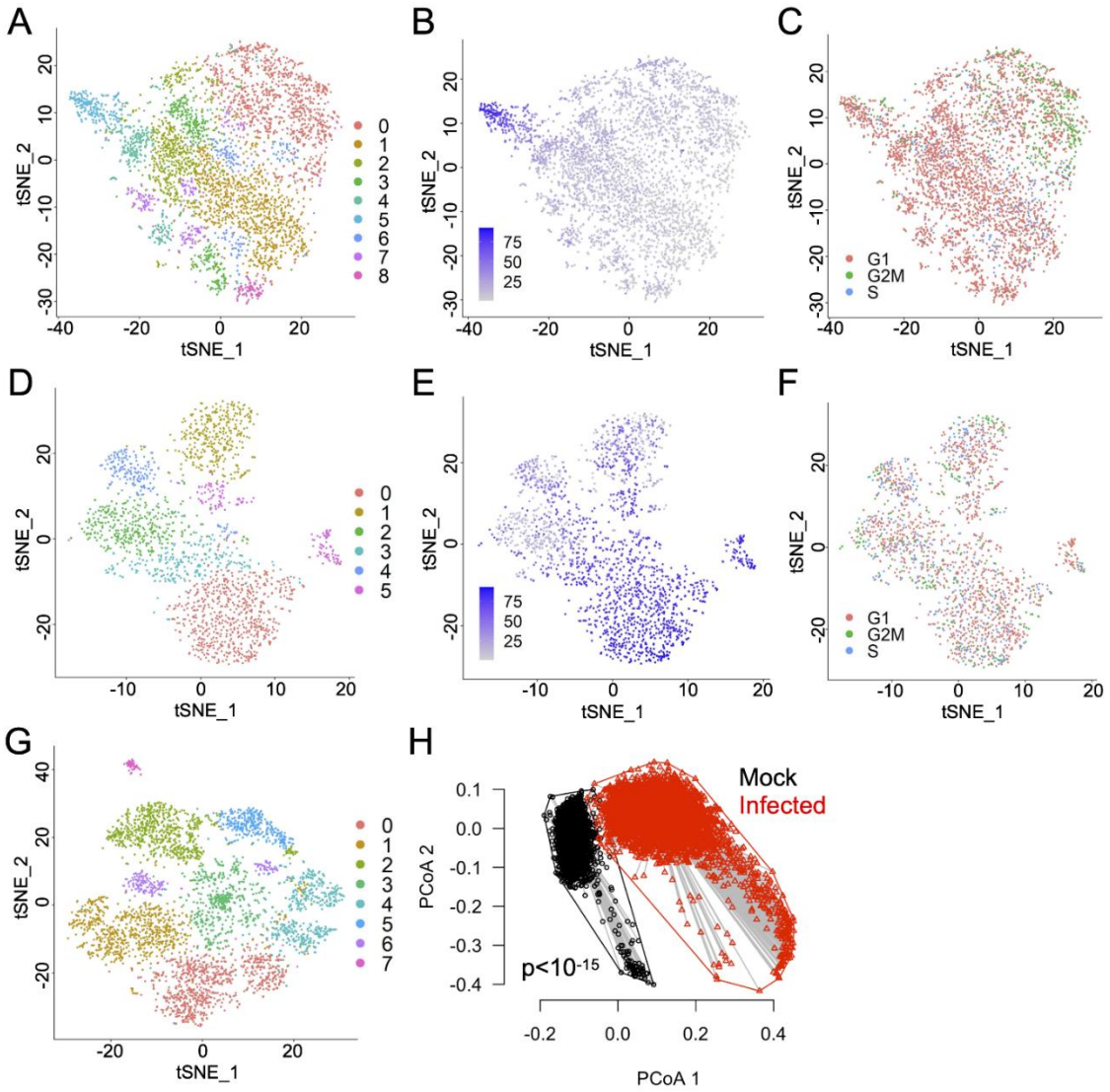

Figure 4.3 Significant heterogeneity in the host transcriptional response to infection. (A) tSNE dimensionality reduction plot showing all Cal07-infected A549 cells clustered based on similarity of host transcription patterns. (B) Same tSNE plot of Cal07-infected cells shown in (A) with each cell colored by the percentage of total cellular poly(A) RNA that is viral in origin. (C) Same tSNE plot of Cal07-infected cells shown in (A) with each cell colored by predicted cell cycle stage, as determined by the Scran package. (D) Same figure as (A) for Perth09. (E) Same figure as (B) for Perth09. (F) Same figure as (C) for Perth09. (G) tSNE dimensionality reduction plot showing mock A549 cells from Cal07 experiment clustered based on similarity of host transcriptional patterns. (H) Principle coordinate axes (PCoA) plot comparing the multivariate dispersions for mock (black) and Cal07-infected (red) A549 cells. The first two axes (PCoA 1 and PCoA 2) in the multivariate homogeneity of group dispersions analysis are used.

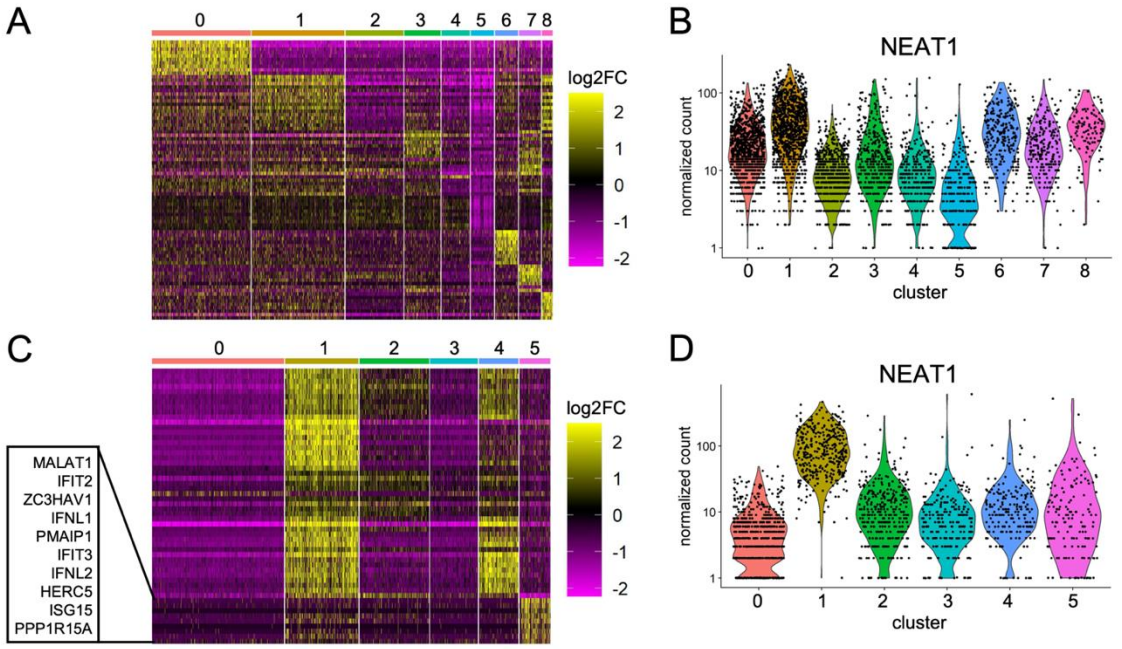

Figure 4.4 Substantial virus strain-specific variation in the expression patterns of critical determinants of IAV infection outcome. (A) Heat map showing differential expression of the top 10 characteristic host genes for each cluster of Cal07-infected cells (from Fig 3A). Individual cells are each represented by a column, grouped by cluster, with individual rows representing relative expression of the top 10 specific host transcripts most significantly (lowest p values) associated with each cluster. (B) Comparison of normalized per cell counts of NEAT1 between clusters of Cal07-infected cells shown in (A). (C) Same heat map as (A) for each cluster from Perth09-infected cells (From Fig 3D), with the top 10 genes defining cluster 5 highlighted. (D) Comparison of normalized per cell counts of NEAT1 between clusters of Perth09-infected cells shown in (C).

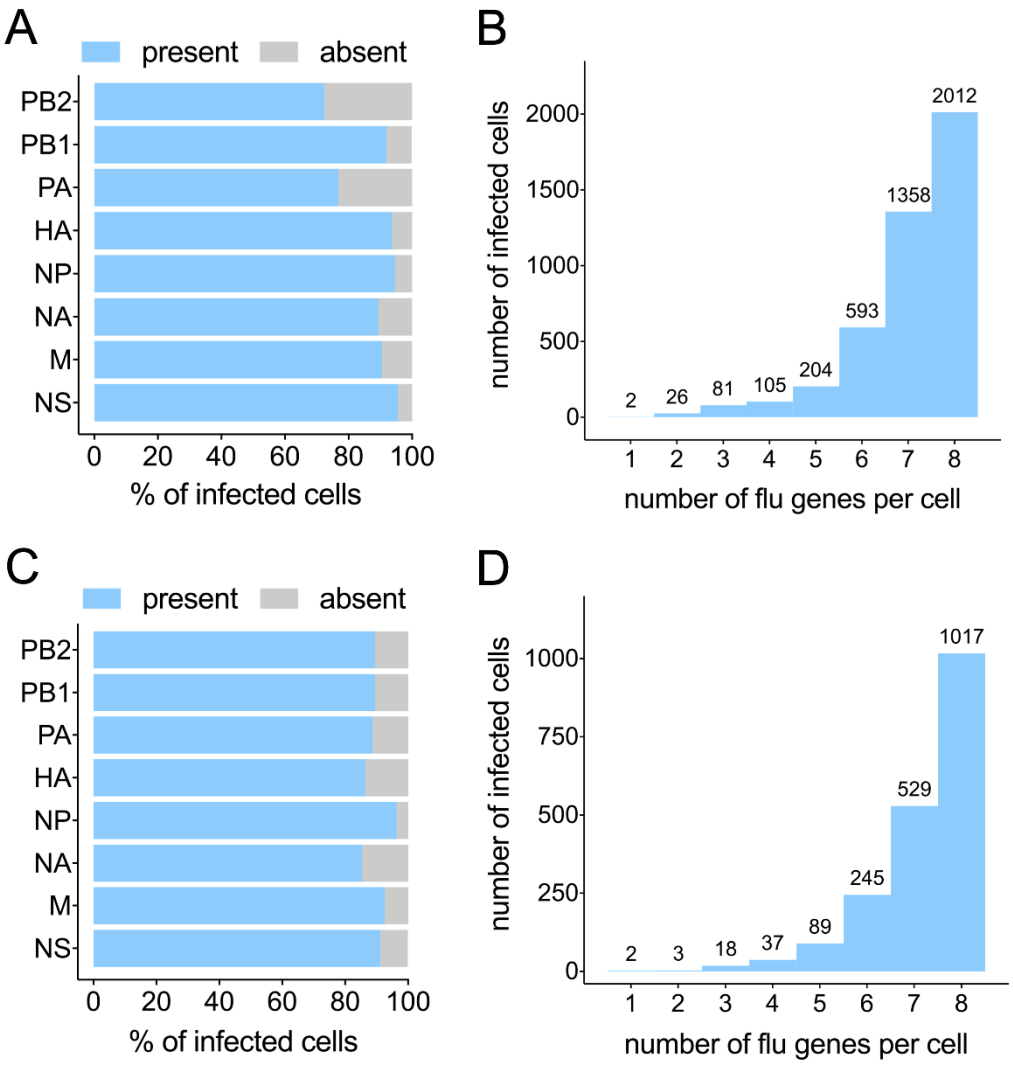

Figure 4.5 Many infected cells have undetectable levels of one or more viral transcripts. (A) The percentage of all Cal07-infected cells called as positive for the indicated gene segments. (B) All Cal07-infected cells binned by the total number of viral gene segments that were called positive, with the actual numbers of cells in each group detailed above. (C) Same figure as (A) for Perth09. (D) Same figure as (B) for Perth09.

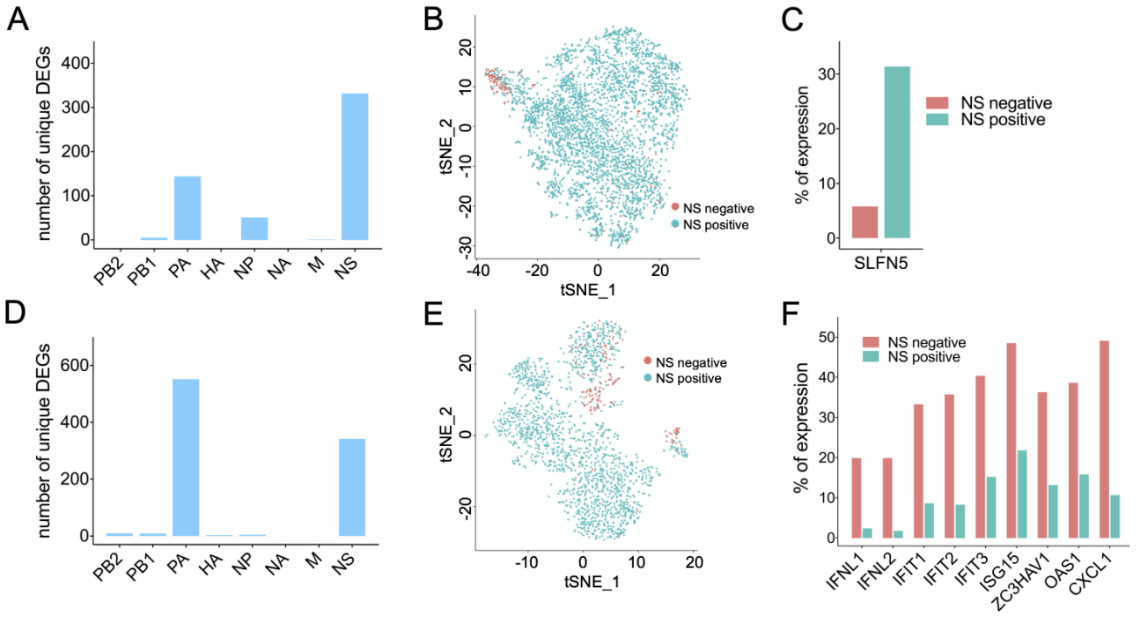

Figure 4.6 Dissection of the effects of individual viral gene expression on the host transcriptional response to infection. (A) The number of host transcripts for which expression levels significantly differ depending on whether the indicated Cal07 gene segment is present or not, according to both MAST and NBID (host genes that are differentially regulated by the expression status of more than one viral segment are excluded). (B) tSNE plot of all Cal07-infected A549 cells colored based on whether NS segment-derived transcripts are detected (Cyan) or not detected (Salmon). (C) Percentages of NS negative and NS positive Cal07-infected A549 cells that have detectable levels of SLFN5. (D) Same figure as (A) for Perth09. (E) Same figure as (B) for Perth09. (F) Percentages of NS negative and NS positive Perth09-infected A549 cells that have detectable levels of the indicated host transcripts.

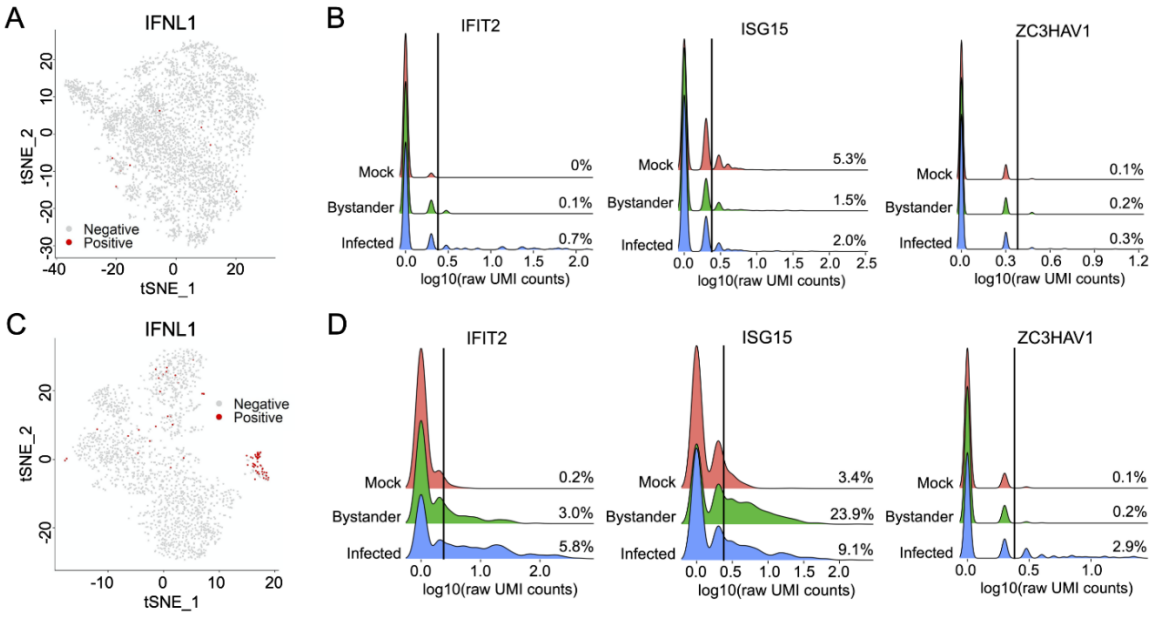

Figure 4.7 H1N1 and H3N2 strains differ significantly in single cell patterns of IFN and ISG transcription. (A) tSNE plots of all Cal07-infected A549 cells with cells that have detectable level of IFNL1 colored in red. (B) Histograms comparing distributions of per-cell UMI counts in log10 scale for the indicated host transcripts across the three libraries (mock, bystander, and infected) for Cal07 experiment. Cells with zero count excluded to avoid dominating the y-scale. Vertical lines indicate cutoff thresholds of 3 UMI counts, with percentages of all cells (including cells with zero count) in each library above the threshold shown on right. (C) Same figure as (A) for Perth09. (D) Same figure as (B) for Perth09.

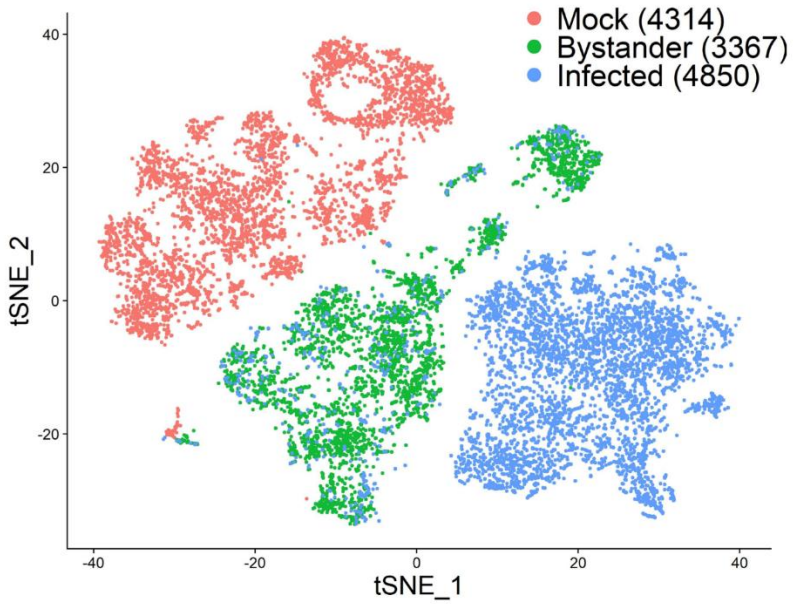

Figure 4.8 Viral and host transcriptional similarity in cells from Cal07 infection. tSNE dimensionality reduction plot showing the extent of overlap between 3 indicated cell populations from Cal07 experiment clustered based on transcriptional similarity.

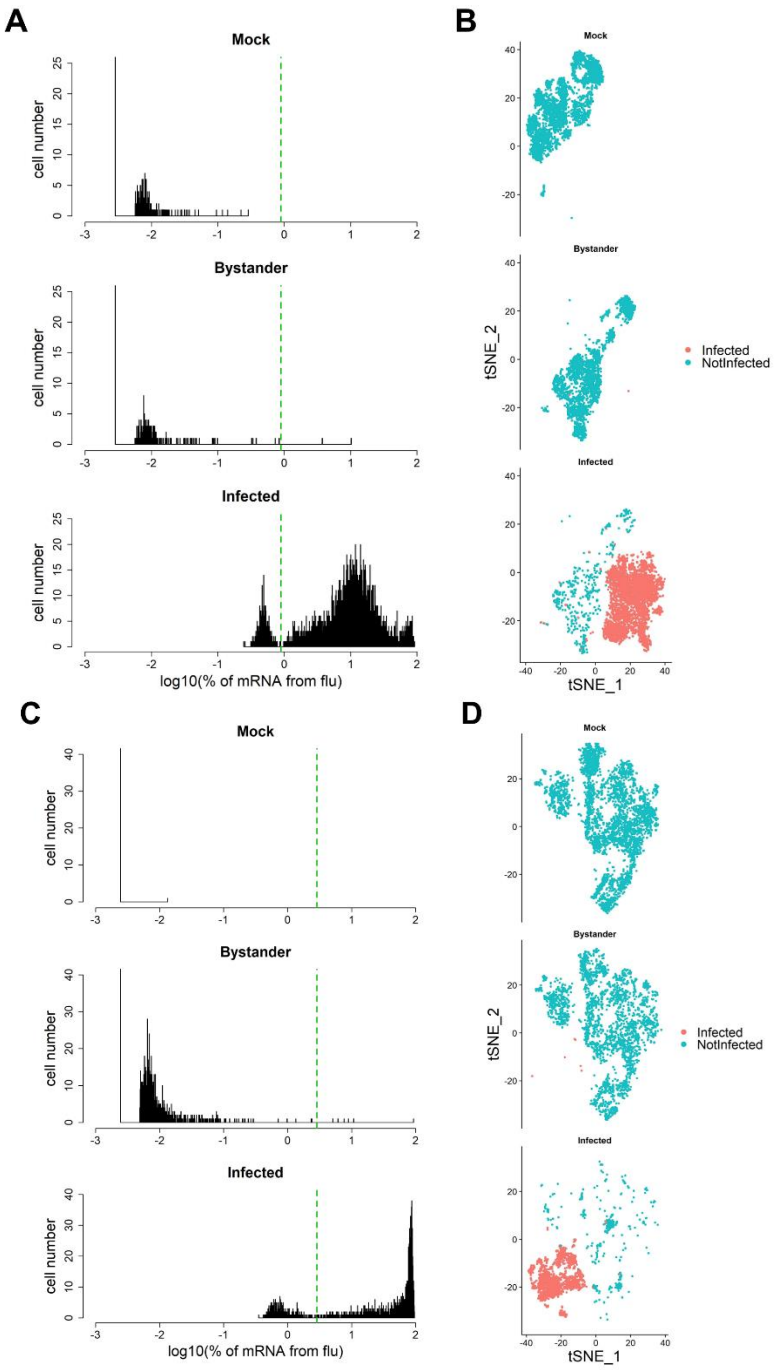

Figure 4.9 Determination of cutoff thresholds used to determine infection status. (A) Histograms comparing distributions of total viral mRNA percentages in log10 scale across the three libraries (mock, bystander, and infected) for Cal07 experiment. Vertical dash line indicates cutoff threshold determined by calculating kernel density estimates on the distribution of infected library and finding the first local minima. (B) Cells from each library clustered as in S1 Fig are shown separately, with uninfected cells (below threshold) colored in cyan and infected cells (above threshold) colored in salmon. (C) Same figure as (A) for Perth09. (D) Same figure as (B) for Perth09.

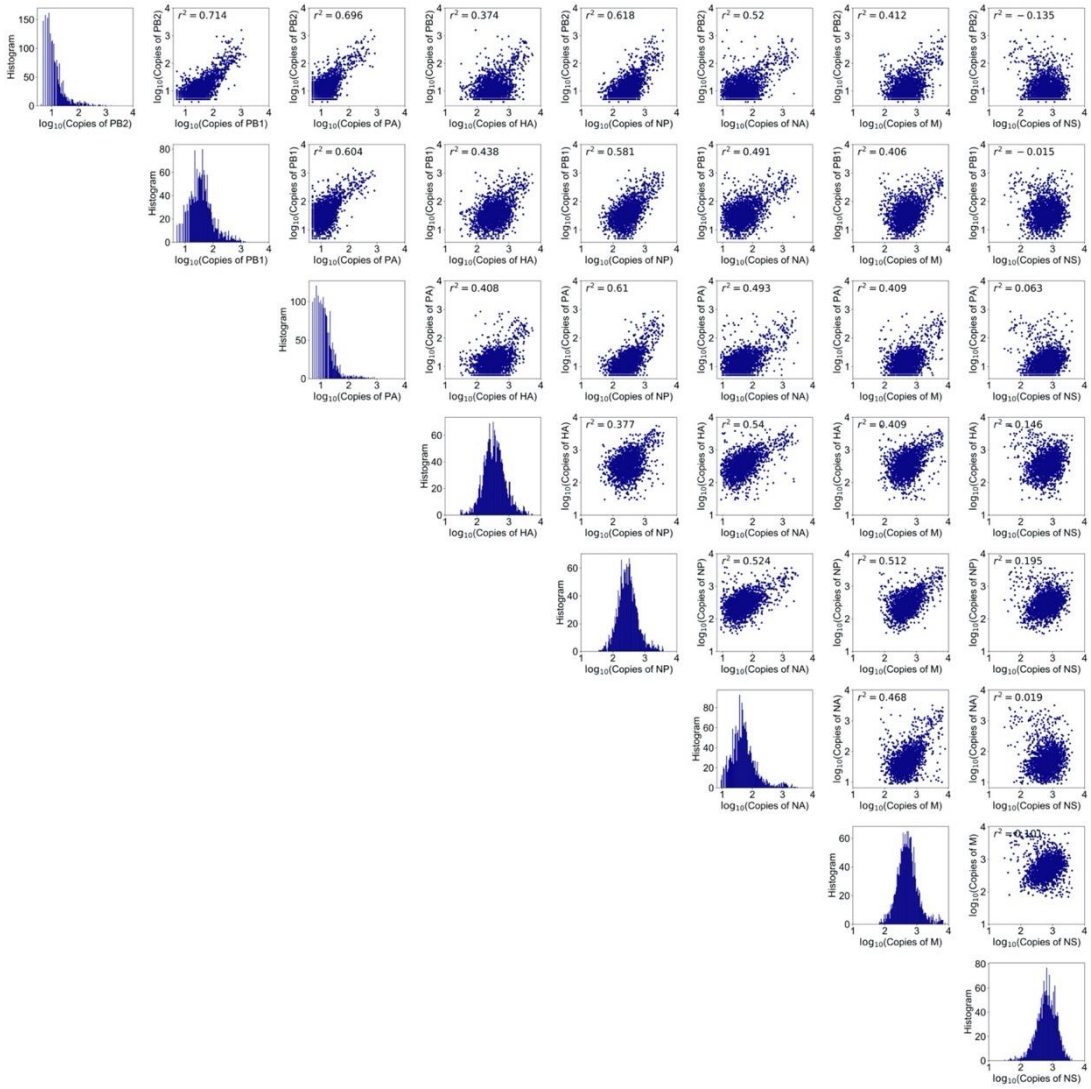

Figure 4.10 All pairwise Cal07 viral gene correlation plots. Normalized per cell copy numbers for the indicated Cal07 genes plotted against each other. Data only show infected cells that are positive for all viral gene segments.

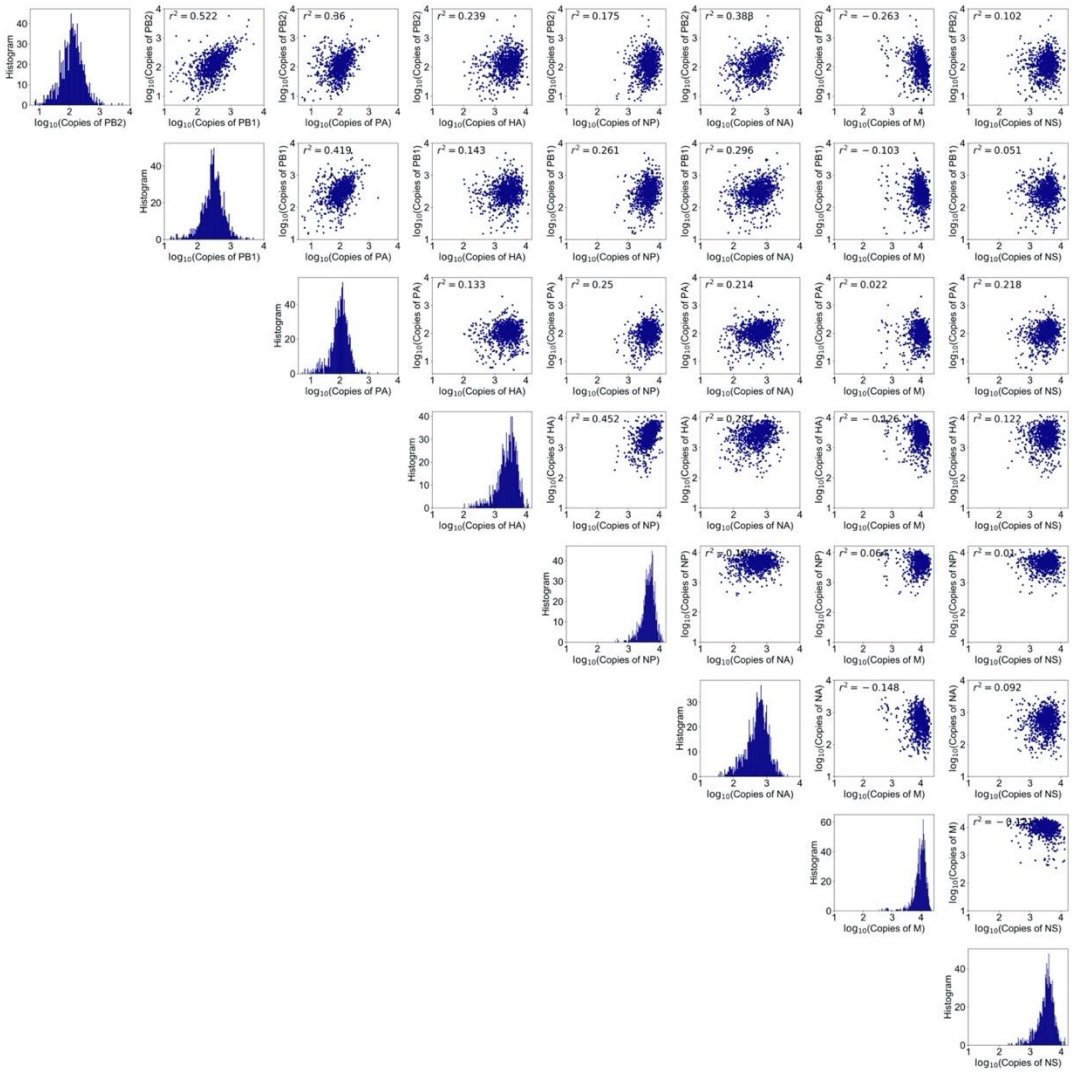

Figure 4.11 All pairwise Perth09 viral gene correlation plots. Normalized per cell copy numbers for the indicated Perth09 genes plotted against each other. Data only show infected cells that are positive for all viral gene segments.

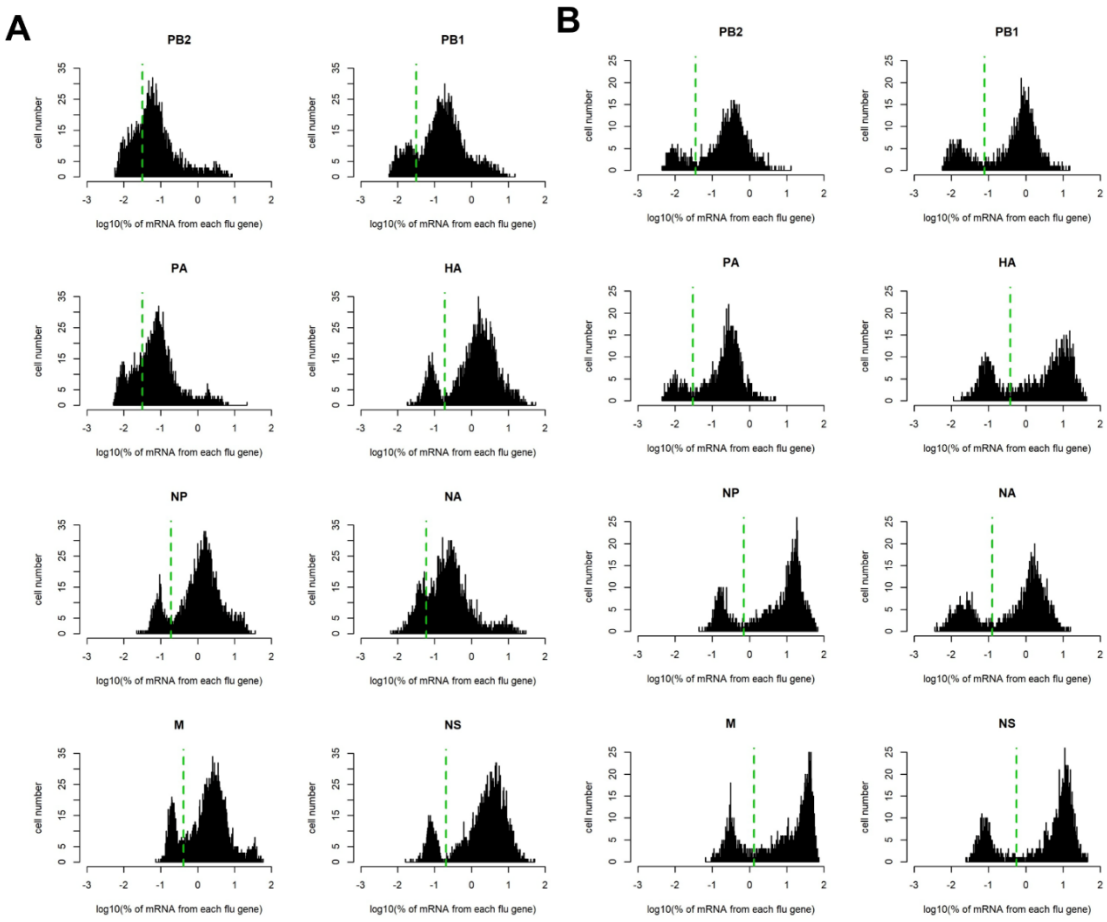

Figure 4.12 Determination of cutoff thresholds used to determine or presence/absence of individual viral gene segments. (A) Histograms show the percentages of mRNA molecules derived from each Cal07 gene segment in log10 scale. Vertical dash lines indicate cutoff thresholds determined by calculating kernel density estimates on the distributions and finding the first local minima. For PB2 and PA that do not have clear bi-modal distributions, the threshold was set to -1.5 (log10 scale), which was a consistent minimum in other low-expression viral genes and extremely close to the maximum value of PB2 and PA in uninfected cells within the infected library. (B) Same figure as (A) for Perth09.

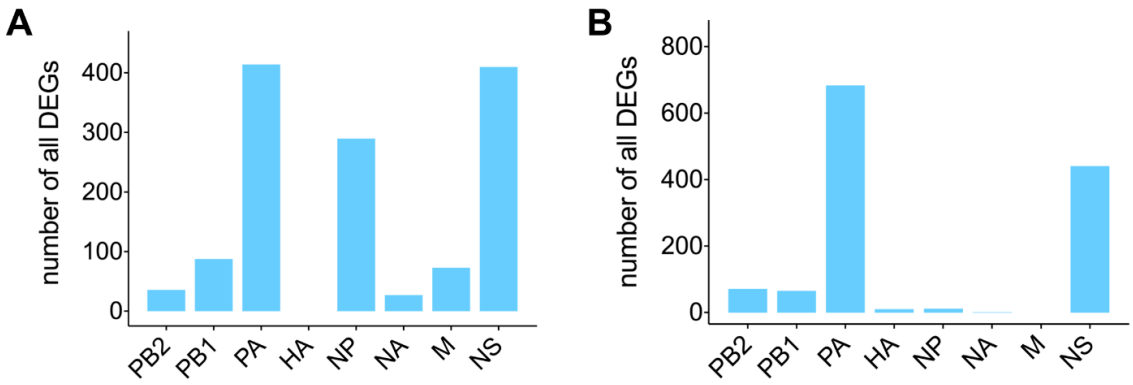

Figure 4.13 Quantification of all differentially expressed host genes correlated with presence/absence of individual viral gene segments. (A) The number of host transcripts for which expression levels significantly differ depending on whether the indicated Cal07 gene segment is present or not, according to both MAST and NBID (host genes that are differentially regulated by the expression status of more than one viral segment are included). (B) Same figure as (A) for Perth09.

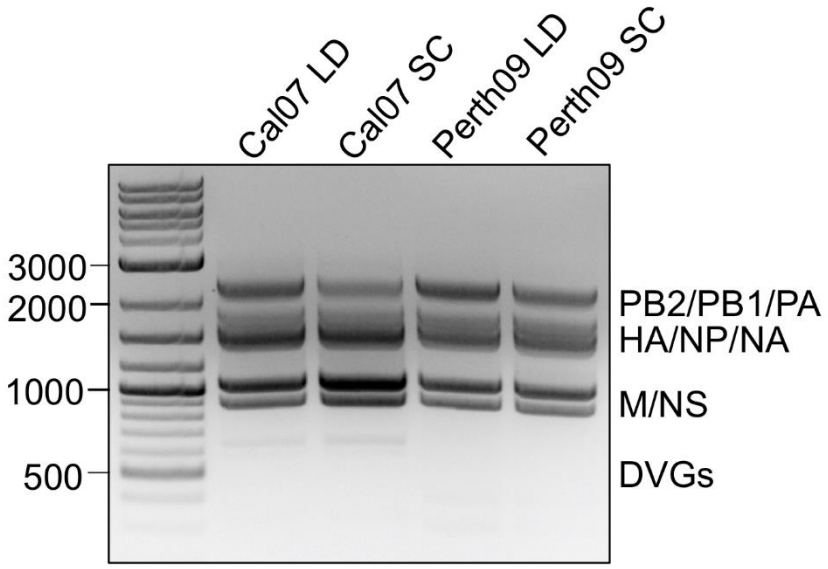

Figure 4.14 Comparison on DVGs content between validated viral stocks with low DVGs and viral stocks used in scRNAseq experiments. PCR products following 8-segment whole-genome amplification from viral cDNAs of the pre-verified viral stocks (Cal07 LD and Perth09 LD have been shown to have minimum DVGs using NGS sequencing in articles published by the lab) and viral stocks used in scRNAseq experiments (Cal07 SC and Perth09 SC) are visualized on 1% agarose gel.

CHAPTER 5: CONCLUSIONS AND DISCUSSION

The most majority of IAV particles are semi-infectious particles (SIPs) that express variable, incomplete subset of viral genes. During natural infection where virus particles within droplets are greatly outnumbered by the airway epithelial cells, the initial infection is likely under low MOI conditions. As a result, most infected cells are singly infected by SIPs that express different combinations of viral genes. Given that IAV requires expression of all viral genes to initiate productive infection, this incomplete, highly heterogeneous gene expression pattern at single particle level is likely the major reason why co-infection is commonly detected *in vivo*. To date, the biological significance and functional consequences of this viral gene expression heterogeneity remain largely unclear. In this thesis, we demonstrated that IAV gene expression heterogeneity regulates viral superinfection potential and host innate immune response.

Using multicolor flow cytometry, we compared superinfection potential in cells expressing different combinations of viral genes and found that viral superinfection potential decreases with the increase of total number of actively replicating viral gene segments in infected cells. In addition, we found that this dose-dependent inhibitory effect on superinfection potential is dependent of viral replicase activity, but largely independent of cell types, activity of individual viral gene products, host innate antiviral response, and viral binding efficiency. It is clear that less potent superinfection exclusion (SIE) in SIPs promotes multiplicity reactivation and increases viral replicative potential. However, the biological significance of SIE for IAV still remains unclear.

In future, more research is definitely needed to determine the mechanisms of SIE. Specifically, a combination of single molecule labeling technique and high-resolution microscopy would be ideal to quantify the viral genomes from superinfecting viruses that are trapped in endosome or cytoplasm and the viral genomes imported into nucleus that do or do not get replicated. To simplify the system, the viruses we used in superinfection assay shared similar genetic backgrounds. It would be interesting to study superinfection between different types of IAV or between IAV and other viruses. However, the concern is that the inhibition on superinfection could result from both SIE and viral interference between viruses that are genetically distant. Another caveat of our study is that we did not apply the superinfection assay to an animal model. Although it would be technically challenging, more study is needed to investigate superinfection *in vivo* and validate the findings in cell culture.

The outcome of IAV infection depends heavily on the host innate immune response to infection. By pairing Fluorescence-Activated Cell Sorting (FACS) with single cell RNA-seq (scRNAseq), we obtained combined host and viral transcriptomes of thousands of singly infected cells. We observed complex single cell patterns of viral gene expression and host transcriptional responses to infection. Further, we found that human H1N1 and H3N2 virus infections differ hugely in viral gene expression dynamics, type III IFN and ISG transcription at single cell level. Finally, we demonstrated that SIPs that fail to express NS in H3N2 infection but not H1N1 infection play a dominant role in inducing type III IFN and ISG.

To verify the findings in this study, more replicates at different time points should be included to increase the statistical power and reproducibility. Moreover, it would be extremely meaningful to validate the strain-dependence in the induction of innate antiviral response *in vivo*. In this study, we revealed that the IFN transcription seems to be extremely rare and random under our experimental condition. In future, more study is definitely needed to identify novel factors (other than NS1 expression) that regulate IFN induction during IAV infection. Finally, host factors coming out of our differential gene expression (DGE) analysis whose expression are correlated with the expression status of individual viral gene should be experimentally verified.

To summarize, we identified the biological consequences of IAV gene expression heterogeneity from two separate directions. First, we demonstrated that incomplete gene expression pattern in SIPs promotes co-infection by exerting less potent SIE, suggesting both multiplicity reactivation and reassortment can be regulated by viral gene expression heterogeneity. Second, we showed that host innate immune response can be disproportionately driven by small subsets of cells infected by SIPs, suggesting pathogenesis of IAV infection might be governed by viral gene expression heterogeneity at single cell level. Altogether, we illustrated that IAV gene expression heterogeneity and SIPs production have important functional consequences and are not merely the byproduct of infection. Further dissection on the intrinsic viral genomic diversity will shed more light on the basic mechanisms of IAV infection, transmission, evolution, and pathogenesis.

REFERENCES

1. Air, Gillian M. 2012. “Influenza Neuraminidase.” *Influenza and Other Respiratory Viruses* 6 (4): 245–56. https://doi.org/10.1111/j.1750-2659.2011.00304.x.

2. Akarsu, Hatice, Wilhelm P. Burmeister, Carlo Petosa, Isabelle Petit, Christoph W. Müller, Rob W. H. Ruigrok, and Florence Baudin. 2003. “Crystal Structure of the M1 Protein-Binding Domain of the Influenza A Virus Nuclear Export Protein (NEP/NS2).” *The EMBO Journal* 22 (18): 4646–55. https://doi.org/10.1093/emboj/cdg449.

3. Alexopoulou, L., A. C. Holt, R. Medzhitov, and R. A. Flavell. 2001. “Recognition of Double-Stranded RNA and Activation of NF-KappaB by Toll-like Receptor 3.” *Nature* 413 (6857): 732–38. https://doi.org/10.1038/35099560.

4. Ali, A., R. T. Avalos, E. Ponimaskin, and D. P. Nayak. 2000. “Influenza Virus Assembly: Effect of Influenza Virus Glycoproteins on the Membrane Association of M1 Protein.” *Journal of Virology* 74 (18): 8709–19. https://doi.org/10.1128/jvi.74.18.8709-8719.2000.

5. Alnaji, Fadi G., Jessica R. Holmes, Gloria Rendon, J. Cristobal Vera, Christopher J. Fields, Brigitte E. Martin, and Christopher B. Brooke. 2019. “Sequencing Framework for the Sensitive Detection and Precise Mapping of Defective Interfering Particle-Associated Deletions across Influenza A and B Viruses.” *Journal of Virology* 93 (11). https://doi.org/10.1128/JVI.00354-19.

6. Amorim, Maria Joao, Emily A. Bruce, Eliot K. C. Read, Agnes Foeglein, Robert Mahen, Amanda D. Stuart, and Paul Digard. 2011. “A Rab11- and Microtubule-Dependent Mechanism for Cytoplasmic Transport of Influenza A Virus Viral RNA.” *Journal of Virology* 85 (9): 4143–56. https://doi.org/10.1128/JVI.02606-10.

7. Anderson, Marti J. 2006. “Distance-Based Tests for Homogeneity of Multivariate Dispersions.” *Biometrics* 62 (1): 245–53. https://doi.org/10.1111/j.1541-0420.2005.00440.x.

8. Andino, Raul, and Esteban Domingo. 2015. “Viral Quasispecies.” *Virology* 479–480 (May): 46–51. https://doi.org/10.1016/j.virol.2015.03.022.

9. Arranz, Rocío, Rocío Coloma, Francisco Javier Chichón, José Javier Conesa, José L. Carrascosa, José M. Valpuesta, Juan Ortín, and Jaime Martín-Benito. 2012. “The Structure of Native Influenza Virion Ribonucleoproteins.” *Science (New York, N.Y.)* 338 (6114): 1634–37. https://doi.org/10.1126/science.1228172.

10. Arslan, A. D., A. Sassano, D. Saleiro, P. Lisowski, E. M. Kosciuczuk, M. Fischietti, F. Eckerdt, E. N. Fish, and L. C. Platanias. 2017. “Human SLFN5 Is a Transcriptional Co-Repressor of STAT1-Mediated Interferon Responses and Promotes the Malignant Phenotype in Glioblastoma.” *Oncogene* 36 (43): 6006–19. https://doi.org/10.1038/onc.2017.205.

11. Ayllon, Juan, and Adolfo García-Sastre. 2015. “The NS1 Protein: A Multitasking Virulence Factor.” *Current Topics in Microbiology and Immunology* 386: 73–107. https://doi.org/10.1007/82_2014_400.

12. Babcock, Hazen P., Chen Chen, and Xiaowei Zhuang. 2004. “Using Single-Particle Tracking to Study Nuclear Trafficking of Viral Genes.” *Biophysical Journal* 87 (4): 2749–58. https://doi.org/10.1529/biophysj.104.042234.

13. Backström Winquist, Ellenor, Samir Abdurahman, Anna Tranell, Sofia Lindström, Susanne Tingsborg, and Stefan Schwartz. 2012. “Inefficient Splicing of Segment 7 and 8 MRNAs Is an Inherent Property of Influenza Virus A/Brevig Mission/1918/1 (H1N1) That Causes Elevated Expression of NS1 Protein.” *Virology* 422 (1): 46–58. https://doi.org/10.1016/j.virol.2011.10.004.

14. Badham, Matthew D., and Jeremy S. Rossman. 2016. “Filamentous Influenza Viruses.” *Current Clinical Microbiology Reports* 3 (3): 155–61. https://doi.org/10.1007/s40588-016-0041-7.

15. Bailey, Charles C., Guocai Zhong, I.-Chueh Huang, and Michael Farzan. 2014. “IFITM-Family Proteins: The Cell’s First Line of Antiviral Defense.” *Annual Review of Virology* 1 (November): 261–83. https://doi.org/10.1146/annurev-virology-031413-085537.

16. Barman, Subrata, Lopa Adhikary, Alok K. Chakrabarti, Carl Bernas, Yoshihiro Kawaoka, and Debi P. Nayak. 2004. “Role of Transmembrane Domain and Cytoplasmic Tail Amino Acid Sequences of Influenza a Virus Neuraminidase in Raft Association and Virus Budding.” *Journal of Virology* 78 (10): 5258–69. https://doi.org/10.1128/jvi.78.10.5258-5269.2004.

17. Barr, Ian G., Colin Russell, Terry G. Besselaar, Nancy J. Cox, Rod S. Daniels, Ruben Donis, Othmar G. Engelhardt, et al. 2014. “WHO Recommendations for the Viruses Used in the 2013-2014 Northern Hemisphere Influenza Vaccine: Epidemiology, Antigenic and Genetic Characteristics of Influenza A(H1N1) Pdm09, A(H3N2) and B Influenza Viruses Collected from October 2012 to January 2013.” *Vaccine* 32 (37): 4713–25. https://doi.org/10.1016/j.vaccine.2014.02.014.

18. Ben-David, Uri, Benjamin Siranosian, Gavin Ha, Helen Tang, Yaara Oren, Kunihiko Hinohara, Craig A. Strathdee, et al. 2018. “Genetic and Transcriptional Evolution Alters Cancer Cell Line Drug Response.” *Nature* 560 (7718): 325–30. https://doi.org/10.1038/s41586-018-0409-3.

19. Bertram, Stephanie, Adeline Heurich, Hayley Lavender, Stefanie Gierer, Simon Danisch, Paula Perin, Jared M. Lucas, Peter S. Nelson, Stefan Pöhlmann, and Elizabeth J. Soilleux. 2012. “Influenza and SARS-Coronavirus Activating Proteases TMPRSS2 and HAT Are Expressed at Multiple Sites in Human Respiratory and Gastrointestinal Tracts.” *PloS One* 7 (4): e35876. https://doi.org/10.1371/journal.pone.0035876.

20. Blasius, Amanda L., and Bruce Beutler. 2010. “Intracellular Toll-like Receptors.” *Immunity* 32 (3): 305–15. https://doi.org/10.1016/j.immuni.2010.03.012.

21. Boni, Maciej F., Yang Zhou, Jeffery K. Taubenberger, and Edward C. Holmes. 2008. “Homologous Recombination Is Very Rare or Absent in Human Influenza A Virus.” *Journal of Virology* 82 (10): 4807–11. https://doi.org/10.1128/JVI.02683-07.

22. Bordería, Antonio V., Ofer Isakov, Gonzalo Moratorio, Rasmus Henningsson, Sonia Agüera-González, Lindsey Organtini, Nina F. Gnädig, et al. 2015. “Group Selection and Contribution of Minority Variants during Virus Adaptation Determines Virus Fitness and Phenotype.” *PLoS Pathogens* 11 (5): e1004838. https://doi.org/10.1371/journal.ppat.1004838.

23. Böttcher, Eva, Tatyana Matrosovich, Michaela Beyerle, Hans-Dieter Klenk, Wolfgang Garten, and Mikhail Matrosovich. 2006. “Proteolytic Activation of Influenza Viruses by Serine Proteases TMPRSS2 and HAT from Human Airway Epithelium.” *Journal of Virology* 80 (19): 9896–98. https://doi.org/10.1128/JVI.01118-06.

24. Böttcher-Friebertshäuser, Eva, Wolfgang Garten, Mikhail Matrosovich, and Hans Dieter Klenk. 2014. “The Hemagglutinin: A Determinant of Pathogenicity.” *Current Topics in Microbiology and Immunology* 385: 3–34. https://doi.org/10.1007/82_2014_384.

25. Bowie, James U. 2005. “Solving the Membrane Protein Folding Problem.” *Nature* 438 (7068): 581–89. https://doi.org/10.1038/nature04395.

26. Brooke, Christopher B. 2014. “Biological Activities of ‘noninfectious’ Influenza A Virus Particles.” *Future Virology* 9 (1): 41–51. https://doi.org/10.2217/fvl.13.118.

27. Brooke, Christopher B. 2017. “Population Diversity and Collective Interactions during Influenza Virus Infection.” *Journal of Virology* 91 (22): e01164-17. https://doi.org/10.1128/JVI.01164-17.

28. Brooke, Christopher B., William L. Ince, Jiajie Wei, Jack R. Bennink, and Jonathan W. Yewdell. 2014. “Influenza A Virus Nucleoprotein Selectively Decreases Neuraminidase Gene-Segment Packaging While Enhancing Viral Fitness and Transmissibility.” *Proceedings of the National Academy of Sciences of the United States of America* 111 (47): 16854–59. https://doi.org/10.1073/pnas.1415396111.

29. Brooke, Christopher B., William L. Ince, Jens Wrammert, Rafi Ahmed, Patrick C. Wilson, Jack R. Bennink, and Jonathan W. Yewdell. 2013. “Most Influenza A Virions Fail to Express at Least One Essential Viral Protein.” *Journal of Virology* 87 (6): 3155–62. https://doi.org/10.1128/JVI.02284-12.

30. Bui, M., G. Whittaker, and A. Helenius. 1996. “Effect of M1 Protein and Low PH on Nuclear Transport of Influenza Virus Ribonucleoproteins.” *Journal of Virology* 70 (12): 8391–8401. https://doi.org/10.1128/JVI.70.12.8391-8401.1996.

31. Bullough, P. A., F. M. Hughson, J. J. Skehel, and D. C. Wiley. 1994. “Structure of Influenza Haemagglutinin at the PH of Membrane Fusion.” *Nature* 371 (6492): 37–43. https://doi.org/10.1038/371037a0.

32. Burnet, F. M. 1948. “Mucins and Mucoids in Relation to Influenza Virus Action; the Destruction of Francis Inhibitor Activity in a Purified Mucoid by Virus Action.” *The Australian Journal of Experimental Biology and Medical Science* 26 (Pt 5): 389–402. https://doi.org/10.1038/icb.1948.40.

33. Burnet, F. M., J. F. Mccrea, and S. G. Anderson. 1947. “Mucin as Substrate of Enzyme Action by Viruses of the Mumps Influenza Group.” *Nature* 160 (4064): 404–5. https://doi.org/10.1038/160404b0.

34. Calder, Lesley J., Sebastian Wasilewski, John A. Berriman, and Peter B. Rosenthal. 2010. “Structural Organization of a Filamentous Influenza A Virus.” *Proceedings of the National Academy of Sciences of the United States of America* 107 (23): 10685–90. https://doi.org/10.1073/pnas.1002123107.

35. Castro Martin, Isabel Fernández de, Guillaume Fournier, Martin Sachse, Javier Pizarro-Cerda, Cristina Risco, and Nadia Naffakh. 2017. “Influenza Virus Genome Reaches the Plasma Membrane via a Modified Endoplasmic Reticulum and Rab11-Dependent Vesicles.” *Nature Communications* 8 (1): 1396. https://doi.org/10.1038/s41467-017-01557-6.

36. Chen, Benjamin J., George P. Leser, Eiji Morita, and Robert A. Lamb. 2007. “Influenza Virus Hemagglutinin and Neuraminidase, but Not the Matrix Protein, Are Required for Assembly and Budding of Plasmid-Derived Virus-like Particles.” *Journal of Virology* 81 (13): 7111–23. https://doi.org/10.1128/JVI.00361-07.

37. Chen, Chen, and Xiaowei Zhuang. 2008. “Epsin 1 Is a Cargo-Specific Adaptor for the Clathrin-Mediated Endocytosis of the Influenza Virus.” *Proceedings of the National Academy of Sciences of the United States of America* 105 (33): 11790–95. https://doi.org/10.1073/pnas.0803711105.

38. Chen, Wenan, Yan Li, John Easton, David Finkelstein, Gang Wu, and Xiang Chen. 2018. “UMI-Count Modeling and Differential Expression Analysis for Single-Cell RNA Sequencing.” *Genome Biology* 19 (1): 70. https://doi.org/10.1186/s13059-018-1438-9.

39. Chen, Z., Y. Li, and R. M. Krug. 1999. “Influenza A Virus NS1 Protein Targets Poly(A)-Binding Protein II of the Cellular 3’-End Processing Machinery.” *The EMBO Journal* 18 (8): 2273–83. https://doi.org/10.1093/emboj/18.8.2273.

40. Chlanda, Petr, Oliver Schraidt, Susann Kummer, James Riches, Heike Oberwinkler, Simone Prinz, Hans-Georg Kräusslich, and John A. G. Briggs. 2015. “Structural Analysis of the Roles of Influenza A Virus Membrane-Associated Proteins in Assembly and Morphology.” *Journal of Virology* 89 (17): 8957–66. https://doi.org/10.1128/JVI.00592-15.

41. Chou, Yi-ying, Nicholas S. Heaton, Qinshan Gao, Peter Palese, Robert Singer, and Timothée Lionnet. 2013. “Colocalization of Different Influenza Viral RNA Segments in the Cytoplasm before Viral Budding as Shown by Single-Molecule Sensitivity FISH Analysis.” *PLoS Pathogens* 9 (5). https://doi.org/10.1371/journal.ppat.1003358.

42. Cohen, Miriam, Xing-Quan Zhang, Hooman P. Senaati, Hui-Wen Chen, Nissi M. Varki, Robert T. Schooley, and Pascal Gagneux. 2013. “Influenza A Penetrates Host Mucus by Cleaving Sialic Acids with Neuraminidase.” *Virology Journal* 10 (November): 321. https://doi.org/10.1186/1743-422X-10-321.

43. Croce, M. V., A. G. Colussi, M. R. Price, and A. Segal-Eiras. 1999. “Identification and Characterization of Different Subpopulations in a Human Lung Adenocarcinoma Cell Line (A549).” *Pathology Oncology Research: POR* 5 (3): 197–204. https://doi.org/10.1053/paor.1999.0212.

44. Cros, Jerome F., Adolfo García-Sastre, and Peter Palese. 2005. “An Unconventional NLS Is Critical for the Nuclear Import of the Influenza A Virus Nucleoprotein and Ribonucleoprotein.” *Traffic (Copenhagen, Denmark)* 6 (3): 205–13. https://doi.org/10.1111/j.1600-0854.2005.00263.x.

45. Daniels, Robert, Brad Kurowski, Arthur E. Johnson, and Daniel N. Hebert. 2003. “N-Linked Glycans Direct the Cotranslational Folding Pathway of Influenza Hemagglutinin.” *Molecular Cell* 11 (1): 79–90. https://doi.org/10.1016/s1097-2765(02)00821-3.

46. Deng, Tao, Frank T. Vreede, and George G. Brownlee. 2006. “Different de Novo Initiation Strategies Are Used by Influenza Virus RNA Polymerase on Its CRNA and Viral RNA Promoters during Viral RNA Replication.” *Journal of Virology* 80 (5): 2337–48. https://doi.org/10.1128/JVI.80.5.2337-2348.2006.

47. Desmyter, J., J. L. Melnick, and W. E. Rawls. 1968. “Defectiveness of Interferon Production and of Rubella Virus Interference in a Line of African Green Monkey Kidney Cells (Vero).” *Journal of Virology* 2 (10): 955–61. https://doi.org/10.1128/JVI.2.10.955-961.1968.

48. Dias, Alexandre, Denis Bouvier, Thibaut Crépin, Andrew A. McCarthy, Darren J. Hart, Florence Baudin, Stephen Cusack, and Rob W. H. Ruigrok. 2009. “The Cap-Snatching Endonuclease of Influenza Virus Polymerase Resides in the PA Subunit.” *Nature* 458 (7240): 914–18. https://doi.org/10.1038/nature07745.

49. Diebold, Sandra S., Tsuneyasu Kaisho, Hiroaki Hemmi, Shizuo Akira, and Caetano Reis e Sousa. 2004. “Innate Antiviral Responses by Means of TLR7-Mediated Recognition of Single-Stranded RNA.” *Science (New York, N.Y.)* 303 (5663): 1529–31. https://doi.org/10.1126/science.1093616.

50. Diefenbacher, Meghan, Jiayi Sun, and Christopher B Brooke. 2018. “The Parts Are Greater than the Whole: The Role of Semi-Infectious Particles in Influenza A Virus Biology.” *Current Opinion in Virology*, Virus vector interactions • Special Section: Multicomponent viral systems, 33 (December): 42–46. https://doi.org/10.1016/j.coviro.2018.07.002.

51. Dixit, Evelyn, Steeve Boulant, Yijing Zhang, Amy S. Y. Lee, Charlotte Odendall, Bennett Shum, Nir Hacohen, et al. 2010. “Peroxisomes Are Signaling Platforms for Antiviral Innate Immunity.” *Cell* 141 (4): 668–81. https://doi.org/10.1016/j.cell.2010.04.018.

52. Domingo-Calap, Pilar, Ernesto Segredo-Otero, María Durán-Moreno, and Rafael Sanjuán. 2019. “Social Evolution of Innate Immunity Evasion in a Virus.” *Nature Microbiology* 4 (6): 1006–13. https://doi.org/10.1038/s41564-019-0379-8.

53. Donald, Heather B., and A. Isaacs. 1954. “Counts of Influenza Virus Particles.” *Microbiology* 10 (3): 457–64. https://doi.org/10.1099/00221287-10-3-457.

54. Dou, Dan, Iván Hernández-Neuta, Hao Wang, Henrik Östbye, Xiaoyan Qian, Swantje Thiele, Patricia Resa-Infante, et al. 2017. “Analysis of IAV Replication and Co-Infection Dynamics by a Versatile RNA Viral Genome Labeling Method.” *Cell Reports* 20 (1): 251–63. https://doi.org/10.1016/j.celrep.2017.06.021.

55. Dou, Dan, Diogo V. da Silva, Johan Nordholm, Hao Wang, and Robert Daniels. 2014. “Type II Transmembrane Domain Hydrophobicity Dictates the Cotranslational Dependence for Inversion.” *Molecular Biology of the Cell* 25 (21): 3363–74. https://doi.org/10.1091/mbc.e14-04-0874.

56. Drake, J. W. 1999. “The Distribution of Rates of Spontaneous Mutation over Viruses, Prokaryotes, and Eukaryotes.” *Annals of the New York Academy of Sciences* 870 (May): 100–107. https://doi.org/10.1111/j.1749-6632.1999.tb08870.x.

57. Drayman, Nir, Parthiv Patel, Luke Vistain, and Savaş Tay. 2019. “HSV-1 Single-Cell Analysis Reveals the Activation of Anti-Viral and Developmental Programs in Distinct Sub-Populations.” *ELife* 8. https://doi.org/10.7554/eLife.46339.

58. Dugan VG, Chen R, Spiro DJ, Sengamalay N, Zaborsky J, Ghedin E, Nolting J, Swayne DE, Runstadler JA, Happ GM, Senne DA, Wang R, Slemons RD, Holmes EC, Taubenberger JK. 2008. “The Evolutionary Genetics and Emergence of Avian Influenza Viruses in Wild Birds.” *PLoS Pathog.* 4(5):e1000076. https://doi.org/10.1371/journal.ppat.1000076

59. Elleman, C. J., and W. S. Barclay. 2004. “The M1 Matrix Protein Controls the Filamentous Phenotype of Influenza A Virus.” *Virology* 321 (1): 144–53. https://doi.org/10.1016/j.virol.2003.12.009.

60. Emeny, J. M., and M. J. Morgan. 1979. “Regulation of the Interferon System: Evidence That Vero Cells Have a Genetic Defect in Interferon Production.” *The Journal of General Virology* 43 (1): 247–52. https://doi.org/10.1099/0022-1317-43-1-247.

61. Essere, Boris, Matthieu Yver, Cyrille Gavazzi, Olivier Terrier, Catherine Isel, Emilie Fournier, Fabienne Giroux, et al. 2013. “Critical Role of Segment-Specific Packaging Signals in Genetic Reassortment of Influenza A Viruses.” *Proceedings of the National Academy of Sciences* 110 (40): E3840–48. https://doi.org/10.1073/pnas.1308649110.

62. Finak, Greg, Andrew McDavid, Masanao Yajima, Jingyuan Deng, Vivian Gersuk, Alex K. Shalek, Chloe K. Slichter, et al. 2015. “MAST: A Flexible Statistical Framework for Assessing Transcriptional Changes and Characterizing Heterogeneity in Single-Cell RNA Sequencing Data.” *Genome Biology* 16 (December): 278. https://doi.org/10.1186/s13059-015-0844-5.

63. Fodor, E., B. L. Seong, and G. G. Brownlee. 1993. “Photochemical Cross-Linking of Influenza A Polymerase to Its Virion RNA Promoter Defines a Polymerase Binding Site at Residues 9 to 12 of the Promoter.” *The Journal of General Virology* 74 (Pt 7) (July): 1327–33. https://doi.org/10.1099/0022-1317-74-7-1327.

64. Folimonova, Svetlana Y. 2012. “Superinfection Exclusion Is an Active Virus-Controlled Function That Requires a Specific Viral Protein.” *Journal of Virology* 86 (10): 5554–61. https://doi.org/10.1128/JVI.00310-12.

65. Fonville, Judith M., Nicolle Marshall, Hui Tao, John Steel, and Anice C. Lowen. 2015. “Influenza Virus Reassortment Is Enhanced by Semi-Infectious Particles but Can Be Suppressed by Defective Interfering Particles.” *PLOS Pathogens* 11 (10): e1005204. https://doi.org/10.1371/journal.ppat.1005204.

66. Fournier, Emilie, Vincent Moules, Boris Essere, Jean-Christophe Paillart, Jean-Daniel Sirbat, Catherine Isel, Annie Cavalier, et al. 2012. “A Supramolecular Assembly Formed by Influenza A Virus Genomic RNA Segments.” *Nucleic Acids Research* 40 (5): 2197–2209. https://doi.org/10.1093/nar/gkr985.

67. Franz, Kate M., William J. Neidermyer, Yee-Joo Tan, Sean P. J. Whelan, and Jonathan C. Kagan. 2018. “STING-Dependent Translation Inhibition Restricts RNA Virus Replication.” *Proceedings of the National Academy of Sciences* 115 (9): E2058–67. https://doi.org/10.1073/pnas.1716937115.

68. Fujii, Yutaka, Hideo Goto, Tokiko Watanabe, Tetsuya Yoshida, and Yoshihiro Kawaoka. 2003. “Selective Incorporation of Influenza Virus RNA Segments into Virions.” *Proceedings of the National Academy of Sciences* 100 (4): 2002–7. https://doi.org/10.1073/pnas.0437772100.

69. Fukuyama, Satoshi, Hiroaki Katsura, Dongming Zhao, Makoto Ozawa, Tomomi Ando, Jason E. Shoemaker, Izumi Ishikawa, et al. 2015. “Multi-Spectral Fluorescent Reporter Influenza Viruses (Color-Flu) as Powerful Tools for in Vivo Studies.” *Nature Communications* 6 (1): 6600. https://doi.org/10.1038/ncomms7600.

70. Gabriel, Gülsah, Karin Klingel, Anna Otte, Swantje Thiele, Ben Hudjetz, Gökhan Arman-Kalcek, Martina Sauter, et al. 2011. “Differential Use of Importin-α Isoforms Governs Cell Tropism and Host Adaptation of Influenza Virus.” *Nature Communications* 2 (1): 156. https://doi.org/10.1038/ncomms1158.

71. Gack, Michaela Ulrike, Randy Allen Albrecht, Tomohiko Urano, Kyung-Soo Inn, I.-Chueh Huang, Elena Carnero, Michael Farzan, Satoshi Inoue, Jae Ung Jung, and Adolfo García-Sastre. 2009. “Influenza A Virus NS1 Targets the Ubiquitin Ligase TRIM25 to Evade Recognition by the Host Viral RNA Sensor RIG-I.” *Cell Host & Microbe* 5 (5): 439–49. https://doi.org/10.1016/j.chom.2009.04.006.

72. Gambaryan, A. S., A. B. Tuzikov, V. E. Piskarev, S. S. Yamnikova, D. K. Lvov, J. S. Robertson, N. V. Bovin, and M. N. Matrosovich. 1997. “Specification of Receptor-Binding Phenotypes of Influenza Virus Isolates from Different Hosts Using Synthetic Sialylglycopolymers: Non-Egg-Adapted Human H1 and H3 Influenza A and Influenza B Viruses Share a Common High Binding Affinity for 6’-Sialyl(N-Acetyllactosamine).” *Virology* 232 (2): 345–50. https://doi.org/10.1006/viro.1997.8572.

73. Gamblin, Steven J., and John J. Skehel. 2010. “Influenza Hemagglutinin and Neuraminidase Membrane Glycoproteins.” *The Journal of Biological Chemistry* 285 (37): 28403–9. https://doi.org/10.1074/jbc.R110.129809.

74. Gavazzi, Cyrille, Matthieu Yver, Catherine Isel, Redmond P. Smyth, Manuel Rosa-Calatrava, Bruno Lina, Vincent Moulès, and Roland Marquet. 2013. “A Functional Sequence-Specific Interaction between Influenza A Virus Genomic RNA Segments.” *Proceedings of the National Academy of Sciences* 110 (41): 16604–9. https://doi.org/10.1073/pnas.1314419110.

75. Gerl, Mathias J., Julio L. Sampaio, Severino Urban, Lucie Kalvodova, Jean-Marc Verbavatz, Beth Binnington, Dirk Lindemann, et al. 2012. “Quantitative Analysis of the Lipidomes of the Influenza Virus Envelope and MDCK Cell Apical Membrane.” *The Journal of Cell Biology* 196 (2): 213–21. https://doi.org/10.1083/jcb.201108175.

76. Gilmore, R., P. Walter, and G. Blobel. 1982. “Protein Translocation across the Endoplasmic Reticulum. II. Isolation and Characterization of the Signal Recognition Particle Receptor.” *The Journal of Cell Biology* 95 (2 Pt 1): 470–77. https://doi.org/10.1083/jcb.95.2.470.

77. Görlich, D., S. Prehn, E. Hartmann, K. U. Kalies, and T. A. Rapoport. 1992. “A Mammalian Homolog of SEC61p and SECYp Is Associated with Ribosomes and Nascent Polypeptides during Translocation.” *Cell* 71 (3): 489–503. https://doi.org/10.1016/0092-8674(92)90517-g.

78. Goto, Hideo, Yukiko Muramoto, Takeshi Noda, and Yoshihiro Kawaoka. 2013. “The Genome-Packaging Signal of the Influenza A Virus Genome Comprises a Genome Incorporation Signal and a Genome-Bundling Signal.” *Journal of Virology* 87 (21): 11316–22. https://doi.org/10.1128/JVI.01301-13.

79. Götz, Veronika, Linda Magar, Dominik Dornfeld, Sebastian Giese, Anne Pohlmann, Dirk Höper, Byung-Whi Kong, et al. 2016. “Influenza A Viruses Escape from MxA Restriction at the Expense of Efficient Nuclear VRNP Import.” *Scientific Reports* 6 (March): 23138. https://doi.org/10.1038/srep23138.

80. Greenbaum, Benjamin D., Olive T. W. Li, Leo L. M. Poon, Arnold J. Levine, and Raul Rabadan. 2012. “Viral Reassortment as an Information Exchange between Viral Segments.” *Proceedings of the National Academy of Sciences of the United States of America* 109 (9): 3341–46. https://doi.org/10.1073/pnas.1113300109.

81. Guilligay, Delphine, Franck Tarendeau, Patricia Resa-Infante, Rocío Coloma, Thibaut Crepin, Peter Sehr, Joe Lewis, et al. 2008. “The Structural Basis for Cap Binding by Influenza Virus Polymerase Subunit PB2.” *Nature Structural & Molecular Biology* 15 (5): 500–506. https://doi.org/10.1038/nsmb.1421.

82. Guo, Feng, Sixing Li, Mehmet Umut Caglar, Zhangming Mao, Wu Liu, Andrew Woodman, Jamie J. Arnold, Claus O. Wilke, Tony Jun Huang, and Craig E. Cameron. 2017. “Single-Cell Virology: On-Chip Investigation of Viral Infection Dynamics.” *Cell Reports* 21 (6): 1692–1704. https://doi.org/10.1016/j.celrep.2017.10.051.

83. Hafemeister, Christoph, and Rahul Satija. 2019. “Normalization and Variance Stabilization of Single-Cell RNA-Seq Data Using Regularized Negative Binomial Regression.” *Genome Biology* 20 (1): 296. https://doi.org/10.1186/s13059-019-1874-1.

84. Hale, Benjamin G., Richard E. Randall, Juan Ortín, and David Jackson. 2008. “The Multifunctional NS1 Protein of Influenza A Viruses.” *The Journal of General Virology* 89 (Pt 10): 2359–76. https://doi.org/10.1099/vir.0.2008/004606-0.

85. Hale, Benjamin G., John Steel, Rafael A. Medina, Balaji Manicassamy, Jianqiang Ye, Danielle Hickman, Rong Hai, et al. 2010. “Inefficient Control of Host Gene Expression by the 2009 Pandemic H1N1 Influenza A Virus NS1 Protein.” *Journal of Virology* 84 (14): 6909–22. https://doi.org/10.1128/JVI.00081-10.

86. Hamilton, Brian S., Gary R. Whittaker, and Susan Daniel. 2012. “Influenza Virus-Mediated Membrane Fusion: Determinants of Hemagglutinin Fusogenic Activity and Experimental Approaches for Assessing Virus Fusion.” *Viruses* 4 (7): 1144–68. https://doi.org/10.3390/v4071144.

87. Harris, Audray, Giovanni Cardone, Dennis C. Winkler, J. Bernard Heymann, Matthew Brecher, Judith M. White, and Alasdair C. Steven. 2006. “Influenza Virus Pleiomorphy Characterized by Cryoelectron Tomography.” *Proceedings of the National Academy of Sciences of the United States of America* 103 (50): 19123–27. https://doi.org/10.1073/pnas.0607614103.

88. Harrison, Stephen C. 2015. “Viral Membrane Fusion.” *Virology* 479–480 (May): 498–507. https://doi.org/10.1016/j.virol.2015.03.043.

89. Hause, Ben M., Emily A. Collin, Runxia Liu, Bing Huang, Zizhang Sheng, Wuxun Lu, Dan Wang, Eric A. Nelson, and Feng Li. 2014. “Characterization of a Novel Influenza Virus in Cattle and Swine: Proposal for a New Genus in the Orthomyxoviridae Family.” *MBio* 5 (2). https://doi.org/10.1128/mBio.00031-14.

90. Hayman, A., S. Comely, A. Lackenby, S. Murphy, J. McCauley, S. Goodbourn, and W. Barclay. 2006. “Variation in the Ability of Human Influenza A Viruses to Induce and Inhibit the IFN-Beta Pathway.” *Virology* 347 (1): 52–64. https://doi.org/10.1016/j.virol.2005.11.024.

91. Hebert, D. N., J. X. Zhang, W. Chen, B. Foellmer, and A. Helenius. 1997. “The Number and Location of Glycans on Influenza Hemagglutinin Determine Folding and Association with Calnexin and Calreticulin.” *The Journal of Cell Biology* 139 (3): 613–23. https://doi.org/10.1083/jcb.139.3.613.

92. Heldt, Frank S., Sascha Y. Kupke, Sebastian Dorl, Udo Reichl, and Timo Frensing. 2015. “Single-Cell Analysis and Stochastic Modelling Unveil Large Cell-to-Cell Variability in Influenza A Virus Infection.” *Nature Communications* 6 (November). https://doi.org/10.1038/ncomms9938.

93. Hensley, Scott E., Suman R. Das, James S. Gibbs, Adam L. Bailey, Loren M. Schmidt, Jack R. Bennink, and Jonathan W. Yewdell. 2011. “Influenza A Virus Hemagglutinin Antibody Escape Promotes Neuraminidase Antigenic Variation and Drug Resistance.” *PloS One* 6 (2): e15190. https://doi.org/10.1371/journal.pone.0015190.

94. Herfst, Sander, Eefje J. A. Schrauwen, Martin Linster, Salin Chutinimitkul, Emmie de Wit, Vincent J. Munster, Erin M. Sorrell, et al. 2012. “Airborne Transmission of Influenza A/H5N1 Virus between Ferrets.” *Science (New York, N.Y.)* 336 (6088): 1534–41. https://doi.org/10.1126/science.1213362.

95. Hirst, G. K. 1943. “Studies of Antigenic Differences Among Strains of Influenza a by Means of Red Cell Agglutination.” *The Journal of Experimental Medicine* 78 (5): 407–23. https://doi.org/10.1084/jem.78.5.407.

96. Hirst, George K. 1973. “Mechanism of Influenza Recombination: I. Factors Influencing Recombination Rates between Temperature-Sensitive Mutants of Strain WSN and the Classification of Mutants into Complementation-Recombination Groups.” *Virology* 55 (1): 81–93. https://doi.org/10.1016/S0042-6822(73)81010-4.

97. Hirst, George K., and Marcel W. Pons. 1973. “Mechanism of Influenza Recombination: II. Virus Aggregation and Its Effect on Plaque Formation by so-Called Noninfective Virus.” *Virology* 56 (2): 620–31. https://doi.org/10.1016/0042-6822(73)90063-9.

98. Hoffmann, Hans-Heinrich, William M. Schneider, and Charles M. Rice. 2015. “Interferons and Viruses: An Evolutionary Arms Race of Molecular Interactions.” *Trends in Immunology* 36 (3): 124–38. https://doi.org/10.1016/j.it.2015.01.004.

99. Holmes, Edward C., Elodie Ghedin, Naomi Miller, Jill Taylor, Yiming Bao, Kirsten St George, Bryan T. Grenfell, et al. 2005. “Whole-Genome Analysis of Human Influenza A Virus Reveals Multiple Persistent Lineages and Reassortment among Recent H3N2 Viruses.” *PLoS Biology* 3 (9): e300. https://doi.org/10.1371/journal.pbio.0030300.

100. Holsinger, L. J., and R. A. Lamb. 1991. “Influenza Virus M2 Integral Membrane Protein Is a Homotetramer Stabilized by Formation of Disulfide Bonds.” *Virology* 183 (1): 32–43. https://doi.org/10.1016/0042-6822(91)90115-r.

101. Honda, Kenya, Yusuke Ohba, Hideyuki Yanai, Hideo Negishi, Tatsuaki Mizutani, Akinori Takaoka, Choji Taya, and Tadatsugu Taniguchi. 2005. “Spatiotemporal Regulation of MyD88-IRF-7 Signalling for Robust Type-I Interferon Induction.” *Nature* 434 (7036): 1035–40. https://doi.org/10.1038/nature03547.

102. Houser, Katherine, and Kanta Subbarao. 2015. “Influenza Vaccines: Challenges and Solutions.” *Cell Host & Microbe* 17 (3): 295–300. https://doi.org/10.1016/j.chom.2015.02.012.

103. Hsu, M. T., J. D. Parvin, S. Gupta, M. Krystal, and P. Palese. 1987. “Genomic RNAs of Influenza Viruses Are Held in a Circular Conformation in Virions and in Infected Cells by a Terminal Panhandle.” *Proceedings of the National Academy of Sciences* 84 (22): 8140–44. https://doi.org/10.1073/pnas.84.22.8140.

104. Huang, I.-Chueh, Wenhui Li, Jianhua Sui, Wayne Marasco, Hyeryun Choe, and Michael Farzan. 2008. “Influenza A Virus Neuraminidase Limits Viral Superinfection.” *Journal of Virology* 82 (10): 4834–43. https://doi.org/10.1128/JVI.00079-08.

105. Huang, R. T., R. Rott, and H. D. Klenk. 1981. “Influenza Viruses Cause Hemolysis and Fusion of Cells.” *Virology* 110 (1): 243–47. https://doi.org/10.1016/0042-6822(81)90030-1.

106. Huang, Shengping, Jingjing Chen, Quanjiao Chen, Huadong Wang, Yanfeng Yao, Jianjun Chen, and Ze Chen. 2013. “A Second CRM1-Dependent Nuclear Export Signal in the Influenza A Virus NS2 Protein Contributes to the Nuclear Export of Viral Ribonucleoproteins.” *Journal of Virology* 87 (2): 767–78. https://doi.org/10.1128/JVI.06519-11.

107. Hurt, Aeron C., Yvonne C. F. Su, Malet Aban, Heidi Peck, Hilda Lau, Chantal Baas, Yi-Mo Deng, et al. 2016. “Evidence for the Introduction, Reassortment, and Persistence of Diverse Influenza A Viruses in Antarctica.” *Journal of Virology* 90 (21): 9674–82. https://doi.org/10.1128/JVI.01404-16.

108. Hutchinson, Edward C., Philip D. Charles, Svenja S. Hester, Benjamin Thomas, David Trudgian, Mónica Martínez-Alonso, and Ervin Fodor. 2014. “Conserved and Host-Specific Features of Influenza Virion Architecture.” *Nature Communications* 5 (September): 4816. https://doi.org/10.1038/ncomms5816.

109. Hutchinson, Edward C., Johann C. von Kirchbach, Julia R. Gog, and Paul Digard. 2010. “Genome Packaging in Influenza A Virus.” *Journal of General Virology* 91 (2): 313–28. https://doi.org/10.1099/vir.0.017608-0.

110. Imai, Masaki, Tokiko Watanabe, Masato Hatta, Subash C. Das, Makoto Ozawa, Kyoko Shinya, Gongxun Zhong, et al. 2012. “Experimental Adaptation of an Influenza H5 HA Confers Respiratory Droplet Transmission to a Reassortant H5 HA/H1N1 Virus in Ferrets.” *Nature* 486 (7403): 420–28. https://doi.org/10.1038/nature10831.

111. Inglis, S C, and C M Brown. 1981. “Spliced and Unspliced RNAs Encoded by Virion RNA Segment 7 of Influenza Virus.” *Nucleic Acids Research* 9 (12): 2727–40.

112. Inglis, S. C., and C. M. Brown. 1984. “Differences in the Control of Virus MRNA Splicing during Permissive or Abortive Infection with Influenza A (Fowl Plague) Virus.” *The Journal of General Virology* 65 (Pt 1) (January): 153–64. https://doi.org/10.1099/0022-1317-65-1-153.

113. Iuliano, A. Danielle, Katherine M. Roguski, Howard H. Chang, David J. Muscatello, Rakhee Palekar, Stefano Tempia, Cheryl Cohen, et al. 2018. “Estimates of Global Seasonal Influenza-Associated Respiratory Mortality: A Modelling Study.” *Lancet (London, England)* 391 (10127): 1285–1300. https://doi.org/10.1016/S0140-6736(17)33293-2.

114. Iwasaki, Akiko, and Padmini S. Pillai. 2014. “Innate Immunity to Influenza Virus Infection.” *Nature Reviews. Immunology* 14 (5): 315–28. https://doi.org/10.1038/nri3665.

115. Jacobs, Nathan T., Nina O. Onuoha, Alice Antia, John Steel, Rustom Antia, and Anice C. Lowen. 2019. “Incomplete Influenza A Virus Genomes Occur Frequently but Are Readily Complemented during Localized Viral Spread.” *Nature Communications* 10 (1): 3526. https://doi.org/10.1038/s41467-019-11428-x.

116. Jeisy-Scott, Victoria, Jin Hyang Kim, William G. Davis, Weiping Cao, Jacqueline M. Katz, and Suryaprakash Sambhara. 2012. “TLR7 Recognition Is Dispensable for Influenza Virus A Infection but Important for the Induction of Hemagglutinin-Specific Antibodies in Response to the 2009 Pandemic Split Vaccine in Mice.” *Journal of Virology* 86 (20): 10988–98. https://doi.org/10.1128/JVI.01064-12.

117. Jong, J. C. de, D. J. Smith, A. S. Lapedes, I. Donatelli, L. Campitelli, G. Barigazzi, K. Van Reeth, et al. 2007. “Antigenic and Genetic Evolution of Swine Influenza A (H3N2) Viruses in Europe.” *Journal of Virology* 81 (8): 4315–22. https://doi.org/10.1128/JVI.02458-06.

118. Jorba, N., Coloma, R., & Ortín, J. 2009. “Genetic Trans-Complementation Establishes a New Model for Influenza Virus RNA Transcription and Replication.” *PLOS Pathogens* 5 (5): e1000462. https://doi.org/10.1371/journal.ppat.1000462.

119. Kato, Hiroki, Shintaro Sato, Mitsutoshi Yoneyama, Masahiro Yamamoto, Satoshi Uematsu, Kosuke Matsui, Tohru Tsujimura, et al. 2005. “Cell Type-Specific Involvement of RIG-I in Antiviral Response.” *Immunity* 23 (1): 19–28. https://doi.org/10.1016/j.immuni.2005.04.010.

120. Katz, Garrett, Younes Benkarroum, Hui Wei, William J. Rice, Doris Bucher, Alexandra Alimova, Al Katz, Joanna Klukowska, Gabor T. Herman, and Paul Gottlieb. 2014. “Morphology of Influenza B/Lee/40 Determined by Cryo-Electron Microscopy.” *PloS One* 9 (2): e88288. https://doi.org/10.1371/journal.pone.0088288.

121. Kawakami, Eiryo, Tokiko Watanabe, Ken Fujii, Hideo Goto, Shinji Watanabe, Takeshi Noda, and Yoshihiro Kawaoka. 2011. “Strand-Specific Real-Time RT-PCR for Distinguishing Influenza VRNA, CRNA, and MRNA.” *Journal of Virological Methods* 173 (1): 1–6. https://doi.org/10.1016/j.jviromet.2010.12.014.

122. Keirstead, N. D., and K. M. Coombs. 1998. “Absence of Superinfection Exclusion during Asynchronous Reovirus Infections of Mouse, Monkey, and Human Cell Lines.” *Virus Research* 54 (2): 225–35. https://doi.org/10.1016/s0168-1702(98)00023-9.

123. Killip, M. J., D. Jackson, M. Pérez-Cidoncha, E. Fodor, and R. E. Randall. 2017. “Single-Cell Studies of IFN-β Promoter Activation by Wild-Type and NS1-Defective Influenza A Viruses.” *The Journal of General Virology* 98 (3): 357–63. https://doi.org/10.1099/jgv.0.000687.

124. Klemm, Carolin, Yvonne Boergeling, Stephan Ludwig, and Christina Ehrhardt. 2018. “Immunomodulatory Nonstructural Proteins of Influenza A Viruses.” *Trends in Microbiology* 26 (7): 624–36. https://doi.org/10.1016/j.tim.2017.12.006.

125. Koel, Björn F., David F. Burke, Theo M. Bestebroer, Stefan van der Vliet, Gerben C. M. Zondag, Gaby Vervaet, Eugene Skepner, et al. 2013. “Substitutions near the Receptor Binding Site Determine Major Antigenic Change during Influenza Virus Evolution.” *Science (New York, N.Y.)* 342 (6161): 976–79. https://doi.org/10.1126/science.1244730.

126. Kordyukova, Larisa V., Marina V. Serebryakova, Ludmila A. Baratova, and Michael Veit. 2008. “S Acylation of the Hemagglutinin of Influenza Viruses: Mass Spectrometry Reveals Site-Specific Attachment of Stearic Acid to a Transmembrane Cysteine.” *Journal of Virology* 82 (18): 9288–92. https://doi.org/10.1128/JVI.00704-08.

127. Kowalinski, Eva, Thomas Lunardi, Andrew A. McCarthy, Jade Louber, Joanna Brunel, Boyan Grigorov, Denis Gerlier, and Stephen Cusack. 2011. “Structural Basis for the Activation of Innate Immune Pattern-Recognition Receptor RIG-I by Viral RNA.” *Cell* 147 (2): 423–35. https://doi.org/10.1016/j.cell.2011.09.039.

128. Krammer, Florian, Gavin J. D. Smith, Ron A. M. Fouchier, Malik Peiris, Katherine Kedzierska, Peter C. Doherty, Peter Palese, et al. 2018. “Influenza.” *Nature Reviews Disease Primers* 4 (1): 1–21. https://doi.org/10.1038/s41572-018-0002-y.

129. Krug, Robert M. 2015. “Functions of the Influenza A Virus NS1 Protein in Antiviral Defense.” *Current Opinion in Virology* 12 (June): 1–6. https://doi.org/10.1016/j.coviro.2015.01.007.

130. Kuiken, T., B. Riteau, R. a. M. Fouchier, and G. F. Rimmelzwaan. 2012. “Pathogenesis of Influenza Virus Infections: The Good, the Bad and the Ugly.” *Current Opinion in Virology* 2 (3): 276–86. https://doi.org/10.1016/j.coviro.2012.02.013.

131. Kumar, A., J. Haque, J. Lacoste, J. Hiscott, and B. R. Williams. 1994. “Double-Stranded RNA-Dependent Protein Kinase Activates Transcription Factor NF-Kappa B by Phosphorylating I Kappa B.” *Proceedings of the National Academy of Sciences of the United States of America* 91 (14): 6288–92. https://doi.org/10.1073/pnas.91.14.6288.

132. Kutter, Jasmin S, Monique I Spronken, Pieter L Fraaij, Ron AM Fouchier, and Sander Herfst. 2018. “Transmission Routes of Respiratory Viruses among Humans.” *Current Opinion in Virology*, Emerging viruses: intraspecies transmission • Viral Immunology, 28 (February): 142–51. https://doi.org/10.1016/j.coviro.2018.01.001.

133. Lai, Jimmy C. C., Wallace W. L. Chan, François Kien, John M. Nicholls, J. S. Malik Peiris, and Jean-Michel Garcia. 2010. “Formation of Virus-like Particles from Human Cell Lines Exclusively Expressing Influenza Neuraminidase.” *The Journal of General Virology* 91 (Pt 9): 2322–30. https://doi.org/10.1099/vir.0.019935-0.

134. Lakdawala, S. S., Wu, Y., Wawrzusin, P., Kabat, J., Broadbent, A. J., Lamirande, E. W., Fodor, E., Altan-Bonnet, N., Shroff, H., & Subbarao, K. 2016. “Correction: Influenza A Virus Assembly Intermediates Fuse in the Cytoplasm.” *PLoS pathogens*, *12*(12). https:// doi: 10.1371/journal.ppat.1006121.

135. Laliberte, Jason P., and Bernard Moss. 2014. “A Novel Mode of Poxvirus Superinfection Exclusion That Prevents Fusion of the Lipid Bilayers of Viral and Cellular Membranes.” *Journal of Virology* 88 (17): 9751–68. https://doi.org/10.1128/JVI.00816-14.

136. Lamb, R A, P W Choppin, R M Chanock, and C J Lai. 1980. “Mapping of the Two Overlapping Genes for Polypeptides NS1 and NS2 on RNA Segment 8 of Influenza Virus Genome.” *Proceedings of the National Academy of Sciences of the United States of America* 77 (4): 1857–61.

137. Lamb, R. A., C. J. Lai, and P. W. Choppin. 1981. “Sequences of MRNAs Derived from Genome RNA Segment 7 of Influenza Virus: Colinear and Interrupted MRNAs Code for Overlapping Proteins.” *Proceedings of the National Academy of Sciences of the United States of America* 78 (7): 4170–74. https://doi.org/10.1073/pnas.78.7.4170.

138. Landeras-Bueno, Sara, and Juan Ortín. 2016. “Regulation of Influenza Virus Infection by Long Non-Coding RNAs.” *Virus Research* 212 (January): 78–84. https://doi.org/10.1016/j.virusres.2015.08.008.

139. Lawson, Devon A., Kai Kessenbrock, Ryan T. Davis, Nicholas Pervolarakis, and Zena Werb. 2018. “Tumour Heterogeneity and Metastasis at Single-Cell Resolution.” *Nature Cell Biology* 20 (12): 1349–60. https://doi.org/10.1038/s41556-018-0236-7.

140. Le Goffic, Ronan, Viviane Balloy, Micheline Lagranderie, Lena Alexopoulou, Nicolas Escriou, Richard Flavell, Michel Chignard, and Mustapha Si-Tahar. 2006. “Detrimental Contribution of the Toll-like Receptor (TLR)3 to Influenza A Virus-Induced Acute Pneumonia.” *PLoS Pathogens* 2 (6): e53. https://doi.org/10.1371/journal.ppat.0020053.

141. Lee, Nara, Valerie Le Sage, Adalena V. Nanni, Dan J. Snyder, Vaughn S. Cooper, and Seema S. Lakdawala. 2017. “Genome-Wide Analysis of Influenza Viral RNA and Nucleoprotein Association.” *Nucleic Acids Research* 45 (15): 8968–77. https://doi.org/10.1093/nar/gkx584.

142. Leonard, Ashley Sobel, Micah T. McClain, Gavin J. D. Smith, David E. Wentworth, Rebecca A. Halpin, Xudong Lin, Amy Ransier, et al. 2017. “The Effective Rate of Influenza Reassortment Is Limited during Human Infection.” *PLOS Pathogens* 13 (2): e1006203. https://doi.org/10.1371/journal.ppat.1006203.

143. Levy, David E., Isabelle J. Marié, and Joan E. Durbin. 2011. “Induction and Function of Type I and III Interferon in Response to Viral Infection.” *Current Opinion in Virology* 1 (6): 476–86. https://doi.org/10.1016/j.coviro.2011.11.001.

144. Lewis, N. S., J. M. Daly, C. A. Russell, D. L. Horton, E. Skepner, N. A. Bryant, D. F. Burke, et al. 2011. “Antigenic and Genetic Evolution of Equine Influenza A (H3N8) Virus from 1968 to 2007.” *Journal of Virology* 85 (23): 12742–49. https://doi.org/10.1128/JVI.05319-11.

145. Li, Chengjun, Masato Hatta, Shinji Watanabe, Gabriele Neumann, and Yoshihiro Kawaoka. 2008. “Compatibility among Polymerase Subunit Proteins Is a Restricting Factor in Reassortment between Equine H7N7 and Human H3N2 Influenza Viruses.” *Journal of Virology* 82 (23): 11880–88. https://doi.org/10.1128/JVI.01445-08.

146. Li, Chengye, Tong Wang, Yuying Zhang, and Fanhua Wei. 2020. “Evasion Mechanisms of the Type I Interferons Responses by Influenza A Virus.” *Critical Reviews in Microbiology* 46 (4): 420–32. https://doi.org/10.1080/1040841X.2020.1794791.

147. Li, Shoudong, Ji-Young Min, Robert M. Krug, and Ganes C. Sen. 2006. “Binding of the Influenza A Virus NS1 Protein to PKR Mediates the Inhibition of Its Activation by Either PACT or Double-Stranded RNA.” *Virology* 349 (1): 13–21. https://doi.org/10.1016/j.virol.2006.01.005.

148. Lingwood, Daniel, and Kai Simons. 2010. “Lipid Rafts as a Membrane-Organizing Principle.” *Science (New York, N.Y.)* 327 (5961): 46–50. https://doi.org/10.1126/science.1174621.

149. Linster, Martin, Sander van Boheemen, Miranda de Graaf, Eefje J. A. Schrauwen, Pascal Lexmond, Benjamin Mänz, Theo M. Bestebroer, et al. 2014. “Identification, Characterization, and Natural Selection of Mutations Driving Airborne Transmission of A/H5N1 Virus.” *Cell* 157 (2): 329–39. https://doi.org/10.1016/j.cell.2014.02.040.

150. Lowen, Anice C. 2017. “Constraints, Drivers, and Implications of Influenza A Virus Reassortment.” *Annual Review of Virology* 4 (1): 105–21. https://doi.org/10.1146/annurev-virology-101416-041726.

151. Ludlow, Martin, Stephen McQuaid, S. Louise Cosby, Roberto Cattaneo, Bert K. Rima, and W. Paul Duprex. 2005. “Measles Virus Superinfection Immunity and Receptor Redistribution in Persistently Infected NT2 Cells.” *The Journal of General Virology* 86 (Pt 8): 2291–2303. https://doi.org/10.1099/vir.0.81052-0.

152. Lun, Aaron T. L., Davis J. McCarthy, and John C. Marioni. 2016. “A Step-by-Step Workflow for Low-Level Analysis of Single-Cell RNA-Seq Data with Bioconductor.” *F1000Research* 5: 2122. https://doi.org/10.12688/f1000research.9501.2.

153. Lun, Aaron T. L., Samantha Riesenfeld, Tallulah Andrews, The Phuong Dao, Tomas Gomes, participants in the 1st Human Cell Atlas Jamboree, and John C. Marioni. 2019. “EmptyDrops: Distinguishing Cells from Empty Droplets in Droplet-Based Single-Cell RNA Sequencing Data.” *Genome Biology* 20 (1): 63. https://doi.org/10.1186/s13059-019-1662-y.

154. Luo, Dahai, Steve C. Ding, Adriana Vela, Andrew Kohlway, Brett D. Lindenbach, and Anna Marie Pyle. 2011. “Structural Insights into RNA Recognition by RIG-I.” *Cell* 147 (2): 409–22. https://doi.org/10.1016/j.cell.2011.09.023.

155. Macosko, Evan Z., Anindita Basu, Rahul Satija, James Nemesh, Karthik Shekhar, Melissa Goldman, Itay Tirosh, et al. 2015. “Highly Parallel Genome-Wide Expression Profiling of Individual Cells Using Nanoliter Droplets.” *Cell* 161 (5): 1202–14. https://doi.org/10.1016/j.cell.2015.05.002.

156. Maeda, T., K. Kawasaki, and S. Ohnishi. 1981. “Interaction of Influenza Virus Hemagglutinin with Target Membrane Lipids Is a Key Step in Virus-Induced Hemolysis and Fusion at PH 5.2.” *Proceedings of the National Academy of Sciences of the United States of America* 78 (7): 4133–37. https://doi.org/10.1073/pnas.78.7.4133.

157. Magnus, P. von. 1951. “Propagation of the PR8 Strain of Influenza A Virus in Chick Embryos. II. The Formation of Incomplete Virus Following Inoculation of Large Doses of Seed Virus.” *Acta Pathologica Et Microbiologica Scandinavica* 28 (3): 278–93. https://doi.org/10.1111/j.1699-0463.1951.tb03693.x.

158. Maljkovic Berry, Irina, Melanie C. Melendrez, Tao Li, Anthony W. Hawksworth, Gary T. Brice, Patrick J. Blair, Eric S. Halsey, et al. 2016. “Frequency of Influenza H3N2 Intra-Subtype Reassortment: Attributes and Implications of Reassortant Spread.” *BMC Biology* 14 (1): 117. https://doi.org/10.1186/s12915-016-0337-3.

159. Mandon, Elisabet C., Steven F. Trueman, and Reid Gilmore. 2013. “Protein Translocation across the Rough Endoplasmic Reticulum.” *Cold Spring Harbor Perspectives in Biology* 5 (2). https://doi.org/10.1101/cshperspect.a013342.

160. Marc, Daniel. 2014. “Influenza Virus Non-Structural Protein NS1: Interferon Antagonism and Beyond.” *The Journal of General Virology* 95 (Pt 12): 2594–2611. https://doi.org/10.1099/vir.0.069542-0.

161. Marshall, Nicolle, Lalita Priyamvada, Zachary Ende, John Steel, and Anice C. Lowen. 2013. “Influenza Virus Reassortment Occurs with High Frequency in the Absence of Segment Mismatch.” *PLOS Pathogens* 9 (6): e1003421. https://doi.org/10.1371/journal.ppat.1003421.

162. Martin, K., and A. Helenius. 1991. “Nuclear Transport of Influenza Virus Ribonucleoproteins: The Viral Matrix Protein (M1) Promotes Export and Inhibits Import.” *Cell* 67 (1): 117–30. https://doi.org/10.1016/0092-8674(91)90576-k.

163. Matrosovich, M., A. Tuzikov, N. Bovin, A. Gambaryan, A. Klimov, M. R. Castrucci, I. Donatelli, and Y. Kawaoka. 2000. “Early Alterations of the Receptor-Binding Properties of H1, H2, and H3 Avian Influenza Virus Hemagglutinins after Their Introduction into Mammals.” *Journal of Virology* 74 (18): 8502–12. https://doi.org/10.1128/jvi.74.18.8502-8512.2000.

164. Matrosovich, Mikhail N., Tatyana Y. Matrosovich, Thomas Gray, Noel A. Roberts, and Hans-Dieter Klenk. 2004. “Neuraminidase Is Important for the Initiation of Influenza Virus Infection in Human Airway Epithelium.” *Journal of Virology* 78 (22): 12665–67. https://doi.org/10.1128/JVI.78.22.12665-12667.2004.

165. McDonald, Sarah M., Martha I. Nelson, Paul E. Turner, and John T. Patton. 2016. “Reassortment in Segmented RNA Viruses: Mechanisms and Outcomes.” *Nature Reviews Microbiology* 14 (7): 448–60. https://doi.org/10.1038/nrmicro.2016.46.

166. McGeoch, D., P. Fellner, and C. Newton. 1976. “Influenza Virus Genome Consists of Eight Distinct RNA Species.” *Proceedings of the National Academy of Sciences of the United States of America* 73 (9): 3045–49. https://doi.org/10.1073/pnas.73.9.3045.

167. Min, Ji-Young, and Robert M. Krug. 2006. “The Primary Function of RNA Binding by the Influenza A Virus NS1 Protein in Infected Cells: Inhibiting the 2’-5’ Oligo (A) Synthetase/RNase L Pathway.” *Proceedings of the National Academy of Sciences of the United States of America* 103 (18): 7100–7105. https://doi.org/10.1073/pnas.0602184103.

168. Mochalova, L., V. Kurova, Y. Shtyrya, E. Korchagina, A. Gambaryan, I. Belyanchikov, and N. Bovin. 2007. “Oligosaccharide Specificity of Influenza H1N1 Virus Neuraminidases.” *Archives of Virology* 152 (11): 2047–57. https://doi.org/10.1007/s00705-007-1024-z.

169. Moeller, Arne, Robert N. Kirchdoerfer, Clinton S. Potter, Bridget Carragher, and Ian A. Wilson. 2012. “Organization of the Influenza Virus Replication Machinery.” *Science (New York, N.Y.)* 338 (6114): 1631–34. https://doi.org/10.1126/science.1227270.

170. Molinari, Noelle-Angelique M., Ismael R. Ortega-Sanchez, Mark L. Messonnier, William W. Thompson, Pascale M. Wortley, Eric Weintraub, and Carolyn B. Bridges. 2007. “The Annual Impact of Seasonal Influenza in the US: Measuring Disease Burden and Costs.” *Vaccine* 25 (27): 5086–96. https://doi.org/10.1016/j.vaccine.2007.03.046.

171. Momose, Fumitaka, Tetsuya Sekimoto, Takashi Ohkura, Shuichi Jo, Atsushi Kawaguchi, Kyosuke Nagata, and Yuko Morikawa. 2011. “Apical Transport of Influenza A Virus Ribonucleoprotein Requires Rab11-Positive Recycling Endosome.” *PloS One* 6 (6): e21123. https://doi.org/10.1371/journal.pone.0021123.

172. Mondal, Arindam, Gregory K. Potts, Anthony R. Dawson, Joshua J. Coon, and Andrew Mehle. 2015. “Phosphorylation at the Homotypic Interface Regulates Nucleoprotein Oligomerization and Assembly of the Influenza Virus Replication Machinery.” *PLoS Pathogens* 11 (4): e1004826. https://doi.org/10.1371/journal.ppat.1004826.

173. Morens, David M., Jeffery K. Taubenberger, and Anthony S. Fauci. 2009. “The Persistent Legacy of the 1918 Influenza Virus.” *The New England Journal of Medicine* 361 (3): 225–29. https://doi.org/10.1056/NEJMp0904819.

174. Murcia, Pablo R., Gregory J. Baillie, Janet Daly, Debra Elton, Carley Jervis, Jennifer A. Mumford, Richard Newton, et al. 2010. “Intra- and Interhost Evolutionary Dynamics of Equine Influenza Virus.” *Journal of Virology* 84 (14): 6943–54. https://doi.org/10.1128/JVI.00112-10.

175. Nakatsu, Sumiho, Hiroshi Sagara, Yuko Sakai-Tagawa, Norio Sugaya, Takeshi Noda, and Yoshihiro Kawaoka. 2016. “Complete and Incomplete Genome Packaging of Influenza A and B Viruses.” *MBio* 7 (5): e01248-16. https://doi.org/10.1128/mBio.01248-16.

176. Nayak, D. P., T. M. Chambers, and R. K. Akkina. 1985. “Defective-Interfering (DI) RNAs of Influenza Viruses: Origin, Structure, Expression, and Interference.” In *Current Topics in Microbiology and Immunology*, edited by M. Cooper, H. Eisen, W. Goebel, P. H. Hofschneider, H. Koprowski, F. Melchers, M. Oldstone, et al., 103–51. Current Topics in Microbiology and Immunology. Berlin, Heidelberg: Springer. https://doi.org/10.1007/978-3-642-70227-3_3.

177. Nelson, Martha I., Laurel Edelman, David J. Spiro, Alex R. Boyne, Jayati Bera, Rebecca Halpin, Naomi Sengamalay, et al. 2008. “Molecular Epidemiology of A/H3N2 and A/H1N1 Influenza Virus during a Single Epidemic Season in the United States.” *PLoS Pathogens* 4 (8): e1000133. https://doi.org/10.1371/journal.ppat.1000133.

178. Nelson MI, Viboud C, Simonsen L, Bennett RT, Griesemer SB, St George K, Taylor J, Spiro DJ, Sengamalay NA, Ghedin E, Taubenberger JK, Holmes EC. 2008. “Multiple Reassortment Events in the Evolutionary History of H1N1 Influenza A Virus Since 1918.” *PLoS Pathog.* 29;4(2):e1000012. https://doi.org/10.1371/journal.ppat.1000012.

179. Nethe, Micha, Ben Berkhout, and Antoinette C. van der Kuyl. 2005. “Retroviral Superinfection Resistance.” *Retrovirology* 2 (August): 52. https://doi.org/10.1186/1742-4690-2-52.

180. Newcomb, Laura L., Rei-Lin Kuo, Qiaozhen Ye, Yunyun Jiang, Yizhi Jane Tao, and Robert M. Krug. 2009. “Interaction of the Influenza a Virus Nucleocapsid Protein with the Viral RNA Polymerase Potentiates Unprimed Viral RNA Replication.” *Journal of Virology* 83 (1): 29–36. https://doi.org/10.1128/JVI.02293-07.

181. Noah, Diana L., Karen Y. Twu, and Robert M. Krug. 2003. “Cellular Antiviral Responses against Influenza A Virus Are Countered at the Posttranscriptional Level by the Viral NS1A Protein via Its Binding to a Cellular Protein Required for the 3’ End Processing of Cellular Pre-MRNAS.” *Virology* 307 (2): 386–95. https://doi.org/10.1016/s0042-6822(02)00127-7.

182. Nobusawa, E., T. Aoyama, H. Kato, Y. Suzuki, Y. Tateno, and K. Nakajima. 1991. “Comparison of Complete Amino Acid Sequences and Receptor-Binding Properties among 13 Serotypes of Hemagglutinins of Influenza A Viruses.” *Virology* 182 (2): 475–85. https://doi.org/10.1016/0042-6822(91)90588-3.

183. Noda, Takeshi, Shin Murakami, Sumiho Nakatsu, Hirotaka Imai, Yukiko Muramoto, Keiko Shindo, Hiroshi Sagara, and Yoshihiro Kawaoka. 2018. “Importance of the 1+7 Configuration of Ribonucleoprotein Complexes for Influenza A Virus Genome Packaging.” *Nature Communications* 9 (1): 54. https://doi.org/10.1038/s41467-017-02517-w.

184. Noda, Takeshi, Hiroshi Sagara, Albert Yen, Ayato Takada, Hiroshi Kida, R. Holland Cheng, and Yoshihiro Kawaoka. 2006. “Architecture of Ribonucleoprotein Complexes in Influenza A Virus Particles.” *Nature* 439 (7075): 490–92. https://doi.org/10.1038/nature04378.

185. Noda, Takeshi, Yukihiko Sugita, Kazuhiro Aoyama, Ai Hirase, Eiryo Kawakami, Atsuo Miyazawa, Hiroshi Sagara, and Yoshihiro Kawaoka. 2012. “Three-Dimensional Analysis of Ribonucleoprotein Complexes in Influenza A Virus.” *Nature Communications* 3 (January): 639. https://doi.org/10.1038/ncomms1647.

186. Nogales, Aitor, Steven F. Baker, Emilio Ortiz-Riaño, Stephen Dewhurst, David J. Topham, and Luis Martínez-Sobrido. 2014. “Influenza A Virus Attenuation by Codon Deoptimization of the NS Gene for Vaccine Development.” *Journal of Virology* 88 (18): 10525–40. https://doi.org/10.1128/JVI.01565-14.

187. Nordholm, Johan, Diogo V. da Silva, Justina Damjanovic, Dan Dou, and Robert Daniels. 2013. “Polar Residues and Their Positional Context Dictate the Transmembrane Domain Interactions of Influenza A Neuraminidases.” *The Journal of Biological Chemistry* 288 (15): 10652–60. https://doi.org/10.1074/jbc.M112.440230.

188. Noton, Sarah L., Elizabeth Medcalf, Dawn Fisher, Anne E. Mullin, Debra Elton, and Paul Digard. 2007. “Identification of the Domains of the Influenza A Virus M1 Matrix Protein Required for NP Binding, Oligomerization and Incorporation into Virions.” *The Journal of General Virology* 88 (Pt 8): 2280–90. https://doi.org/10.1099/vir.0.82809-0.

189. Odendall, Charlotte, and Jonathan C. Kagan. 2015. “The Unique Regulation and Functions of Type III Interferons in Antiviral Immunity.” *Current Opinion in Virology* 12 (June): 47–52. https://doi.org/10.1016/j.coviro.2015.02.003.

190. Ohkuma, S., and B. Poole. 1978. “Fluorescence Probe Measurement of the Intralysosomal PH in Living Cells and the Perturbation of PH by Various Agents.” *Proceedings of the National Academy of Sciences of the United States of America* 75 (7): 3327–31. https://doi.org/10.1073/pnas.75.7.3327.

191. Österlund, Pamela, Mari Strengell, L. Peter Sarin, Minna M. Poranen, Riku Fagerlund, Krister Melén, and Ilkka Julkunen. 2012. “Incoming Influenza A Virus Evades Early Host Recognition, While Influenza B Virus Induces Interferon Expression Directly upon Entry.” *Journal of Virology* 86 (20): 11183–93. https://doi.org/10.1128/JVI.01050-12.

192. Palese, Peter, Kiyotake Tobita, Masahiro Ueda, and Richard W. Compans. 1974. “Characterization of Temperature Sensitive Influenza Virus Mutants Defective in Neuraminidase.” *Virology* 61 (2): 397–410. https://doi.org/10.1016/0042-6822(74)90276-1.

193. Pang, Iris K., and Akiko Iwasaki. 2011. “Inflammasomes as Mediators of Immunity against Influenza Virus.” *Trends in Immunology* 32 (1): 34–41. https://doi.org/10.1016/j.it.2010.11.004.

194. Papalexi, Efthymia, and Rahul Satija. 2018. “Single-Cell RNA Sequencing to Explore Immune Cell Heterogeneity.” *Nature Reviews. Immunology* 18 (1): 35–45. https://doi.org/10.1038/nri.2017.76.

195. Patel, R. C., and G. C. Sen. 1998. “PACT, a Protein Activator of the Interferon-Induced Protein Kinase, PKR.” *The EMBO Journal* 17 (15): 4379–90. https://doi.org/10.1093/emboj/17.15.4379.

196. Pauly, Matthew D, Megan C Procario, and Adam S Lauring. 2017a. “A Novel Twelve Class Fluctuation Test Reveals Higher than Expected Mutation Rates for Influenza A Viruses.” Edited by Karla Kirkegaard. *ELife* 6 (June): e26437. https://doi.org/10.7554/eLife.26437.

197. Pflug, Alexander, Delphine Guilligay, Stefan Reich, and Stephen Cusack. 2014. “Structure of Influenza A Polymerase Bound to the Viral RNA Promoter.” *Nature* 516 (7531): 355–60. https://doi.org/10.1038/nature14008.

198. Phipps, Kara L., Ketaki Ganti, Nathan T. Jacobs, Chung-Young Lee, Silvia Carnaccini, Maria C. White, Miglena Manandhar, et al. 2020. “Collective Interactions Augment Influenza A Virus Replication in a Host-Dependent Manner.” *Nature Microbiology*, July, 1–12. https://doi.org/10.1038/s41564-020-0749-2.

199. Phipps KL, Marshall N, Tao H, Danzy S, Onuoha N, Steel J, Lowen AC. 2017. “Seasonal H3N2 and 2009 Pandemic H1N1 Influenza A Viruses Reassort Efficiently but Produce Attenuated Progeny.” *Journal of Virology.* 91(17):e00830-17. https://jvi.asm.org/content/91/17/e00830-17.

200. Pichlmair, Andreas, Oliver Schulz, Choon Ping Tan, Tanja I. Näslund, Peter Liljeström, Friedemann Weber, and Caetano Reis e Sousa. 2006. “RIG-I-Mediated Antiviral Responses to Single-Stranded RNA Bearing 5’-Phosphates.” *Science (New York, N.Y.)* 314 (5801): 997–1001. https://doi.org/10.1126/science.1132998.

201. Pinto, Lawrence H., and Robert A. Lamb. 2006. “The M2 Proton Channels of Influenza A and B Viruses.” *The Journal of Biological Chemistry* 281 (14): 8997–9000. https://doi.org/10.1074/jbc.R500020200.

202. Plotch, S. J., M. Bouloy, I. Ulmanen, and R. M. Krug. 1981. “A Unique Cap(M7GpppXm)-Dependent Influenza Virion Endonuclease Cleaves Capped RNAs to Generate the Primers That Initiate Viral RNA Transcription.” *Cell* 23 (3): 847–58. https://doi.org/10.1016/0092-8674(81)90449-9.

203. Plotkin, Joshua B., and Jonathan Dushoff. 2003. “Codon Bias and Frequency-Dependent Selection on the Hemagglutinin Epitopes of Influenza A Virus.” *Proceedings of the National Academy of Sciences* 100 (12): 7152–57. https://doi.org/10.1073/pnas.1132114100.

204. Poon, L. L., D. C. Pritlove, E. Fodor, and G. G. Brownlee. 1999. “Direct Evidence That the Poly(A) Tail of Influenza A Virus MRNA Is Synthesized by Reiterative Copying of a U Track in the Virion RNA Template.” *Journal of Virology* 73 (4): 3473–76. https://doi.org/10.1128/JVI.73.4.3473-3476.1999.

205. Rambaut, Andrew, Oliver G. Pybus, Martha I. Nelson, Cecile Viboud, Jeffery K. Taubenberger, and Edward C. Holmes. 2008. “The Genomic and Epidemiological Dynamics of Human Influenza A Virus.” *Nature* 453 (7195): 615–19. https://doi.org/10.1038/nature06945.

206. Ramig, R. F. 1990. “Superinfecting Rotaviruses Are Not Excluded from Genetic Interactions during Asynchronous Mixed Infections in Vitro.” *Virology* 176 (1): 308–10. https://doi.org/10.1016/0042-6822(90)90260-x.

207. Ramos, Irene, Gregory Smith, Frederique Ruf-Zamojski, Carles Martínez-Romero, Miguel Fribourg, Edwin A. Carbajal, Boris M. Hartmann, et al. 2019. “Innate Immune Response to Influenza Virus at Single-Cell Resolution in Human Epithelial Cells Revealed Paracrine Induction of Interferon Lambda 1.” *Journal of Virology* 93 (20). https://doi.org/10.1128/JVI.00559-19.

208. Reich, Stefan, Delphine Guilligay, Alexander Pflug, Hélène Malet, Imre Berger, Thibaut Crépin, Darren Hart, et al. 2014. “Structural Insight into Cap-Snatching and RNA Synthesis by Influenza Polymerase.” *Nature* 516 (7531): 361–66. https://doi.org/10.1038/nature14009.

209. Robb, Nicole C., Aartjan J. W. Te Velthuis, Ralph Wieneke, Robert Tampé, Thorben Cordes, Ervin Fodor, and Achillefs N. Kapanidis. 2016. “Single-Molecule FRET Reveals the Pre-Initiation and Initiation Conformations of Influenza Virus Promoter RNA.” *Nucleic Acids Research* 44 (21): 10304–15. https://doi.org/10.1093/nar/gkw884.

210. Rossman, Jeremy S., Xianghong Jing, George P. Leser, and Robert A. Lamb. 2010. “Influenza Virus M2 Protein Mediates ESCRT-Independent Membrane Scission.” *Cell* 142 (6): 902–13. https://doi.org/10.1016/j.cell.2010.08.029.

211. Rossman, Jeremy S., and Robert A. Lamb. 2013. “Viral Membrane Scission.” *Annual Review of Cell and Developmental Biology* 29: 551–69. https://doi.org/10.1146/annurev-cellbio-101011-155838.

212. Russell, Alistair B., Elizaveta Elshina, Jacob R. Kowalsky, Aartjan J. W. te Velthuis, and Jesse D. Bloom. 2019. “Single-Cell Virus Sequencing of Influenza Infections That Trigger Innate Immunity.” *Journal of Virology* 93 (14). https://doi.org/10.1128/JVI.00500-19.

213. Russell, Alistair B., Cole Trapnell, and Jesse D. Bloom. 2018. “Extreme Heterogeneity of Influenza Virus Infection in Single Cells.” *ELife* 7 (February). https://doi.org/10.7554/eLife.32303.

214. Rust, Michael J., Melike Lakadamyali, Feng Zhang, and Xiaowei Zhuang. 2004. “Assembly of Endocytic Machinery around Individual Influenza Viruses during Viral Entry.” *Nature Structural & Molecular Biology* 11 (6): 567–73. https://doi.org/10.1038/nsmb769.

215. Saira, Kazima, Xudong Lin, Jay V. DePasse, Rebecca Halpin, Alan Twaddle, Timothy Stockwell, Brian Angus, et al. 2013. “Sequence Analysis of in Vivo Defective Interfering-like RNA of Influenza A H1N1 Pandemic Virus.” *Journal of Virology* 87 (14): 8064–74. https://doi.org/10.1128/JVI.00240-13.

216. Saito, T., G. Taylor, and R. G. Webster. 1995. “Steps in Maturation of Influenza A Virus Neuraminidase.” *Journal of Virology* 69 (8): 5011–17. https://doi.org/10.1128/JVI.69.8.5011-5017.1995.

217. Sandbulte, Matthew R., Kim B. Westgeest, Jin Gao, Xiyan Xu, Alexander I. Klimov, Colin A. Russell, David F. Burke, Derek J. Smith, Ron A. M. Fouchier, and Maryna C. Eichelberger. 2011. “Discordant Antigenic Drift of Neuraminidase and Hemagglutinin in H1N1 and H3N2 Influenza Viruses.” *Proceedings of the National Academy of Sciences of the United States of America* 108 (51): 20748–53. https://doi.org/10.1073/pnas.1113801108.

218. Sanjuán, Rafael. 2017. “Collective Infectious Units in Viruses.” *Trends in Microbiology* 25 (5): 402–12. https://doi.org/10.1016/j.tim.2017.02.003.

219. Sasaki, Yasnory T. F., Takashi Ideue, Miho Sano, Toutai Mituyama, and Tetsuro Hirose. 2009. “MENepsilon/Beta Noncoding RNAs Are Essential for Structural Integrity of Nuclear Paraspeckles.” *Proceedings of the National Academy of Sciences of the United States of America* 106 (8): 2525–30. https://doi.org/10.1073/pnas.0807899106.

220. Satterly, Neal, Pei-Ling Tsai, Jan van Deursen, Daniel R. Nussenzveig, Yaming Wang, Paula A. Faria, Agata Levay, David E. Levy, and Beatriz M. A. Fontoura. 2007. “Influenza Virus Targets the MRNA Export Machinery and the Nuclear Pore Complex.” *Proceedings of the National Academy of Sciences of the United States of America* 104 (6): 1853–58. https://doi.org/10.1073/pnas.0610977104.

221. Schaller, Torsten, Nicole Appel, George Koutsoudakis, Stephanie Kallis, Volker Lohmann, Thomas Pietschmann, and Ralf Bartenschlager. 2007. “Analysis of Hepatitis C Virus Superinfection Exclusion by Using Novel Fluorochrome Gene-Tagged Viral Genomes.” *Journal of Virology* 81 (9): 4591–4603. https://doi.org/10.1128/JVI.02144-06.

222. Schelker, Max, Caroline Maria Mair, Fabian Jolmes, Robert-William Welke, Edda Klipp, Andreas Herrmann, Max Flöttmann, and Christian Sieben. 2016. “Viral RNA Degradation and Diffusion Act as a Bottleneck for the Influenza A Virus Infection Efficiency.” *PLOS Computational Biology* 12 (10): e1005075. https://doi.org/10.1371/journal.pcbi.1005075.

223. Schulte, Michael B., and Raul Andino. 2014. “Single-Cell Analysis Uncovers Extensive Biological Noise in Poliovirus Replication.” *Journal of Virology* 88 (11): 6205–12. https://doi.org/10.1128/JVI.03539-13.

224. Schulz, Oliver, Andreas Pichlmair, Jan Rehwinkel, Neil C. Rogers, Donalyn Scheuner, Hiroki Kato, Osamu Takeuchi, Shizuo Akira, Randal J. Kaufman, and Caetano Reis e Sousa. 2010. “Protein Kinase R Contributes to Immunity against Specific Viruses by Regulating Interferon MRNA Integrity.” *Cell Host & Microbe* 7 (5): 354–61. https://doi.org/10.1016/j.chom.2010.04.007.

225. Shimizu, Teppei, Naoki Takizawa, Ken Watanabe, Kyosuke Nagata, and Nobuyuki Kobayashi. 2011. “Crucial Role of the Influenza Virus NS2 (NEP) C-Terminal Domain in M1 Binding and Nuclear Export of VRNP.” *FEBS Letters* 585 (1): 41–46. https://doi.org/10.1016/j.febslet.2010.11.017.

226. Simon, K. O., J. J. Cardamone, P. A. Whitaker-Dowling, J. S. Youngner, and C. C. Widnell. 1990. “Cellular Mechanisms in the Superinfection Exclusion of Vesicular Stomatitis Virus.” *Virology* 177 (1): 375–79. https://doi.org/10.1016/0042-6822(90)90494-c.

227. Sjaastad, Louisa E., Elizabeth J. Fay, Jessica K. Fiege, Marissa G. Macchietto, Ian A. Stone, Matthew W. Markman, Steven Shen, and Ryan A. Langlois. 2018. “Distinct Antiviral Signatures Revealed by the Magnitude and Round of Influenza Virus Replication in Vivo.” *Proceedings of the National Academy of Sciences of the United States of America* 115 (38): 9610–15. https://doi.org/10.1073/pnas.1807516115.

228. Smith, Gavin J. D., Dhanasekaran Vijaykrishna, Justin Bahl, Samantha J. Lycett, Michael Worobey, Oliver G. Pybus, Siu Kit Ma, et al. 2009. “Origins and Evolutionary Genomics of the 2009 Swine-Origin H1N1 Influenza A Epidemic.” *Nature* 459 (7250): 1122–25. https://doi.org/10.1038/nature08182.

229. Sobel Leonard, Ashley, Micah T. McClain, Gavin J. D. Smith, David E. Wentworth, Rebecca A. Halpin, Xudong Lin, Amy Ransier, et al. 2017. “The Effective Rate of Influenza Reassortment Is Limited during Human Infection.” *PLoS Pathogens* 13 (2): e1006203. https://doi.org/10.1371/journal.ppat.1006203.

230. Steel, John, and Anice C. Lowen. 2014. “Influenza A Virus Reassortment.” In *Influenza Pathogenesis and Control - Volume I*, edited by Richard W. Compans and Michael B. A. Oldstone, 377–401. Current Topics in Microbiology and Immunology. Cham: Springer International Publishing. https://doi.org/10.1007/82_2014_395.

231. Steuerman, Yael, Merav Cohen, Naama Peshes-Yaloz, Liran Valadarsky, Ofir Cohn, Eyal David, Amit Frishberg, et al. 2018. “Dissection of Influenza Infection In Vivo by Single-Cell RNA Sequencing.” *Cell Systems* 6 (6): 679-691.e4. https://doi.org/10.1016/j.cels.2018.05.008.

232. Stieneke-Gröber, A., M. Vey, H. Angliker, E. Shaw, G. Thomas, C. Roberts, H. D. Klenk, and W. Garten. 1992. “Influenza Virus Hemagglutinin with Multibasic Cleavage Site Is Activated by Furin, a Subtilisin-like Endoprotease.” *The EMBO Journal* 11 (7): 2407–14.

233. Stuart, Tim, Andrew Butler, Paul Hoffman, Christoph Hafemeister, Efthymia Papalexi, William M. Mauck, Yuhan Hao, Marlon Stoeckius, Peter Smibert, and Rahul Satija. 2019. “Comprehensive Integration of Single-Cell Data.” *Cell* 177 (7): 1888-1902.e21. https://doi.org/10.1016/j.cell.2019.05.031.

234. Stuart, Tim, and Rahul Satija. 2019. “Integrative Single-Cell Analysis.” *Nature Reviews. Genetics* 20 (5): 257–72. https://doi.org/10.1038/s41576-019-0093-7.

235. Sugita, Yukihiko, Hiroshi Sagara, Takeshi Noda, and Yoshihiro Kawaoka. 2013. “Configuration of Viral Ribonucleoprotein Complexes within the Influenza A Virion.” *Journal of Virology* 87 (23): 12879–84. https://doi.org/10.1128/JVI.02096-13.

236. Takeda, Makoto, George P. Leser, Charles J. Russell, and Robert A. Lamb. 2003. “Influenza Virus Hemagglutinin Concentrates in Lipid Raft Microdomains for Efficient Viral Fusion.” *Proceedings of the National Academy of Sciences of the United States of America* 100 (25): 14610–17. https://doi.org/10.1073/pnas.2235620100.

237. Takeuchi, Osamu, and Shizuo Akira. 2009. “Innate Immunity to Virus Infection.” *Immunological Reviews* 227 (1): 75–86. https://doi.org/10.1111/j.1600-065X.2008.00737.x.

238. Talon, J., C. M. Horvath, R. Polley, C. F. Basler, T. Muster, P. Palese, and A. García-Sastre. 2000. “Activation of Interferon Regulatory Factor 3 Is Inhibited by the Influenza A Virus NS1 Protein.” *Journal of Virology* 74 (17): 7989–96. https://doi.org/10.1128/jvi.74.17.7989-7996.2000.

239. Talon, J., M. Salvatore, R. E. O’Neill, Y. Nakaya, H. Zheng, T. Muster, A. García-Sastre, and P. Palese. 2000. “Influenza A and B Viruses Expressing Altered NS1 Proteins: A Vaccine Approach.” *Proceedings of the National Academy of Sciences of the United States of America* 97 (8): 4309–14. https://doi.org/10.1073/pnas.070525997.

240. Tao, Hui, John Steel, and Anice C. Lowen. 2014. “Intrahost Dynamics of Influenza Virus Reassortment.” *Journal of Virology* 88 (13): 7485–92. https://doi.org/10.1128/JVI.00715-14.

241. Tao H, Li L, White MC, Steel J, Lowen AC. 2015. “Influenza A Virus Coinfection through Transmission Can Support High Levels of Reassortment”. *Journal of Virology.* 89(16):8453-61. https://jvi.asm.org/content/89/16/8453.

242. Taubenberger, Jeffery K., and John C. Kash. 2010. “Influenza Virus Evolution, Host Adaptation and Pandemic Formation.” *Cell Host & Microbe* 7 (6): 440–51. https://doi.org/10.1016/j.chom.2010.05.009.

243. Taubenberger, Jeffery K., and David M. Morens. 2010. “Influenza: The Once and Future Pandemic.” *Public Health Reports (Washington, D.C.: 1974)* 125 Suppl 3 (April): 16–26.

244. Thyagarajan, Bargavi, and Jesse D. Bloom. 2014. “The Inherent Mutational Tolerance and Antigenic Evolvability of Influenza Hemagglutinin.” *ELife* 3 (July). https://doi.org/10.7554/eLife.03300.

245. Tong, Suxiang, Yan Li, Pierre Rivailler, Christina Conrardy, Danilo A. Alvarez Castillo, Li-Mei Chen, Sergio Recuenco, et al. 2012. “A Distinct Lineage of Influenza A Virus from Bats.” *Proceedings of the National Academy of Sciences of the United States of America* 109 (11): 4269–74. https://doi.org/10.1073/pnas.1116200109.

246. Tong, Suxiang, Xueyong Zhu, Yan Li, Mang Shi, Jing Zhang, Melissa Bourgeois, Hua Yang, et al. 2013. “New World Bats Harbor Diverse Influenza A Viruses.” *PLoS Pathogens* 9 (10): e1003657. https://doi.org/10.1371/journal.ppat.1003657.

247. Tscherne, Donna M., Matthew J. Evans, Thomas von Hahn, Christopher T. Jones, Zania Stamataki, Jane A. McKeating, Brett D. Lindenbach, and Charles M. Rice. 2007. “Superinfection Exclusion in Cells Infected with Hepatitis C Virus.” *Journal of Virology* 81 (8): 3693–3703. https://doi.org/10.1128/JVI.01748-06.

248. Turan, Kadir, Masaki Mibayashi, Kenji Sugiyama, Shoko Saito, Akiko Numajiri, and Kyosuke Nagata. 2004. “Nuclear MxA Proteins Form a Complex with Influenza Virus NP and Inhibit the Transcription of the Engineered Influenza Virus Genome.” *Nucleic Acids Research* 32 (2): 643–52. https://doi.org/10.1093/nar/gkh192.

249. Valcárcel, J., A. Portela, and J. Ortín. 1991. “Regulated M1 MRNA Splicing in Influenza Virus-Infected Cells.” *The Journal of General Virology* 72 (Pt 6) (June): 1301–8. https://doi.org/10.1099/0022-1317-72-6-1301.

250. Vasilijevic, Jasmina, Noelia Zamarreño, Juan Carlos Oliveros, Ariel Rodriguez-Frandsen, Guillermo Gómez, Guadalupe Rodriguez, Mercedes Pérez-Ruiz, et al. 2017. “Reduced Accumulation of Defective Viral Genomes Contributes to Severe Outcome in Influenza Virus Infected Patients.” *PLoS Pathogens* 13 (10): e1006650. https://doi.org/10.1371/journal.ppat.1006650.

251. Vignuzzi, Marco, and Carolina B. López. 2019. “Defective Viral Genomes Are Key Drivers of the Virus-Host Interaction.” *Nature Microbiology* 4 (7): 1075–87. https://doi.org/10.1038/s41564-019-0465-y.

252. Voeten, J. T., T. M. Bestebroer, N. J. Nieuwkoop, R. A. Fouchier, A. D. Osterhaus, and G. F. Rimmelzwaan. 2000. “Antigenic Drift in the Influenza A Virus (H3N2) Nucleoprotein and Escape from Recognition by Cytotoxic T Lymphocytes.” *Journal of Virology* 74 (15): 6800–6807. https://doi.org/10.1128/jvi.74.15.6800-6807.2000.

253. Vries, Erik de, Wenjuan Du, Hongbo Guo, and Cornelis A. M. de Haan. 2020. “Influenza A Virus Hemagglutinin–Neuraminidase–Receptor Balance: Preserving Virus Motility.” *Trends in Microbiology* 28 (1): 57–67. https://doi.org/10.1016/j.tim.2019.08.010.

254. Wack, Andreas, Ewa Terczyńska-Dyla, and Rune Hartmann. 2015. “Guarding the Frontiers: The Biology of Type III Interferons.” *Nature Immunology* 16 (8): 802–9. https://doi.org/10.1038/ni.3212.

255. Wang, Chang, Christian V. Forst, Tsui-Wen Chou, Adam Geber, Minghui Wang, Wissam Hamou, Melissa Smith, et al. 2020. “Cell-to-Cell Variation in Defective Virus Expression and Effects on Host Responses during Influenza Virus Infection.” *MBio* 11 (1). https://doi.org/10.1128/mBio.02880-19.

256. Wang, Ning, Emily J. Glidden, Stephanie R. Murphy, Bradley R. Pearse, and Daniel N. Hebert. 2008. “The Cotranslational Maturation Program for the Type II Membrane Glycoprotein Influenza Neuraminidase.” *The Journal of Biological Chemistry* 283 (49): 33826–37. https://doi.org/10.1074/jbc.M806897200.

257. Wang, P., P. Palese, and R. E. O’Neill. 1997. “The NPI-1/NPI-3 (Karyopherin Alpha) Binding Site on the Influenza a Virus Nucleoprotein NP Is a Nonconventional Nuclear Localization Signal.” *Journal of Virology* 71 (3): 1850–56. https://doi.org/10.1128/JVI.71.3.1850-1856.1997.

258. Wang, X., M. Li, H. Zheng, T. Muster, P. Palese, A. A. Beg, and A. García-Sastre. 2000. “Influenza A Virus NS1 Protein Prevents Activation of NF-KappaB and Induction of Alpha/Beta Interferon.” *Journal of Virology* 74 (24): 11566–73. https://doi.org/10.1128/jvi.74.24.11566-11573.2000.

259. Watanabe, Nobuo, Dale A. Dickinson, David M. Krzywanski, Karen E. Iles, Hongqiao Zhang, Charles J. Venglarik, and Henry Jay Forman. 2002. “A549 Subclones Demonstrate Heterogeneity in Toxicological Sensitivity and Antioxidant Profile.” *American Journal of Physiology. Lung Cellular and Molecular Physiology* 283 (4): L726-736. https://doi.org/10.1152/ajplung.00025.2002.

260. Webster, R. G., W. J. Bean, O. T. Gorman, T. M. Chambers, and Y. Kawaoka. 1992. “Evolution and Ecology of Influenza A Viruses.” *Microbiological Reviews* 56 (1): 152–79.

261. Webster, R. G., and W. G. Laver. 1967. “Preparation and Properties of Antibody Directed Specifically against the Neuraminidase of Influenza Virus.” *Journal of Immunology (Baltimore, Md.: 1950)* 99 (1): 49–55.

262. Weis, W., J. H. Brown, S. Cusack, J. C. Paulson, J. J. Skehel, and D. C. Wiley. 1988. “Structure of the Influenza Virus Haemagglutinin Complexed with Its Receptor, Sialic Acid.” *Nature* 333 (6172): 426–31. https://doi.org/10.1038/333426a0.

263. Westgeest, Kim B., Colin A. Russell, Xudong Lin, Monique I. J. Spronken, Theo M. Bestebroer, Justin Bahl, Ruud van Beek, et al. 2014. “Genomewide Analysis of Reassortment and Evolution of Human Influenza A(H3N2) Viruses Circulating between 1968 and 2011.” *Journal of Virology* 88 (5): 2844–57. https://doi.org/10.1128/JVI.02163-13.

264. White, David O., and Ian M. Cheyne. 1966. “Early Events in the Eclipse Phase of Influenza and Parainfluenza Virus Infection.” *Virology* 29 (1): 49–59. https://doi.org/10.1016/0042-6822(66)90195-4.

265. White, Do, Hm Day, Ej Batchelder, Im Cheyne, and Aj Wansbrough. 1965. “Delay in the Multiplication of Influenza Virus.” *Virology* 25 (February): 289–302. https://doi.org/10.1016/0042-6822(65)90207-2.

266. White, Judith M., and Gary R. Whittaker. 2016. “Fusion of Enveloped Viruses in Endosomes.” *Traffic (Copenhagen, Denmark)* 17 (6): 593–614. https://doi.org/10.1111/tra.12389.

267. White MC, Steel J, Lowen AC. 2017. “Heterologous Packaging Signals on Segment 4, but Not Segment 6 or Segment 8, Limit Influenza A Virus Reassortment. *Journal of Virology*.” 91(11):e00195-17. https://jvi.asm.org/content/91/11/e00195-17.

268. Williams, Graham D., Dana Townsend, Kristine M. Wylie, Preston J. Kim, Gaya K. Amarasinghe, Sebla B. Kutluay, and Adrianus C. M. Boon. 2018. “Nucleotide Resolution Mapping of Influenza A Virus Nucleoprotein-RNA Interactions Reveals RNA Features Required for Replication.” *Nature Communications* 9 (1): 465. https://doi.org/10.1038/s41467-018-02886-w.

269. Wu, Winco W. H., Lindsay L. Weaver, and Nelly Panté. 2007. “Ultrastructural Analysis of the Nuclear Localization Sequences on Influenza A Ribonucleoprotein Complexes.” *Journal of Molecular Biology* 374 (4): 910–16. https://doi.org/10.1016/j.jmb.2007.10.022.

270. Xiao, Yinghong, Patrick Timothy Dolan, Elizabeth Faul Goldstein, Min Li, Mikhail Farkov, Leonid Brodsky, and Raul Andino. 2017. “Poliovirus Intrahost Evolution Is Required to Overcome Tissue-Specific Innate Immune Responses.” *Nature Communications* 8 (1): 375. https://doi.org/10.1038/s41467-017-00354-5.

271. Xue, Katherine S., Terry Stevens-Ayers, Angela P. Campbell, Janet A. Englund, Steven A. Pergam, Michael Boeckh, and Jesse D. Bloom. 2017. “Parallel Evolution of Influenza across Multiple Spatiotemporal Scales.” *ELife* 6. https://doi.org/10.7554/eLife.26875.

272. Yondola, Mark A., Fiona Fernandes, Alan Belicha-Villanueva, Melissa Uccelini, Qinshan Gao, Carol Carter, and Peter Palese. 2011. “Budding Capability of the Influenza Virus Neuraminidase Can Be Modulated by Tetherin.” *Journal of Virology* 85 (6): 2480–91. https://doi.org/10.1128/JVI.02188-10.

273. Yoon, Sun-Woo, Richard J. Webby, and Robert G. Webster. 2014. “Evolution and Ecology of Influenza A Viruses.” *Current Topics in Microbiology and Immunology* 385: 359–75. https://doi.org/10.1007/82_2014_396.

274. York, Ashley, and Ervin Fodor. 2013. “Biogenesis, Assembly, and Export of Viral Messenger Ribonucleoproteins in the Influenza A Virus Infected Cell.” *RNA Biology* 10 (8): 1274–82. https://doi.org/10.4161/rna.25356.

275. York, Ashley, Narin Hengrung, Frank T. Vreede, Juha T. Huiskonen, and Ervin Fodor. 2013. “Isolation and Characterization of the Positive-Sense Replicative Intermediate of a Negative-Strand RNA Virus.” *Proceedings of the National Academy of Sciences of the United States of America* 110 (45): E4238-4245. https://doi.org/10.1073/pnas.1315068110.

276. Zanin, Mark, Bindumadhav Marathe, Sook-San Wong, Sun-Woo Yoon, Emily Collin, Christine Oshansky, Jeremy Jones, Benjamin Hause, and Richard Webby. 2015. “Pandemic Swine H1N1 Influenza Viruses with Almost Undetectable Neuraminidase Activity Are Not Transmitted via Aerosols in Ferrets and Are Inhibited by Human Mucus but Not Swine Mucus.” *Journal of Virology* 89 (11): 5935–48. https://doi.org/10.1128/JVI.02537-14.

277. Zanini, Fabio, Szu-Yuan Pu, Elena Bekerman, Shirit Einav, and Stephen R. Quake. 2018. “Single-Cell Transcriptional Dynamics of Flavivirus Infection.” *ELife* 7. https://doi.org/10.7554/eLife.32942.

278. Zebedee, S. L., and R. A. Lamb. 1988. “Influenza A Virus M2 Protein: Monoclonal Antibody Restriction of Virus Growth and Detection of M2 in Virions.” *Journal of Virology* 62 (8): 2762–72. https://doi.org/10.1128/JVI.62.8.2762-2772.1988.

279. Zhang, Feifei, Lingling Wu, Jie Qian, Bo Qu, Shiwei Xia, Ting La, Yanfang Wu, et al. 2016. “Identification of the Long Noncoding RNA NEAT1 as a Novel Inflammatory Regulator Acting through MAPK Pathway in Human Lupus.” *Journal of Autoimmunity* 75 (December): 96–104. https://doi.org/10.1016/j.jaut.2016.07.012.

280. Zhang, Jie, Andrew Pekosz, and Robert A. Lamb. 2000. “Influenza Virus Assembly and Lipid Raft Microdomains: A Role for the Cytoplasmic Tails of the Spike Glycoproteins.” *Journal of Virology* 74 (10): 4634–44. https://doi.org/10.1128/JVI.74.10.4634-4644.2000.

281. Zhang, Pengfei, Limian Cao, Rongbin Zhou, Xiaolu Yang, and Mian Wu. 2019. “The LncRNA Neat1 Promotes Activation of Inflammasomes in Macrophages.” *Nature Communications* 10 (1): 1495. https://doi.org/10.1038/s41467-019-09482-6.

282. Zhang, Shijian, Jinlan Wang, Qiang Wang, and Tetsuya Toyoda. 2010. “Internal Initiation of Influenza Virus Replication of Viral RNA and Complementary RNA in Vitro.” *The Journal of Biological Chemistry* 285 (52): 41194–201. https://doi.org/10.1074/jbc.M110.130062.

283. Zhang, Xiao-Feng, Rong Sun, Qin Guo, Shaoyan Zhang, Tea Meulia, Randal Halfmann, Dawei Li, and Feng Qu. 2017. “A Self-Perpetuating Repressive State of a Viral Replication Protein Blocks Superinfection by the Same Virus.” *PLoS Pathogens* 13 (3): e1006253. https://doi.org/10.1371/journal.ppat.1006253.

284. Zhirnov, Oleg P., Mine R. Ikizler, and Peter F. Wright. 2002. “Cleavage of Influenza a Virus Hemagglutinin in Human Respiratory Epithelium Is Cell Associated and Sensitive to Exogenous Antiproteases.” *Journal of Virology* 76 (17): 8682–89. https://doi.org/10.1128/jvi.76.17.8682-8689.2002.

285. Zhou, Xiang, Jennifer J. Michal, Lifan Zhang, Bo Ding, Joan K. Lunney, Bang Liu, and Zhihua Jiang. 2013. “Interferon Induced IFIT Family Genes in Host Antiviral Defense.” *International Journal of Biological Sciences* 9 (2): 200–208. https://doi.org/10.7150/ijbs.5613.

286. Zou, Gang, Bo Zhang, Pei-Yin Lim, Zhiming Yuan, Kristen A. Bernard, and Pei-Yong Shi. 2009. “Exclusion of West Nile Virus Superinfection through RNA Replication.” *Journal of Virology* 83 (22): 11765–76. https://doi.org/10.1128/JVI.01205-09.

287. Zurcher, T, G Luo, and P Palese. 1994. “Mutations at Palmitylation Sites of the Influenza Virus Hemagglutinin Affect Virus Formation.” *Journal of Virology* 68 (9): 5748–54.